Fall 12-2011

Quantifying Rates of Autocompaction in the Pearl River Marsh, Louisiana

Jeremiah Nicholas Prouhet
University of Southern Mississippi

The University of Southern Mississippi

QUANTIFYING RATES OF AUTOCOMPACTION

IN THE PEARL RIVER MARSH, LOUISIANA

by

Jeremiah Nicholas Prouhet

A Thesis
Submitted to the Graduate School
of The University of Southern Mississippi
in Partial Fulfillment of the Requirements
for the Degree of Master of Science

Approved:

Kevin Yeager
Director

Charlotte Brunner

Mark Kulp

Susan A Siltanen
Dean of the Graduate School

December 2011

ABSTRACT

QUANTIFYING RATES OF AUTOCOMPACTION

IN THE PEARL RIVER MARSH, LOUISIANA

by

Jeremiah Nicholas Prouhet

December 2011

Annual rates of shallow autocompaction (< 1 m) were calculated in the upper ~one meter of sediment from six cores of a transect in the Pearl River Marsh (PRM), Louisiana, in order to determine the most significant sedimentary property controlling this process. Compaction-free wedge cores were sub-sampled at one centimeter intervals to collect the following data: age control, using ^{137}Cs and ^{210}Pb, and sedimentary variables, specifically, particulate organic carbon, bulk density, median grain size, porosity, and water content. An upper and an underlying sedimentary unit (named the ^{137}Cs and ^{210}Pb units) were defined between radiometric datum levels, and their sedimentary properties were statistically tested for significant differences using the non-parametric Mann-Whitney test. Rates of autocompaction were calculated from the model of Williams (2003), and both rates of autocompaction and sedimentation were tested for significant differences between the upper and lower sedimentary units.

The upper unit in the six cores generally had lower bulk density, higher water content, higher porosity, and higher particulate organic carbon than the underlying unit, but with some interesting exceptions. Additionally, annual autocompaction and sedimentation rates were greatest in the overlying unit at stations PR02 (0.39 ± 0.05 cm/y) and PR05 (0.42 ± 0.03 cm/y) and greatest in the underlying unit at stations PR02 (0.22 ± 0.08 cm/y) and PR03 (0.18 ± 0.06 cm/y). Based on Spearman correlations, rates of autocompaction were most strongly correlated to and influenced by rates of sedimentation rather than the other sedimentary variables:

particulate organic carbon, bulk density, median grain size, porosity, and water content. The rates of sedimentation and autocompaction from this study were similar to rates measured in similar studies that use different methodologies to calculate compaction. This study demonstrates that rates of autocompaction are highly variable in near-surface sediments and that these rates significantly decrease with increased depth.

ACKNOWLEDGMENTS

This research project would have been impossible without the support of many people. The author would like to express gratitude to Dr. Kevin Yeager, who was abundantly helpful and offered invaluable assistance, support, and guidance.

Deepest gratitude also is due to the members of the graduate committee, Dr. Charlotte Brunner and Dr. Mark Kulp. Without their knowledge and assistance, this study would not have been successful.

The author would also like to express his love and gratitude to his beloved family for their understanding and endless support throughout the duration of this thesis.

TABLE OF CONTENTS

LIST OF TABLES

Table

LIST OF ILLUSTRATIONS

Figure

CHAPTER I

INTRODUCTION

According to Allen (2000), "The continuous, progressive, irreversible, and asymptotic process of sediment autocompaction plays a significant, but so far largely neglected role in determining the coevolving character of the Holocene landscape and sedimentary sequences formed in coastal marshlands" (p. 239). Autocompaction is neither well-understood nor well-characterized at local, let alone at regional scales; therefore, broad assumptions of regional autocompaction rates are likely not realistic (Allen, 2000; Cahoon, Reed, & Day, 1995; Meckel, 2007). Developing or refining a way to model autocompaction at the near surface will improve understanding of short-term (~100 yBP) marsh elevation changes.

Autocompaction rates of near-surface sediments have been modeled by Turner, Milan, and Swenson (2006) and Williams (2003). Turner et al. and Williams used fallout radionuclides for chronological control. However, the limits of their approaches are associated primarily with the quality and quantity of physical data collected. The underlying theory of autocompaction developed by Williams (2003) appears sound, but the data set supporting the results should be broadened. Turner et al. (2006) claimed that compaction of marsh sediments can be directly tied to accretion rates based on the ratio of $^{137}Cs/^{210}Pb$ in shallow marsh sediments. Included data should include the physical parameters believed to be most important in terms of sediment deformation and compaction and also the errors associated with the calculations of autocompaction rates.

Previous studies about autocompaction use a limited data set in the determination of this process. Dry sediment bulk density and rates of accretion are important to

understand sediment compressibility but may not be the most important physical variables. How do the sedimentation rate, grain size, water content, porosity, and organic matter content affect autocompaction rates in a marsh environment? Can a conceptual model that includes these parameters be developed allowing up-scaling to other marsh systems that share similar characteristics?

Hypothesis

The hypothesis of this research set out to investigate if sedimentation rates are as important as sediment composition (inorganic/organic, component), variations in porosity, and variations in the water content at controlling the rate of autocompaction.

Objectives

To test this hypothesis, sediment cores were collected from the PRM, and physical sedimentary properties were measured and calculated including the following: bulk density (B_d), sedimentary particulate organic carbon (POC), porosity (φ), median grain size (d.50), water content, ^{137}Cs and $^{210}Pb_{xs}$ activities, and rates of annual sedimentation derived from isotopic chronostratigraphic horizons. Once physical data were collected, rates of autocompaction were calculated from a model developed by Williams (2003) for both the ^{137}Cs and ^{210}Pb sedimentary units. Variations in the sedimentary data were compared to the calculated rates of autocompaction to evaluate if changes of bulk density, POC content, porosity, average grain size, changing water content, or rates of sedimentation are influencing how sediments compact on decadal and centennial time scales. Specific objectives included the following:

1. *Quantify rates of autocompaction*. Sediment cores collected from the PRM were sampled for bulk density and radionuclides to calculate averaged rates of autocompaction.
2. *Develop a high-resolution data set of sedimentary properties for the upper 90 cm*. Sediment cores were analyzed in detail (at 1 cm vertical resolution) to resolve small changes in the sediment texture and composition that would likely be missed using larger sampling intervals (meters).
3. *Examine autocompaction rates relative to a suite of sediment physical properties*. Sediment cores were processed for physical properties (sedimentation rate, bulk density [B_d], sedimentary POC, porosity [φ], median grain size [d.50], and water content) and correlations between autocompaction rates and physical properties were investigated.

CHAPTER II

REVIEW OF RELATED LITERATURE

Autocompaction of near surface, marsh sediments is a poorly understood process that is often underestimated or overly generalized (Allen, 1998; Kaye & Barghoorn, 1964; Meckel, Brink, & Williams, 2006; Pizzuto & Schwendt, 1997). The scarcity of reliable, quantitative data hinders understanding of the contribution of autocompaction to coastal subsidence of surface sediments.

While regional, deep subsidence primarily results from natural resource withdrawal (Meckel et al., 2006; Meckel, 2007; Morton, Tiling, & Ferina, 2003; Nunn, 2003; Wilson & Grace, 1942) or aseismic, tectonic processes (Dokka, Sella, & Dixon, 2006; Gagliano, 2005; Gonzales & Törnqvist, 2006; Shinkel & Dokka, 2004; Törnqvist, Bick, van der Board, & de Jong, 2006), shallow (<10 m) autocompaction is more localized and could be dominantly controlled by sediment supply, sediment textures, and the *in situ* production of organic sediments (Cahoon et al., 1995; Williams, 2003).

Autocompaction creates accommodation space from the gradual subsidence of deposited sediments on a local and regional scale. Lower marsh elevation leads to longer periods of marsh inundation of low relief areas if sediment supply and *in situ* sediment production are insufficient.

On a regional scale, coastal subsidence is a complex process controlled by site-specific sedimentary properties, relative sea level (RSL) rise, eustatic sea level rise (Penland & Ramsey, 1990; Reed, 1989), land use (Gambolati, Putti Teatini, & Gasparetto-Stori, 2006), natural resource (oil, natural gas, water) withdrawal (Meckel, 2007; Morton et al., 2003; Nunn, 2003; Wilson & Grace, 1942), and tectonics (Gagliano,

2005; Gonzales & Törnqvist, 2006; Shinkle & Dokka, 2004; Törnqvist et al., 2006). A rise in eustatic sea level caused by global warming, coupled with subsidence of coastal areas, is rapidly inundating and destroying wetlands, which are economically and ecologically vital (Törnqvist et al., 2008).

On a local scale, shallow autocompaction can lead to the development of marsh hot spots that can accelerate interior marsh erosion (Morton, Bernier & Ferina, 2005). These hot spots are areas that rapidly subside below the active marsh platform and fill with fresh or saline water. They begin as small, isolated patches of standing water that are surrounded by healthy marsh vegetation but increase in size over time (Leibowitz & Hill, 1987). Some become large enough that wind-driven wave action further erodes their banks, increasing the pond's width and depth (DeLaune, Nyman, & Patric, 1994; DeLaune & Pezeshki, 2003; Morton et al., 2003; Morton et al., 2005). As the marsh deteriorates, these ponds gradually enlarge and merge with one another transitioning the wetland to open water with a few remnant islands.

Autocompaction is an interaction of biological, hydro-chemical, and physical processes that typically operate on distinctly different time scales (see Figure 1) (van Asselen, Stouthamer, & van Asch, 2009). These time scales range from immediately after sediment is deposited to thousands of years after burial (van Asselen et al., 2009). This research is focused on the physical component of autocompaction but addresses the other components in brief here.

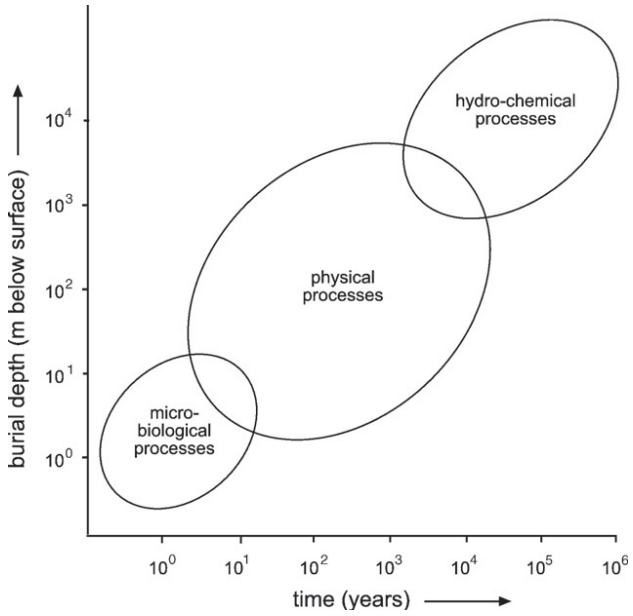

Figure 1. Dominant processes contributing to compaction at different time scales and depths. These processes operate at different time scales and at different depths with some overlap (van Asselen et al., 2009).

Relevant biological activities in marshes include plant growth, decomposition (mechanical, chemical and microbial), and bioturbation by micro, macro, and mega fauna (Ford & Grace, 1998; McCraith, Gardner, Welthey, & Moore, 2003). The decomposition and destruction of organic matter by fauna reduce the accumulated litter at the marsh surface with larger fauna capable of destroying the living plant root system.

The living plant root system forms a tightly interwoven network that increases marsh soil strength (DeLaune et al., 1994). If the root mat dies, there is a loss of turgor pressure in the thousands of tiny rootlets that support the marsh surface; this may lead to marsh subsidence below the ambient water level (McKee & Mendelssohn, 1989). While some organic sediments are provided to the marsh by flooding, most organic sediments result from the *in situ* production and decay of plant materials. The accretion of *in situ* organic sediments is controlled by floral productivity, species density, species diversity,

and the decay rate of marsh plants. The decay rate is primarily a function of microbial decomposition, which is influenced by temperature, soil water content, oxygen availability, microbial population, soil animal population, and plant material type (Charman, 2002). In low-energy marsh environments with intermediate salinities (0-5 ppt) *Spartina patens* decomposes very slowly due to its chemical composition and morphology, as compared to *Spartina alterniflora* (Foote & Reynolds, 1997). However, the factors controlling decomposition rates are highly variable, so these rates will vary along gradients of elevation, ground water flow, and oxygen supply in the marsh (van Asselen et al., 2009). Variability in decay rates lead to different rates of volume reduction at the marsh surface, both spatially and temporally. Through time in tidal, fresh-water marshes, the regional variability suggests that the organic component of autochthonous sediment production contributes significantly to the overall accretion of the marsh platform (Neubauer, 2008).

The biological breakdown of organic carbon begins within the first 24 hours after a plant dies or loses leaves (Valiela, Teal, & Allen, 1985). Over the first month, this decomposition can reduce the carbon content by 30%, leading to a reduction in litter volume (Neubauer, Anderson, Constantine & Kuehl, 2002). This reduction in leaf litter biomass can significantly affect the marsh platform elevation in a short period. The process of plant decomposition can be broken down into three phases (Valiela et al., 1985):

1. *The leaching phase* occurs within the first 24 hours, when 20-40% of the soluble plant biomass is removed.

2. *The decomposition phase* occurs when labile materials decay after colonization of fungi and the subsequent consumption of the fungal colony by invertebrates and bacteria.
3. The *refractory phase* is when all remaining plant materials are lignified (Foote & Reynolds, 1997).

Oxidation of organic matter is considered to be the most important process in the chemical reduction of sediment volume (Gambolati et al., 2006). Degradation of organic matter produces both carbon dioxide (CO_2) and methane (CH_4) gas. The release of these gases from the sediment will influence the surface elevation through the collapse of pore spaces due to reduced internal pressure (McKee & Mendelssohn, 1989). Aerobic respiration is typically limited to only near surface sediments (top few centimeters) (Tailfort, Neuhubuer, & Bristow, 2007). Oxygen can be replenished by physically mixing the sediment through bioturbation or by influxes of fresh pore water from tidal creeks. Below this oxic zone, less efficient electron accepting processes (denitrification, Mn(IV) reduction, Fe(III) reduction, sulfate reduction, and finally fermentation) are utilized (Bianchi, 2007) for respiration. Remineralization of organic matter into its most basic components causes the volume of the sediment to decrease, resulting in more accommodation space and reduction of the surface elevation (Neubauer, 2008).

The final stage of compaction is the hydro-chemical process of cementation. This process consolidates loose sediment into consolidated rock (van Asselen et al., 2009). Once the sediment has been cemented together, the possibility of further compaction is limited to a deeper seated process. Physical compression and consolidation also contribute to a decrease in sediment volume (Williams, 2003) that can outpace vertical

accretion leading to a reduction in surface elevation (Kooi & De Vries, 1998; Shennan & Horton, 2002).

In general, modeling of marsh autocompaction has been approached using two different methods. First is a forward modeling method, which calculates the amount of autocompaction an uncompacted sedimentary unit will experience during a specified length of time (Meckel, Brink, & Williams, 2007; van Asselen et al., 2009). Second, which is used here, is the backward modeling method that starts from a compacted state and estimates the decompaction correction (Massey, Paul, Gehrels, & Charman, 2006). Some experiments to calculate the amount of surfical compaction have been conducted under the assumption that organic-rich silt deposits are homogenous and do not vary in texture or organic composition along isochronous beds (Allen, 1998). Deposition of storm layers or proximity to source of allochthonous sediments are known to influence the composition of peat and other marsh facies (e.g., Cahoon, 2006; Williams, 2003). Simple decompaction of peat or organic-rich silts based on geotechnical parameters, as described by Kuecher (1994), does not account for different types of organic matter (grass, wood, rush stem) or its rate of delivery to the marsh over time. Other simple 1-dimensional vertical models have been developed and used (Callaway & Day, 1996; Rybcyzk, Curco, Canico, Prat & Day, 1996; Rybcyzk, Day, Rismond, Scarton, & Arc, 1996) to model thin (0.25 m) Holocene-age peats that were recently accumulated with limited geographic application.

Dry Bulk Density as a Proxy for Autocompaction

A recent review by van Asselen et al. (2009) showed that a broad set of sedimentary properties should be used to calculate rates of autocompaction in marsh

settings. Using a combination of dry bulk density, water content, grain size, radiometric dating, and sedimentary POC concentration data should give insight on how these parameters interact to reduce marsh elevation (van Asselen et al., 2009). The need was recognized by van Asselen et al. (2009) to sample organic-rich sediments using a device that introduces little to no artifact compaction (core shortening), such as a Wardenaar corer (Wardenaar, 1987) or a block sampler (Lefebvre, Langlois, Lupien, & Lavalée, 1984).

Bird, Fifield, Chua, and Goh (2004) documented correlations between dry bulk density, grain size, and organic matter content in un-compacted, modern peat samples (0 – 20 cm). However, these sedimentary relationships were originally based upon data from a deeply buried mangrove swamp peat bed, overlain by ~9 m of clastic sediment. From this deeply buried peat, Bird et al. (2004) concluded that grain size and organic content weighed heavily on the compaction rate of organic-rich and/or fine grained sediments. Research by Allen (1998) and Long, Waller, and Stupples (2006) in northern Europe also calculated rates of autocompaction in peat beds that were buried by several meters of clastic sediments. However, these settings differ substantially from the PRM, where fine-grained and organic-rich sediments are located in the near surface without a thick overburden of clastic sediment.

Basal Peat and ^{14}C as a Proxy for Autocompaction

Dating of basal peats using ^{14}C is a common practice in calculating a single rate of compaction for a sedimentary unit several meters thick (Bloom, 1964; Haslett et al., 1998; Törnqvist, Newsome, Borg, Jong, & Kurnik, 2004). Basal peats in the Mississippi River delta, where present, constitute the initial sedimentary unit in the Holocene

transgressive sequence. This datum typically overlies the relatively consolidated Pleistocene basement, which experiences negligible compaction (Bloom, 1964; Haslett et al., 1998; Törnqvist et al., 2004). With the basal peat directly overlying this incompressible basement, any subsidence at the surface is assumed to be limited entirely to the Holocene sedimentary unit.

Törnqvist et al. (2008) relied on 250 shallow boreholes (of ~15 m depth) to find a common datum level of an extensive, peat-forming, bald cypress swamp deposit overlain by clastic sediments of variable thicknesses in Bayou Lafourche, Louisiana. Using ^{14}C dating of the basal peat deposits to establish chronological control, Törnqvist et al. (2008) measured the relationship of overburden to compaction. This approach assumes linear compaction through the thickness of the entire sedimentary section and does not account for non-linear compaction, i.e., rapid autocompaction of near-surface sediments, followed by much slower, incremental autocompaction of deeper, older sediments (Dokka, 2008; van Asselen et al., 2009). Törnqvist et al. (2008) did find a significant linear relationship between total compaction rates and overburden thickness ($r^2 = 0.83$, $n = 103$) but found that rates of compaction were greater on a centennial scale (10 mm/y) when compared to modeled rates on a millennial scale (5 mm/y).

Haslett et al. (1998) used ^{14}C dating of basal peat, heavy metal deposits, and biostratigraphy to calculate a rate of sediment compaction. Haslett et al.'s (1998) methods for collecting samples included an Eijkelkamp gouge auger (Russian peat corer), followed by drilling a number of boreholes using an unspecified method to reach the base of the basal peat layer. The total compaction within the basal peat layer was 2.2 m, with the amount of compaction that occurred at the near surface (<1 m depth) being estimated.

Compaction reduced the original thickness of the basal peat by up to 47% with a calculated rate of 0.12 cm/y over a +3000 timescale.

CHAPTER III

METHODOLOGY

Study Area

The PRM is located east of Slidell, Louisiana, in the terraced, lower Pearl River valley. It is dominated at the surface by sediments with organic-rich silts, variable amounts of plant material, and high water contents. Other sedimentary facies common in the shallow stratigraphy of the study area include sandbars, natural levees, crevasse splays, and bay muds.

The Holocene and Pleistocene deposits of this region are underlain by approximately 10 to 15 km of Upper Cretaceous through Upper Tertiary deposits (Galloway, 2001; McBride, 1998). Most Cenozoic sediments of the northern Gulf of Mexico were deposited during Miocene depositional phases that took place within a range of deltaic and shelf environments (Galloway, 2001; McGookey, 1975).

At the last Quaternary glacial maximum (18,000 y BP), sea level within the Gulf of Mexico was approximately 120 m below present-day elevation due to the large volumes of water bound as ice sheets (Fairbanks, 1989; Fisk & McFarlan, 1955; Flint, 1963). In response to the marine regression that preceded the marine low stand, the Pearl River extended out onto and incised into the continental shelf, intersecting the shelf edge (~120 m isobath) approximately 145 km south of the river's present deltaic depocenter (Frazier, 1974; Kindinger, Balson, & Flocks, 1994). Extension of the river to the shelf edge led to the creation of a shelf margin delta, comprised of sediment derived from the Pearl River drainage basin and continental shelf sediment excavated and mobilized as river extension and incision proceeded (Frazier, 1974; Greene, Rodriguez, & Anderson,

2007). Stratigraphic data presented by Frazier (1974) indicate that the Pearl River incised to a depth of ~75 m below present-day sea level, and its deposits consist of approximately 8 m of silty sands and silty clays that represent delta front deposits, interpreted on the basis of stratigraphic position and facies composition (Frazier 1974; Li, 1994). These delta front deposits were a result of deltaic progradation once the Pearl River system reached equilibrium. As marine transgression began following the late Wisconsin sea level low stand, the Pearl River system retreated northward and valley infilling took place.

It has been suggested that the Pearl River responded in a manner similar to other major Gulf Coast river systems during the late Quaternary (Frazier, 1974; Saucier, 1994). During transgression (~18,000 to 3,000 y BP), the river underwent depositional and geomorphological changes that included a landward shift in deltaic position and evolution from a braided to a meandering system as base level rose and the downstream gradient decreased (Schumm, Dumont, & Holbrook, 2000). Rising water levels in the Gulf of Mexico eventually outpaced the rate of vertical accretion of the lower Pearl River valley, and, much like the Mississippi River, estuarine environments in the form of back-stepping bayhead delta deposits were created in the absence of a deltaic plain (Catuneanu, 2003). The formation of estuarine and bayhead delta environments within the lower river valley also were associated with the deposition of widespread back-swamp facies in portions of the river adjacent to the coastal zone. Beginning ~6,000 years BP, the rate of sea level rise in the Gulf of Mexico began to decrease (Saucier & Snead, 1989), which allowed the Pearl River to evolve from a drowned estuarine

environment to one that once again enabled deltaic progradation (Hanson, 2000; Otvos, 2005; Otvos & Giardino, 2004)

The Pearl River entered into its current depositional framework beginning ~2,000 years BP when the Mississippi River avulsed and abandoned the St. Bernard delta complex (Kindinger, 1998; Saucier & Snead, 1989). The study area (see Figure 2) encompasses a small portion of the PRM, which currently covers 22,000 contiguous acres and is incised into the Hammond alloformation (Heinrich, 2006).

Source: Google Earth (2010)

Figure 2. Part of the Pearl River marsh. The Pearl River is a bifurcated river system that has one major channel (West Pearl River) and several smaller channels.

Quaternary deposits blanket the entire river basin and exist as stream terraces and alluvial valley fill. Underlying Miocene and Pliocene age deposits are generally laminated and consist of varying thicknesses of alternating sands and clays (Frazier, 1974). The Miocene and Pliocene deposits are virtually identical lithologically and

together form a gulfward thickening wedge of sand, silt, and clay beds, thousands of feet thick at the southern limit (Otvos, 2005; Saucier & Snead, 1989).

There are five general vegetative settings commonly found in the marshes of southern Louisiana: bottom-land hardwood forest, cypress-tupelo forest, scrub, fresh-water marsh, and salt-water marsh (White, 1983). The scrub setting is transitional between tree- and herb-dominated environments, so it contains plants found in both areas. Plant species found at this study site varied in density and diversity with changes in elevation and distance from the river. The greatest density of plants along this transect was found in the marsh interiors on both sides of the river, with densities averaging 100% coverage (PR_01_08, PR_06_08). The northern most station, PR_01_08, stands out as a high elevation location, with many trees, high marsh, and upland species in the area. Species richness was the highest in this location, with 14 species noted. Still, this area was dominated by *Spartina patens*, while the many other species were mixed in at lower densities. Station PR_02_08 was also dominated by *Spartina patens* mixed with lower densities of *Sagittaria latifolia, Baccharis halimifolia,* and *Iva frutescens*. Station PR_03_08 was dominated by *Panicum virgatum*, with lower densities of *Juncus roemarianus* and *Cuscuta granovii* comprising the other plant species. There is a contrast between the species on the two sides of the river, with coverage at PR_03_08 dominated by *Panicum virgatum* and coverage at PR_04_08 dominated by *Phragmites australis*. Station PR_04_08 is the first station on the southern bank of the West Middle Pearl River and is located on the downward marsh facing flank of the natural levee. The dominant plant species at PR_04_08 was *Phragmites australis* with lower densities of *Typha spp*., *Juncus roemarianus, Panicum virgatum, Iva frutescens,* and *Baccharis halimifolia*.

Station PR_05_08 in the marsh interior near the natural levee was dominated by *Spartina patens* with lower densities of species including *Calystegia sepium* and *Panicum virgatum,* and minor coverage by *Aster subulatus* and *Setaria geniculata.* The most southern station PR_06_08 far into the marsh interior was dominated by *Spartina patens* intermixed with lower densities of *Juncus roemarianus* and minor coverage of *Cuscuta granovii* (R. Feagin, personal communication, March, 15, 2011).

Pearl River is one of several major river systems draining the Tertiary and Quaternary age coastal plains east of the Mississippi River (Snowden & Forsthoff, 1976). Pearl River splits into three discrete channels in its lower valley, the East, West, and Middle Pearl Rivers, with the West Pearl River carrying the most water. Pearl River is an example of a wave dominated, drowned river valley (Dalrymple, Zaitlin, & Boyd, 1992) with a bay head delta draining into Lake Borgne (East Pearl River), Little Lake (Middle Pearl River), and the Rigolets (West Pearl River).

Sample Collection

The sampling transect crosses the West Middle Pearl River along a linear reach of the river (see Figure 3) south of Highway 90. This reach is thought to be located within the surface expression of an active growth fault, which strikes approximately east-west through the PRM (K. Yeager, personal communication, October 10, 2011).

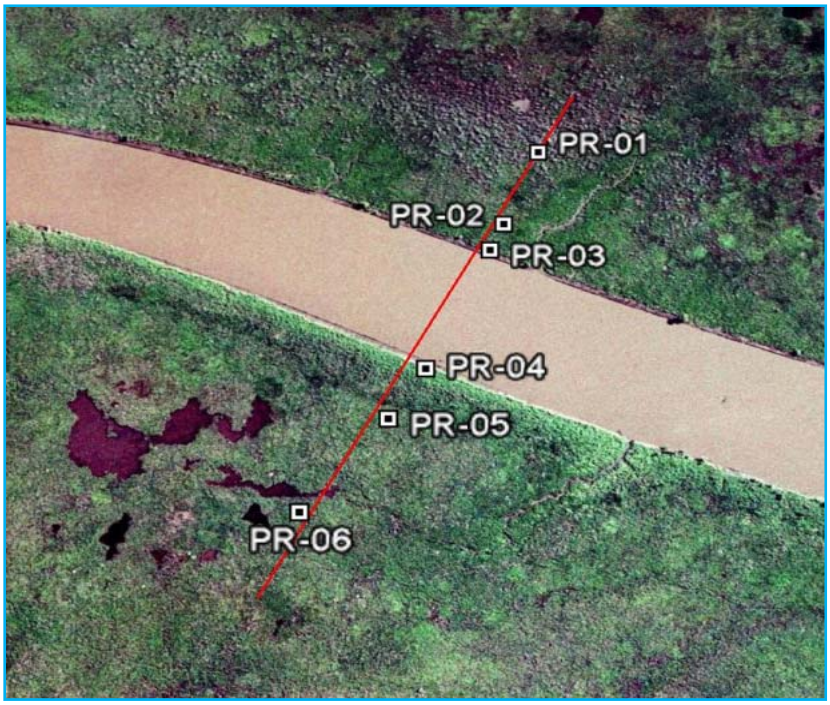

Figure 3. Transect of coring stations in the PRM. The transect bisects the West Middle Pearl River with three stations located on the northern bank and three stations located on the southern bank. Sediment core samples were collected from each station using a wedge corer, Russian peat corer, and a vibra-corer, with the wedge and peat core samples producing the data for this study.

Wedge Corer

Collection of unshortened (not artificially compacted) and undisturbed sediment from the six locations was a very high priority. When attempting to measure bulk physical properties of sediments, artifact compaction common to many traditional coring devices (vibra-corer or piston corer) becomes a problem (Morton & White, 1997).

The wedge corer is an improvement over existing box coring devices, because it eliminates the need to dig the coring device out of the sediment (van Asselen et al., 2009). This sampling method reduces the amount of area at the sampling site that is disturbed, allowing for other cores to be collected in close proximity. The basic design of the wedge corer has four components: a back plate, the plate cover, and two side panels,

all constructed of 0.125 inch thick stainless steel (Inglett, Vollier Roychoudhury, & van Cappellen, 2004). The main body of the wedge corer is formed by the two side plates and back plate. Along the inside edge of the two side plates are machined grooves just wider than the front plate, allowing the front plate to slide into the wedge without becoming dislodged during extraction (Inglett et al., 2004). To assist with entry into the sediment and cut through plant roots, the insertion edges are all sharpened, which also reduces the possibility of dragging material down core. The wedge corer is pushed into the substrate with the sharpened steel edge cutting through the root mat to refusal or until it is fully inserted into the substrate. The face plate is then inserted, which cleaves and compartmentalizes a wedge-shaped block of sediment, thus minimizing sediment compaction and allowing non-destructive removal of the core sample (Inglett et al., 2004). The large, cross-sectional surface area of the wedge corer allows for rapid inspection of near surface sediments for bioturbation, facies changes, and also eases sub-sampling. A disadvantage of the wedge corer is the limited depth of penetration, which is ~1 m in soft sediments.

Russian Peat Corer

The Russian peat corer is a side gouge-auger that introduces little to no vertical sediment compaction but does introduce some lateral sediment compaction. Each sampled interval (50 cm) is completely contained within the sample chamber and protected from the surrounding sediments by a steel door as it is removed from the substrate. This corer has excellent depth of penetration for marsh environments, up to ~6 m. The Russian peat corer works well in soft, loosely consolidated sediments, such as those common in marshes. Its shape allows for easy penetration into the substrate and

easy withdrawal. One drawback of this technique is the small core diameter (5 cm), which allows only a small amount of sample to be collected.

Vibra-Corer

This sampling technique is popular because of its ease of use, excellent depth penetration (5-10^{+} m), and low cost. Conventional vibra-coring of soft, unconsolidated sediments can destroy many fine sedimentary features and commonly alters sediment dry bulk density values. Altering bulk densities will result in a bias in calculated rates of autocompaction when using any technique that relies upon accurate sediment bulk densities to derive autocompaction rates. As the thin core barrel vibrates, the surrounding sediments undergo liquefaction, which allows the core barrel to penetrate. Those sediment grains adjacent to the core barrel can be translated vertically and laterally, thus distorting the lithofacies and expelling water from the sediments.

Visual and Physical Analysis

All cores were immediately transported to the laboratory to be photographed under natural light and visually described for structure, color, and texture. Descriptions were completed immediately after the cores were exposed to air in order to minimize color changes due to the oxidation of anoxic sediments. The Munsell color guide was used to assign colors throughout the length of all cores collected, and the Kent State University texture/fabric guidelines were used as indicators of bulk facies changes down core.

Cores collected at each station were immediately sub-sampled for bulk density after description at 2 cm intervals with a calibrated syringe (10 cm^3). Where bulk facies changes were encountered, the centimeter above and below were also sampled. Each

bulk density plug was then placed into a pre-weighed tin and weighed wet, oven dried for at least 48 hours at 70°C, and weighed immediately upon removal from the oven. From the dry bulk density, porosity, grain density, water content, volume of solids, volume of pore water, and volume of salt when dry was calculated.

The cores were then sectioned for further physical and chemical analyses. Vibra-cores were next sectioned at 2-cm intervals, and samples were weighed wet in a pre-weighed tin. From this 2 cm section, a small portion of sediment was retained for wet archival and held in cold storage; the remainder of the sample was desiccated at 70°C for 48 hours or until dry. Once dry, these samples were removed from the oven, weighed, and then divided into three aliquots. One aliquot was used for grain size analysis, one was processed for radiochemistry and elemental analysis, and one was retained for archive purposes after desiccation. Upon further review of the data, the material from the vibra-core was used only for gross stratigraphic interpretations.

The wedge cores were sectioned at 1 cm intervals from 1-70 cm and then at 2 cm intervals from 70 cm to the end of each core. From each section, a 4-ounce vial of sediment was removed to be archived in cold storage, with the remainder being desiccated at 70°C for 48 hours or until dry. Once dry, these samples were removed from the oven, weighed, and then divided into four aliquots. One aliquot was used for grain size analysis, one processed for radiochemistry and elemental analysis, and one retained for archive purposes.

Peat cores were sampled only for bulk density values and described for lithostratigraphy. After the collection of bulk density samples from each 2-cm section, the small diameter of the peat core sample (5 cm) inhibited further sample collection.

Radiochemical Analysis

Radiochemistry is an important tool for sedimentation, erosion, sediment mixing, and chronology studies on land and in oceans (Appleby & Oldfield, 1978; Appleby, Richardson, & Nolan, 1991; Goldberg, 1963; Oldfield et al., 1979; Olid et al., 2008; Pennington, Cambray, Eakins, & Harkness, 1976). The isotopic markers used for sediment mixing and sedimentation rates (^{7}Be, ^{137}Cs, ^{210}Pb) are found throughout the PRM with well-established dating procedure documented for each isotope (Santschi, Li, Bell, Trier, & Kawtaluk, 1980; Yeager, Santschi, Phillips, & Herberet, 2005; Yeager et al., 2007; Yeager, Santschi, & Rowe, 2004; Yeager, Santschi, Schindler, Andres, & Weaver, 2006). Isotopic markers allow sediments to be dated with high levels of accuracy providing the ability to calculate shallow mixing rates (^{7}Be) and average rates of sedimentation over short (~45 y BP) and medium (~120 y BP) periods of time.

Beryllium-7 ($t_{1/2}$ = 53d, Eγ = 477 keV) and Cesium-137 ($t_{1/2}$ = 30.07, Eγ = 661 keV) were measured using high resolution gamma spectrometry with Camberra HPGe well detectors and multi-channel analyzers (model DSA 1000). Samples were contained in plastic test tubes (inner diameter 1.3 cm, height 9.4 cm), and standards (^{137}Cs and ^{226}Ra: NIST, SRM #4357; ^{7}Be: Isotope Products Laboratory CN #6007) were prepared and run on each detector in geometries identical to those for sediment samples to determine representative efficiencies. Efficiency errors based on standards were less than ± 2%, and samples were counted, on average, for 3 to 4 days to reach a standard deviation for all isotopes on the order of 3% to 5%. All activities were decay-corrected to the date of collection. Cesium-137 found in sediments is the result of fallout from above-ground, nuclear weapons testing, which began in the early 1950s and peaked in

1963 and 1964 (Bird et al., 2004). The Cesium-137 method is attractive based on the low cost of sample preparation and quality of age resolution. The sub-surface peak of ^{137}Cs activity is used to calculate sediment accumulation rates and establish chronological control of near-surface sediments (Williams, 2003). Equation 1 illustrates the method used to calculate the sedimentation rate

$$S = (D_{pk}/t) \quad (1)$$

where S is equal to the sediment accumulation rate (in either cm y^{-1} or g cm^{-2} y^{-1}), t is the time since 1963 (y), and D_{pk} is the depth (cm) or mass depth (g cm^{-2}) of the maximum ^{137}Cs peak.

Lead-210 ($t_{1/2}$ = 22.3 y) is part of the ^{238}U decay series (see Figure 4) and is naturally and continuously produced by the decay of ^{222}Rn, which is a noble gas that is supplied to the atmosphere directly from surface soils and sediments. Atmospheric ^{210}Pb is supplied to Earth's surface by wet and dry deposition (Olid et al., 2008), and its particle-reactive nature makes it an ideal dating tool for sediments within water bodies and on dry land. The use of ^{210}Pb for dating sediments was first proposed by Goldberg (1963) and then successfully applied to peat deposits by El-Daoushy, Tolonen, & Rosenberg (1982) and Oldfield et al. (1979). The period during which ^{210}Pb can be used for dating sediments is about the last 100 years (Orson, Warren, & Niering, 1998; Turner et al., 2006). The continuous, atmospheric deposition of ^{210}Pb, combined with its half life (22 y), allows for deeper chronological control to be achieved than by using ^{137}Cs alone. Also, ^{210}Pb is able to delineate the depth of relatively long-term, near-surface sediment mixing over its temporal range.

	^{238}U Series						
U	^{238}U 4.51x 10^{9}y		^{234}U 2.48x 10^{5}y				
Pa	↓	^{234}Pa 1.18m ↗	↓				
Th	^{234}Th 24.1d ↗		^{230}Th 7.52x 10^{4}y				
Ac			↓				
Ra			^{226}Ra 1601y				
Fr			↓				
Rn			^{222}Rn 3.825d				
At			↓				
Po			^{218}Po 3.05m		^{214}Po 1.6x 10^{-4}s		^{210}Po 138.4d
Bi			↓	^{214}Bi 19.7m ↗	↓	^{210}Bi 5.0d ↗	↓
Pb			^{214}Pb 26.8m ↗		^{210}Pb 21.4y ↗		^{206}Pb stable

Figure 4. Decay series for ^{238}U, y = years, d = days, m = minutes and s = seconds (modified from Kendall & McDonnell, 1998).

Alpha spectrometry was used to resolve ^{210}Pb via a ^{209}Po tracer (Isotope Products Laboratory, #6209-100N), assuming equilibrium between ^{210}Pb and ^{210}Po. Measurements of ^{209}Po and ^{210}Po were made using a Canberra alpha spectrometer (Model 7200) and a Canberra integrated multi-channel analyzer. Lead-210 samples were spiked with the ^{209}Po tracer and then completely digested in a mixture of strong acids (HCl, HNO_3, HF). Ascorbic acid then was added to bind with Fe(III), and a Ag disk was added to the sample

under low heat to provide a suitable surface for the spontaneous deposition of the Polonium isotopes (Santschi et al., 1999; Yeager et al., 2004). The total activity of ^{210}Pb in sediment is comprised of supported ^{210}Pb (resulting from the decay of *in situ* ^{226}Ra) and unsupported or 'excess' ^{210}Pb ($^{210}Pb_{xs}$), which is supplied by atmospheric deposition and used for the determination of sediment chronology and sedimentation rates. To model the data, the constant flux constant supply (CF-CS) model was used. The CF-CS model of ^{210}Pb delivery to the sediment assumes that there is a constant flux of $^{210}Pb_{xs}$ from the atmosphere to the sediment through wet and dry fallout (Appleby & Oldfield, 1978; Oldfield et. al., 1979; Oldfield & Appleby, 1984; Robbins, 1978). This flux rate is independent of any changes in sedimentation rates. In the CF-CS model, the cumulative, $^{210}Pb_{xs}$ activity (A) below the sediment age *t* is given by

$$A = A_{(0)}e^{-\lambda t} \quad (2)$$

where $A_{(0)}$ is the total unsupported activity and λ is the ^{210}Pb decay constant (0.031 y^{-1}). The sediment age at depth x is given by

$$t = 1/\lambda \ln (A_{(0)} / A) \quad (3)$$

where A is the total $^{210}Pb_{xs}$ activity in the sediment column beneath depth (x), $A_{(0)}$ is the total $^{210}Pb_{xs}$ activity in the sediment column, and *t* = time (y), (Allen, Rae, Longworth, Haster, & Ivanovich, 1993). When ^{210}Pb is delivered to Earth's surface by atmospheric deposition, it quickly adsorbs onto particles (Owens & Walling, 1996; Wallbrink & Murray, 1996), which then have an excess amount of ^{210}Pb. Once communication with the atmosphere has been severed by burial, the unsupported or "excess" ^{210}Pb will begin to diminish as a function of radioactive decay, working its way toward secular

equilibrium. After ~100-120 years, all of the excess ^{210}Pb is gone, and ^{210}Pb activity concentrations will reach steady state.

Analysis of Particulate Organic Carbon

Elemental carbon analysis of the sediments collected from the wedge core provides a high resolution profile of the particulate organic carbon content. The pre-treatment of the sediment requires that all inorganic carbon (carbonate) be removed from the sample by HCl vaporization (Harris, Horwath, & Van Kessel, 2001; Hedges & Stern, 1984). An aliquot of dry sediment (~0.02 to 0.10 g) was placed into a silver capsule, weighed, and then enclosed in a sealed desiccator for 24 hours with 100 ml of concentrated HCl acid. Once the acid vaporization was complete, the samples were dried at 70 ºC for 24 hours. After drying, the samples were crushed inside of a larger tin capsule and stored in a desiccator until analysis.

Using a Costech ECS 4010 CHN/OS combustion analyzer, sedimentary POC content was directly measured from the wedge core sediments. This instrument is controlled by a microprocessor that uses flash combustion/chromatographic separation and multi-detector techniques to isolate and identify the percentage of carbon found in the sediment.

Autocompaction Modeling

To calculate shallow autocompaction of PRM sediments, a backwards model developed by Williams (2003) was chosen. The Williams (2003) study was conducted in Trinity Bay, Texas, which contains similar plant species (*Spartina* spp.*)*, is also microtidal, oligohaline to brackish, and has similar sediments (dominantly silt-size

sediments). Most importantly, this model allows for the calculation of autocompaction rates over a decadal time scale.

The Williams (2003) model makes several assumptions about the rates of sedimentation, how sediment compacts over time, and the relationship between bulk density and layer thickness. It is important to understand these assumptions and the limits that they place on the model. The assumptions are as follows:

1. Sedimentation produces an average annual layer of sediment with uniform initial composition, thickness (T), and dry bulk density (B). The surface sediment layer (T_1) is assumed to be uncompacted.
2. As each sediment layer is buried under successive annual layers, it compacts at an exponentially declining rate until a finite limit to compaction is reached at depth (D_n). The thickness of a completely compacted sediment layer is T_n.
3. Dry bulk density is inversely proportional to sediment layer thickness. As a layer compacts and its thickness decreases, dry bulk density will increase up to a finite limit and then remain constant. The dry bulk density of a completely compacted sediment layer is B_n. The thickness of any layer "a" can be calculated as

$$T_a = B_1/B_a \cdot T_1 \quad (4)$$

4. Each annual sediment layer of thickness T_1 is ultimately compacted to a thickness of T_n; therefore, the average annual autocompaction (C) must be

$$C = T_1 - T_n \quad (5)$$

and the annual surface elevation change (δ_e) must be

$$\delta_e = T_n. \quad (6)$$

5. If the depth to the 1963 ^{137}Cs peak (D_P) is known, then the average thickness of sediment layers 1 - p equals D_p/p (depth/number of annual layers). The dry bulk density of layer p is B_p. The thickness of layer p is $(B_1/B_p)(T_1)$. The average dry bulk density of layers 1 - p is $B_{av1\text{-}p}$ was determined using those values between the year one and 1963 and 1964 ^{137}Cs-defined horizons (D_{pk}).
6. Because dry bulk density is inversely proportional to sediment layer thickness, it is assumed that the average dry bulk density ($B_{av1\text{-}p}$) coincides with the average layer thickness (D_p/p). From (3) above it follows that

$$(B_1/B_{av1\text{-}p}) * (T_1) = D_p/p \text{ or} \quad (7)$$

$$T_1 = (D_p/p)/(B_1/B_{av1\text{-}p}). \quad (8)$$

This same method can be used to determine the amount of autocompaction of any layer below the 1963 and 1964 ^{137}Cs peak, if there is chronological control.

Modeling autocompaction within the ^{137}Cs sedimentary unit in the PRM required a modification to the Williams (2003) model. The upper 10-15 cm of sediment in the PRM shows evidence of substantial mixing from Hurricane Katrina in 2005. This heavy mixing in the ^{137}Cs sedimentary unit requires that the base of the mixed layer now become year one. The Williams (2003) study did not remove the bioturbated mix layer before calculating autocompaction rates, because the surface sediment bulk density values were less than those found at the 1963 and 1964 ^{137}Cs peak. However, the nature of bioturbators is to mix the surface sediments with the deeper sediments and vice versa. This mixing leads to a translocation of the isotopes associated with a specific time of deposition for each individual grain. The depth to which the bioturbation occurs is a function of marsh elevation (high, middle, or low marsh) and the type of flora and fauna

indigenous to the marsh (Hippensteel et al., 2002). The study area's elevation is important to consider because previous studies have determined that bioturbation and mix layer thickness are both greater at low marsh elevations than in the high marsh elevations (Hippensteel, Martin, Nikitina, & Pizzuto, 2002). Consequently, it is hypothesized that sedimentary layers would remain relatively intact in the high marsh as compared to the low marsh (Leorri, Martin, & Horton, 2009). Provided that the bulk density rates follow the assumptions set forth by the Williams (2003) model, there would not be a reason to remove this bioturbated mixed layer from the equation. An example of the equation used to determine D_P is shown below:

$$D_P = D_{pk} - D_{mix\ zone} = 27.5\ cm - 16.5\ cm;\ D_P = 11\ cm \quad (9)$$

where $D_{mix\ zone}$ is determined using sedimentary property data.

To calculate autocompaction rates for the underlying $^{210}Pb_{xs}$ sedimentary unit, the variables D_n and B_n remain the same as in the calculation for the ^{137}Cs layer. Now the peak of the ^{137}Cs layer becomes "year one" (B_1), and the depth that falls closest to the 100-year datum is used as the ending point (D_p).

Statistical and Graphical Analysis

The first step in statistical analysis of the sedimentary property data (POC, bulk density, porosity, d.50, and water content) is to determine if the data are normally distributed around a mean value. The normality of the data will dictate if parametric (normally distributed data around a mean with equal variance) or non-parametric (non-normally distributed data) statistics are needed (Zar, 1984). Normality was first assessed quickly with graphical histograms and then more rigorously evaluated with the

Kolmogorov-Smirnov (K-S) test of normality. The K-S test is a non-parametric test for the equality of two independent variables and is more rigorous than visual examination.

The non-parametric Mann-Whitney (M-W) statistical test is a measure of significant change in two independent, non-parametric data sets. The M-W test only requires that the data be both ordinal, independent of each other, and make no assumption about the distribution of the data. This test is an alternative to the independent group t test, when the assumption of normality or variance is not met. M-W uses ranks of the data rather than their raw values to calculate the statistic. However, since this test does not make a distribution assumption, it is not as powerful as the *t* test. The results of the M-W test are tempered by a Bonferroni corrected alpha, limiting the chance of Type 1 errors.

Isolating and identifying driving mechanisms of autocompaction were accomplished using Spearman rank correlations and linear regression. Spearman's rank is a nonparametric (distribution-free) rank statistic measuring the strength of the association between two variables (Lehmann & D'Abrera, 1998). The Spearman correlation assigns a value to the relationship between -1 and 1; the closer the value to one, the stronger the relationship between the two parameters. Correlations that fall between 1 to 0.5 or -0.5 to -1 are deemed strong statistical relationships, whereas coefficients between 0.49 and -0.49, which have a *p* value > .05, are deemed insignificant (Zar, 1984). Using SigmaPlot v. 12, the Spearman rank order correlations between variable medians and depth were determined ($\alpha = 0.05$) for each of the two sedimentary units; the ^{137}Cs sedimentary unit was analyzed separately from the $^{210}Pb_{xs}$ sedimentary unit. As an example, depth was compared to POC, d.50, bulk density, water

content, and porosity to judge the strength of the relationship and to determine the significance of the relationship.

Whisker or box plot graphs were chosen to display the data from the ^{137}Cs sedimentary and ^{210}Pb sedimentary units. The whisker plot is an easily understood way to graphically depict groups of numerical data with the smallest and largest observations being the whiskers (range of data), lower quartile being the base of the box (if orientated vertical), the upper quartile being the top of the box (if orientated vertical), and all outliers are plotted outside the whiskers (Zar, 1984). These graphs display the differences in populations without making any assumptions about the underlying statistical distribution. Whisker plots also display the mean and median values of the data which can indicate the degree of dispersion and skewness of the data.

CHAPTER IV

RESULTS

A complete list of sedimentary properties and tabular data (bulk density, porosity, POC, water content by weight, isotope activities, and elevations) for all cores can be found in Appendix A with the Spearman correlations found in Appendix B.

Stratigraphy of the Pearl River Marsh Transect

The upper sedimentary sections of the PRM (see Figure 5) are dominated by root rich facies, including organic-rich silts and clays, all above subtidal deposits with inter-bedded sand lenses. All cores at the near surface have root rich facies overlying organic-rich silty sediment (see Table 1). These root-rich facies constitute the current marsh surface and have large roots, rush stems, and other relatively intact macro-organic matter. The underlying organic-rich silt is mostly micro-organic matter that has been further degraded by biological, physical, and chemical processes over time. The root rich and organic-rich silt facies extend to a maximum depth of 4.40 m (PR_01_08) and a minimum depth of 0.25 m (PR_04_08) along this transect.

The underlying sedimentary unit is a clay layer that is found in all cores, except PR_02_08 and PR_06_08, between 2 – 4.5 m depth. This clay unit is thin (~ 2 – 6 cm) and has a maximum depth of 6 m at station PR_01_08 and a minimum depth of 2.09 m at station PR_05_08. The deepest stratigraphic unit is a mud with roots facies and is subtidal estuarine or channel deposits based on the foraminiferal assemblage (Yeager et al., 2011). Sand lenses were found only at stations PR_03_08 and PR_04_08, which are both located near the river edge. Similar lithologies were found by Hanson (1999) and Kuykendall (2010) in the PRM.

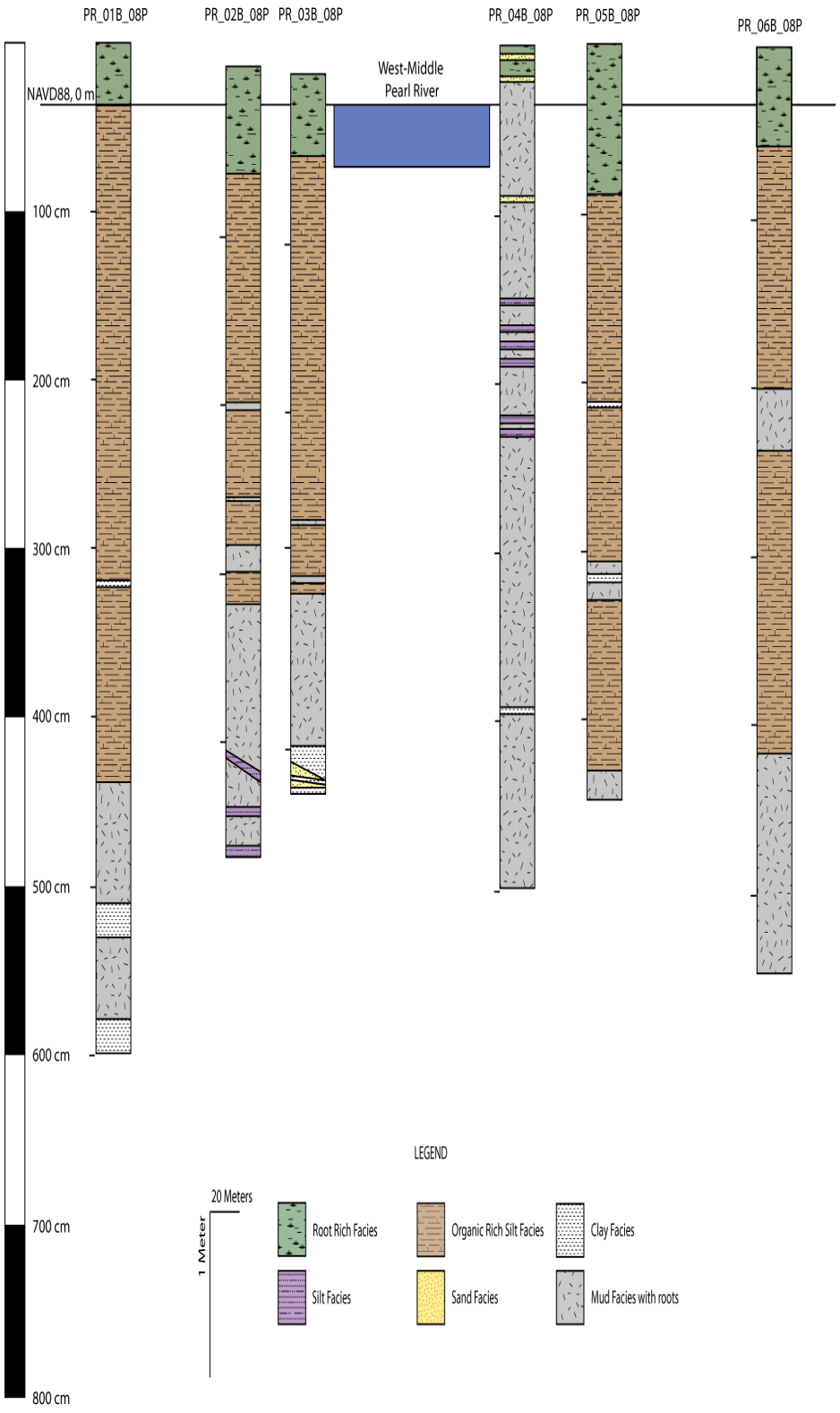

Figure 5. Cross section of the Pearl River marsh transect Peat (P) cores. Cores vertically corrected to the NAVD88 and horizontally corrected to the GPS locations of collection.

Table 1

Major Sedimentary Units and Their Associated Thickness in the PRM Transect

Station	1st Marsh / Organic Rich Silt Facies (cm)	1st Clay Facies (cm)	Organic-Rich Silty Clay (cm)
PR_01_08	0 – 323	323 - 325	440 - 600
PR_02_08	0 – 206	206 - 209	320 - 464
PR_03_08	0 – 267	267 - 269	304 - 409
PR_04_08	0 – 22	376 - 378	23 - 500
PR_05_08	0 – 210	315 - 321	310 - 330; 425 - 450
PR_06_08	0 – 208	Not present	208 - 242; 420 - 450

Base of the Mixed Layer Defined

The surface (first centimeter) bulk density values collected were greater (within the mixed layer) than bulk density values at the ^{137}Cs peak, except for cores PR_04_08W and PR_05_08W (see Appendix A). This violates the autocompaction model assumption that D_b values increase with increasing depth; therefore, it was necessary to remove the mixed layer from the model. When the mixed layer is removed from data set, the base of the mixed layer becomes "layer one." This new layer one is buried under 10-15 cm of sediment and, therefore, has been subjected to some small amount of natural compaction. This natural compaction results in the modeled rates of autocompaction being a minimum rate.

Contributors to the minimum autocompaction rate are the differential rates of large scale compaction in the deeper sediments and small scale compaction in shallow sediments. Below both chronostratigraphic blocks of sediment (^{137}Cs and $^{210}Pb_{xs}$), there is a downward movement of the entire Holocene sequence. This large scale, deeper compaction causes the isotopic markers, used for age control, to be translocated down-section through time. Hence, these isotopic marker horizons have moved down-section

from their original depositional position over time and this movement cannot be corrected in the compaction equation. On a smaller scale, individual grains of sediment, and their associated isotopes, are transported both deeper and shallower within the sediment column through a combination of compaction, bioturbation, and plant root growth (Foote & Reynolds, 1997; Ford & Grace, 1998; McCraith et al., 2003). The isotope ^{137}Cs has a higher affinity to organic carbon as compared to ^{210}Pb (Spencer et al.,2003; Wasserman et al., 2008). Organic carbon is readily moved up and down in the sediment column by bioturbation, making this ^{137}Cs more mobile than ^{210}Pb (McCraith et al., 2003). With the ^{137}Cs isotope having higher affinity for organic carbon and organic carbon is more compressible than inorganic minerals, ^{137}Cs is more likely to be found at a deeper depth than where originally deposited. Anything that might translate the isotopic marker down-section, on a small scale or a large scale, can bias the calculation of autocompaction. The logic and methods employed to define and eliminate this mixed layer are described next.

The mixed layer of the PRM along this transect is defined as the upper ~ 10-15 cm of sediment, which has recently or is currently being modified and reworked through bioturbation or, in the PRM, recently by storm surge (with evidence of Hurricane Katrina in 2005. The uppermost mixed layer in the PRM is actively being turned over, mainly by biological processes, to depths from 2 to < 4 cm (see Figure 6) on a time scale of ~1 year (determined by ^{7}Be $t_{1/2}$ = 53.12 d). This shallow mixing is evident in all wedge cores and is assumed to be ubiquitous in shallow sediments throughout the PRM.

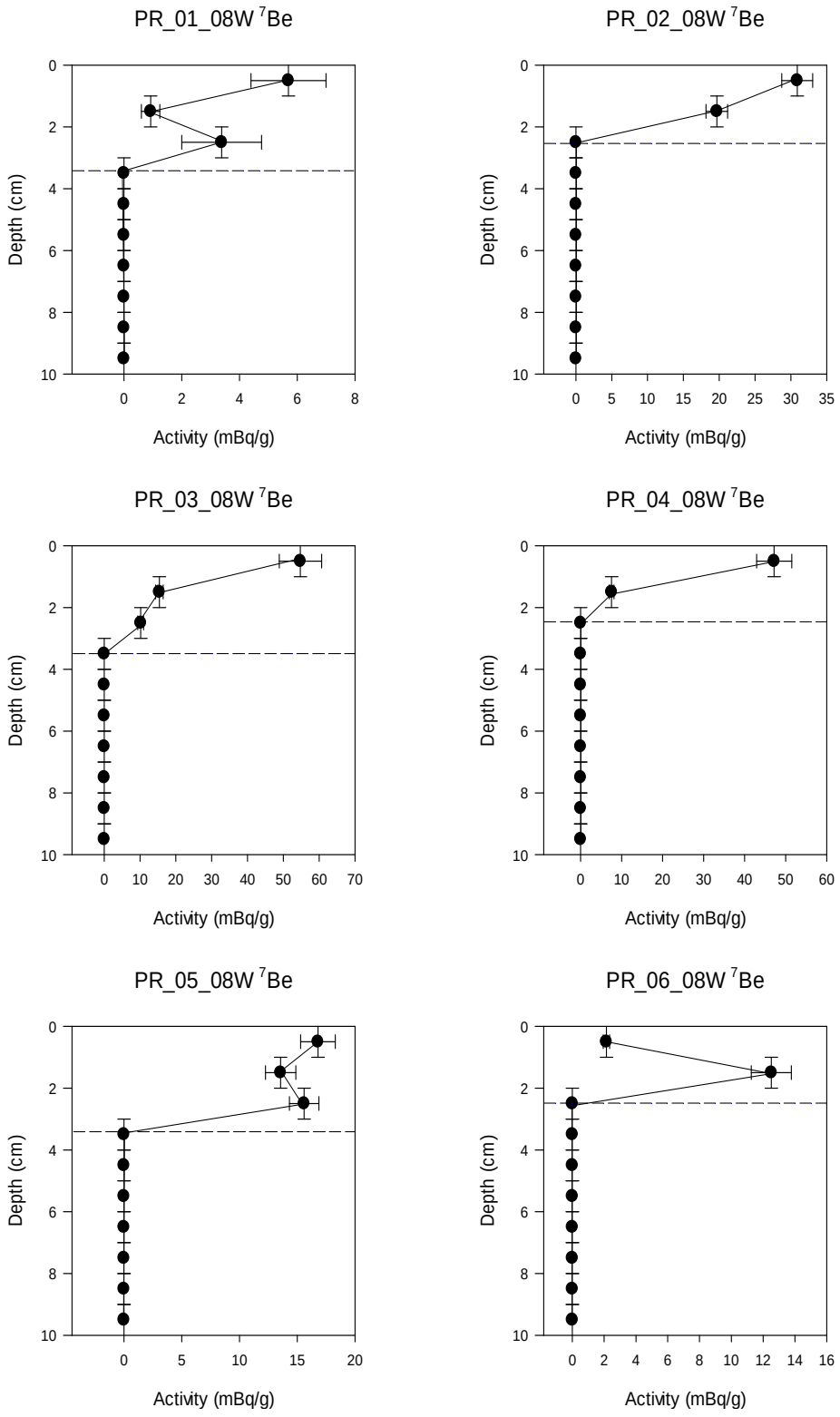

Figure 6. ^{7}Be profiles from PRM wedge cores showing short-term ($\leq$ 1 y), active mixing. Dashed lines denote the base of the short-term mixed layer.

The storm layer from Hurricane Katrina is included as part of the recently mixed layer and is recognized based on two variables: particulate organic carbon (POC) and lead-210. The POC content abruptly changes in concentration in the upper 10-15 cm of all wedge cores. Hurricane Katrina's impact resulted in the removal of the organic-rich marsh surface and the deposition of a less organic-rich storm layer. Figure 7 shows that in all wedge cores, the maximum POC concentrations are not found at the surface, where the carbon source is located, but at depth of 10-15 cm. Reduction in the organic contents of near surface marsh sediments after hurricanes has been seen in the Chenier Plain of southern Louisiana after Hurricane Rita (Faulkner et al., 2006), in the PRM after Hurricane Katrina (McKee & Cherry, 2009), and in Ocean Springs, Mississippi, and Mobile, Alabama, after Hurricanes Katrina and Rita (Horton, Rossi, & Hawkes, 2008). Hence, the base of the mixed layer is considered the base of the storm layer.

The $^{210}Pb_{xs}$ profile is a second proxy used to identify the base of the mixed layer. Profiles of $^{210}Pb_{xs}$ present clear evidence of sediment removal and subsequent deposition caused by Hurricane Katrina in 2005. Evidence of inorganic-rich material deposition post-Katrina is seen in all cores except PR_03_08 and PR_04_08. An ideal $^{210}Pb_{xs}$ profile should exhibit an exponential decrease in activity with increasing depth from the surface until secular equilibrium is reached. Profiles of $^{210}Pb_{xs}$ along the PRM transect show evidence of substantial mixing in the upper ~10-15 cm of all sections. This mixing is evident in the upper profiles where there is clearly much less isotopic activity near the surface when compared to the maximum, except for PR_03_08 and PR_04_08 (see Figure 8). These data, in conjunction with the POC and ^{7}Be data, allowed for the delineation of the mixed layer in all transect cores.

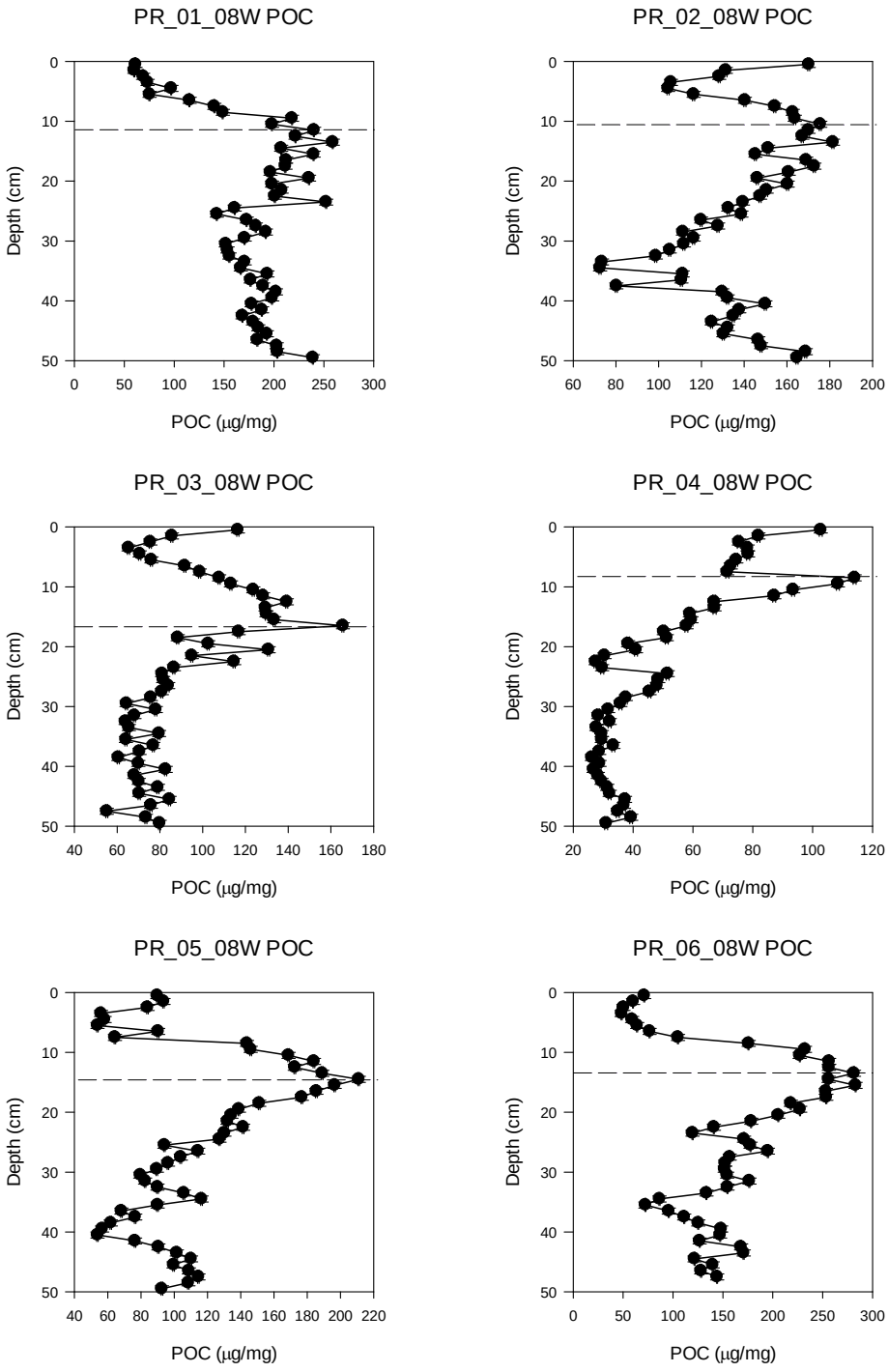

Figure 7. POC profiles from all PRM transect wedge cores with the dashed line representing the base of the mix layer.

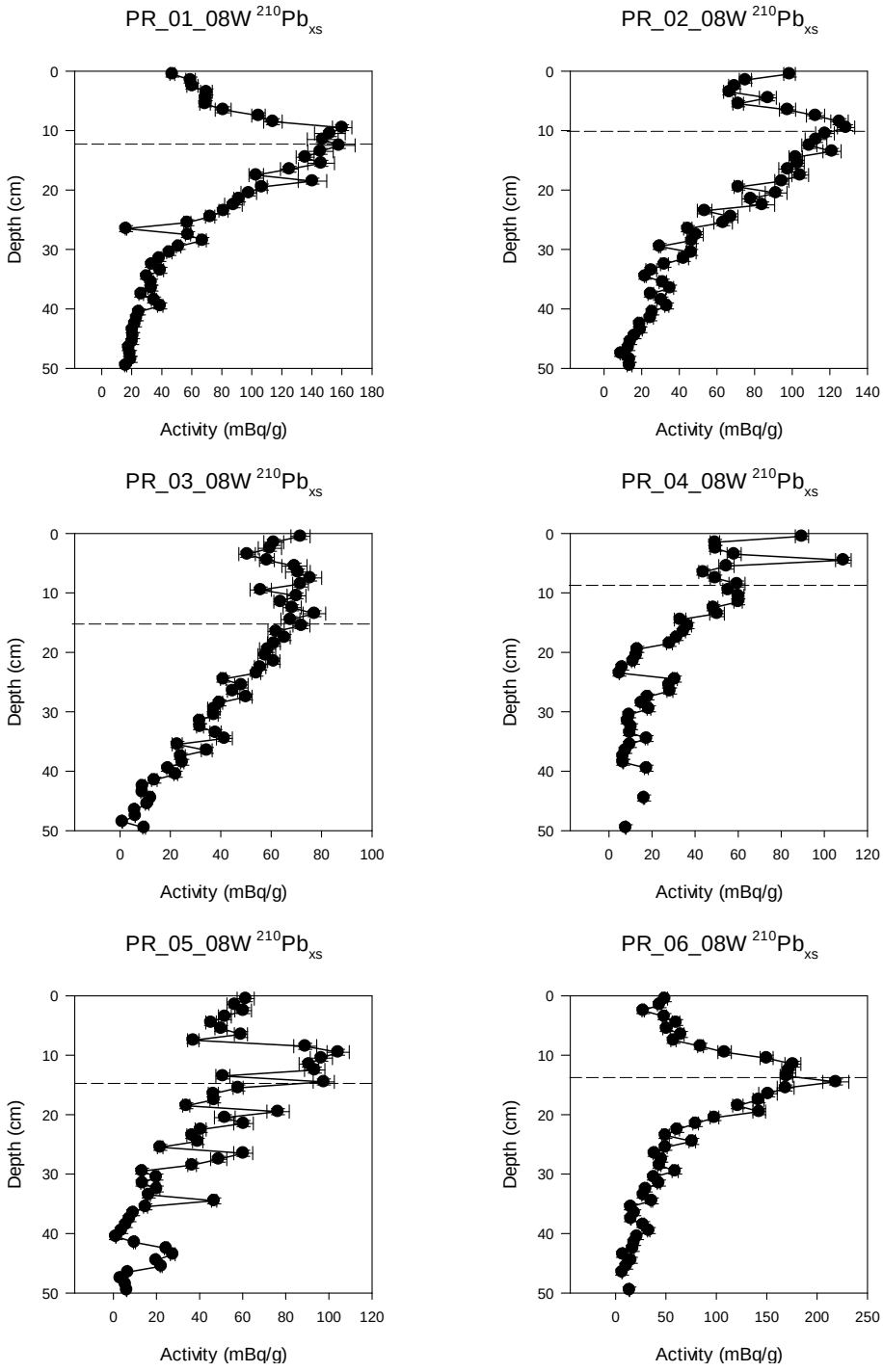

Figure 8. $^{210}Pb_{xs}$ profiles from PRM wedge cores showing activity from the surface to secular equilibrium. Depth from the surface is represented on the Y-axis in centimeters, and the activity of $^{210}Pb_{xs}$ is represented on the X-axis in mBq/g. The dashed line represents the base of the mix layer.

Chronostratigraphic Control

The method used to calculate rates of autocompaction requires strict chronological control. Measurements of the fallout isotopes ^{137}Cs and ^{210}Pb were made for each of the six wedge cores to establish this chronological control. These data were then used to calculate sediment age of corresponding depths at high levels of confidence over the last century. There is strong agreement between the isotopic data at the 1963/1964 Cesium peak and the $^{210}Pb_{xs}$ modeled data, providing confidence in the choice of the CF-CS model used for $^{210}Pb_{xs}$ dating.

Chronostratigraphic Control: ^{137}Cs Sedimentary Unit

The wedge cores show well-defined ^{137}Cs peaks between a minimum depth of 25.5 ± 0.5 cm (PR_03_08W) and a maximum depth of 30.5 ± 0.5 cm (PR_05_08W). In all wedge cores, the ^{137}Cs activity concentrations are significant (non-zero) at the surface and increase down section to an identifiable peak that corresponds to the 1963/1964 maximum in global fallout (see Figure 9).

The ^{137}Cs unit is defined here as the sediment section located between the base of the mixed layer and the maximum peak of ^{137}Cs. This ^{137}Cs sedimentary unit has a maximum thickness of 20 cm (PR_05_08W) and a minimum thickness of 12 cm (PR_01_08W) (see Table 2).

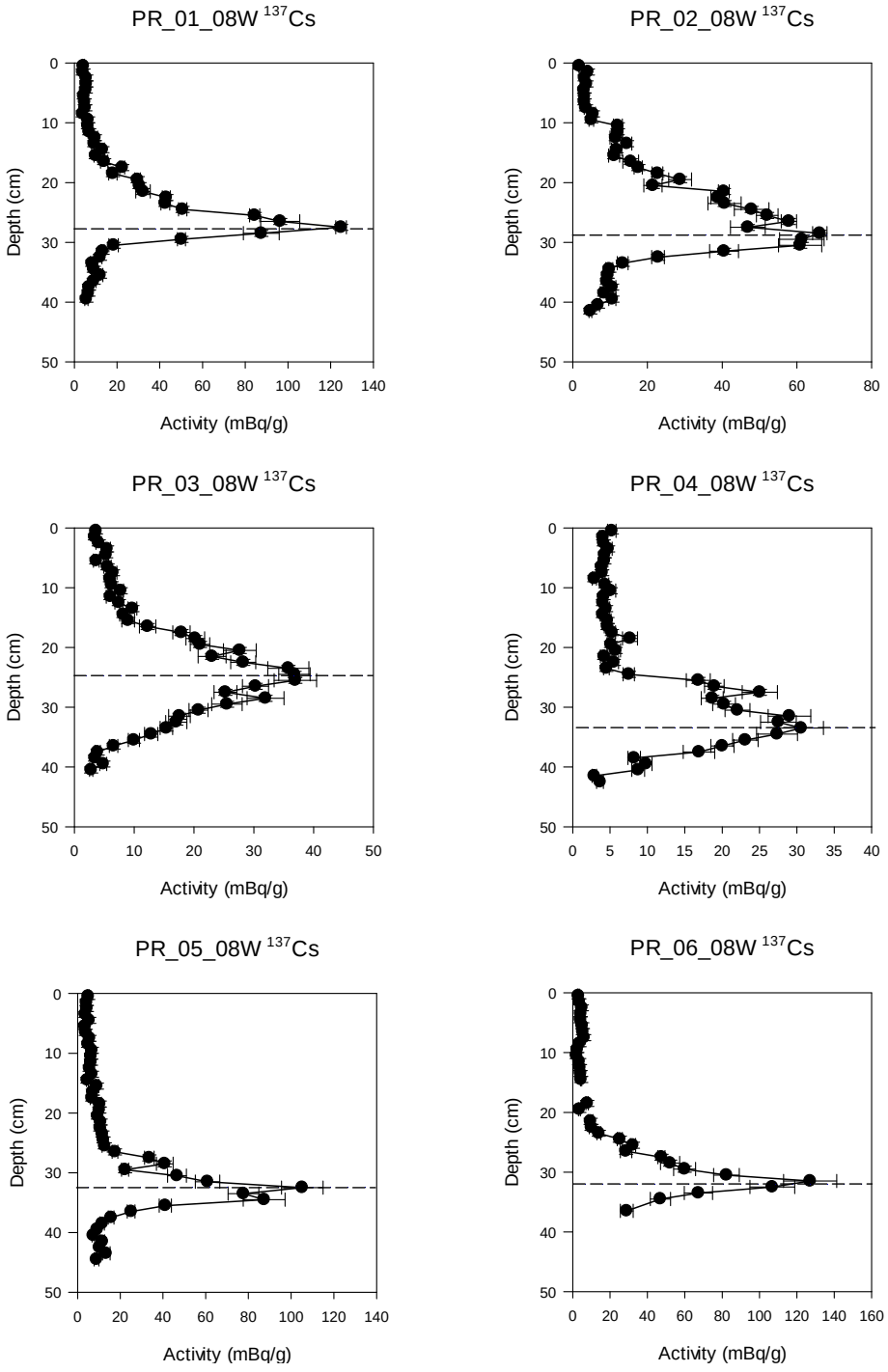

Figure 9. ^{137}Cs profiles from the six stations in the PRM transect. Dashed lines denote depth of the ^{137}Cs peak D_{pk}.

Table 2

Each Station with the Base of the Mixed Layer, the Depth of the ^{137}Cs peaks and $^{201}Pb_{xs}$ Depth and Age About the 100-year Datum for all Cores used to Calculate Average Rates of Autocompaction

Station	Base of the Mix Layer (cm)	^{137}Cs Sediment Age (y)	^{137}Cs Peak Maximum (cm)	$^{210}Pb_{xs}$ Sediment Age (y)	$^{210}Pb_{xs}$ Sediment Depth (cm)
PR_01_08W	15.5 ± 0.5	41.5	27.5 ± 0.5	99.87	42.5 ± 0.5
PR_02_08W	8.5 ± 0.5	41.5	28.5 ± 0.5	97.58	45.5 ± 0.5
PR_03_08W	10.5 ± 0.5	41.5	25.5 ± 0.5	96.04	40.5 ± 0.5
PR_04_08W	10.5 ± 0.5	41.5	27.5 ± 0.5	104.92	44.5 ± 0.5
PR_05_08W	12.5 ± 0.5	41.5	30.5 ± 0.5	118.19	36.5 ± 0.5
PR_06_08W	13.5 ± 0.5	41.5	29.5 ± 0.5	94.87	37.5 ± 0.5

Chronostratigraphic Control: $^{210}Pb_{ex}$ Sedimentary Unit

All transect wedge cores have well-defined $^{210}Pb_{xs}$ profiles that allowed use of the CF-CS model to date sediments beyond the age range of ^{137}Cs. In all cores, a sharp increase in $^{210}Pb_{xs}$ activity concentrations is evident in the upper ~10-15 cm of section, except for PR_03_08W and PR_04_08W, followed by an exponential decrease in activity concentrations until secular equilibrium is reached below 50 cm. The activity concentrations peak between a minimum depth of 4.5 ± 0.5 cm (PR_04_08W) and a maximum depth of 14.5 ± 0.5 cm (PR_06_08W). This peak of maximum activity is assumed to be the boundary between the Hurricane Katrina mixed layer and the undisturbed underlying marsh sediments.

Modeling rates of autocompaction in the ^{210}Pb sedimentary unit requires identifying the top layer and base. The top layer of the ^{210}Pb unit is defined by the maximum activity of the ^{137}Cs fall out isotope, which is tied to the 1963/1964 time horizon. The base ^{210}Pb unit then is constrained with alpha spectrometry giving

chronostratigraphic control between 100 and 150 years after communication with the atmosphere is severed. After 100 and 150 years have expired, the ^{210}Pb isotope reached secular equilibrium, which is where the quantity of ^{210}Pb isotope remains constant because its production rate is equal to its decay rate (Appleby & Oldfield, 1978). Secular equilibrium for $^{210}Pb_{xs}$ is reached after 5 to 7 half-lives ($t_{1/2}$ = 22.3 y) have elapsed or ~110-150 years. To remain within the limits of the ^{210}Pb dating methods, the sediment layer with the age closest to 100 years was picked as the base of the ^{210}Pb unit. Picking the ~100 year datum across all six cores removed the possibility of increased burial time having a greater affect on the calculated rates of autocompaction. For all six wedge cores, ^{210}Pb reached secular equilibrium at depths from 36 to 45 cm below the surface, with corresponding ages greater than 96 years.

Whisker Plots of Sedimentary Properties

Representing the sedimentary property data graphically with whisker plots gives a generalized representation of variability across the transect. The whiskers on the graph represent the range of the data, with outliers being the points outside the whiskers. The base of the box is the 25th percentile, and the top of the box representing the 75th percentile of the data. Red lines within the box are the median values, and the black lines are the mean value for the data set.

The POC whisker plots show a general increase in the concentration of particulate organic carbon in the sediment, with increased distance from the river (PR03 and PR04 located closest to the river edge) (see Figure 10).

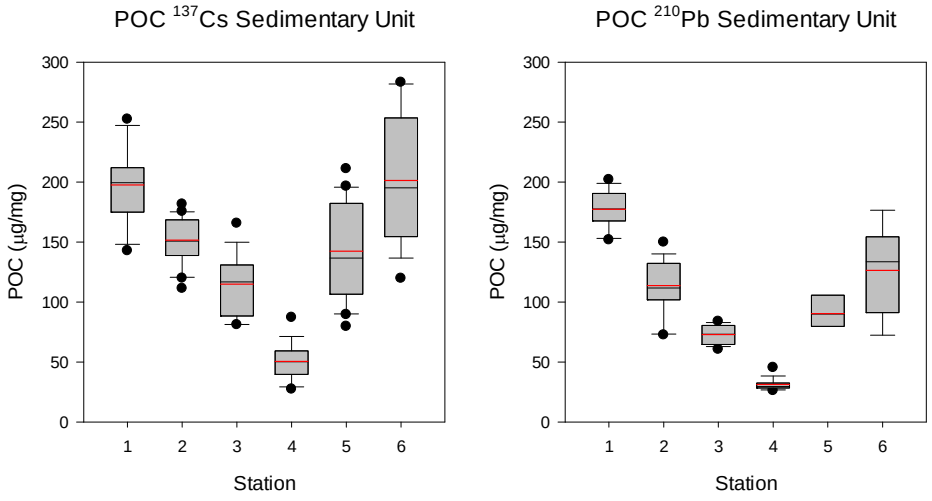

Figure 10. Whisker plots for POC in the ^{137}Cs and ^{210}Pb sedimentary units.

It appears that both sedimentary units share similar trends in the distribution of the bulk density median values and ranges. Bulk density values appear highest at stations PR03 and PR04 and lowest at stations PR02 and PR06 in both sedimentary units (see Figure 11). In the upper sedimentary unit, station PR04 has the greatest range of variability and largest median d.50 value, whereas station PR06 appears to have the lowest range of variability and the lowest median d.50 value.

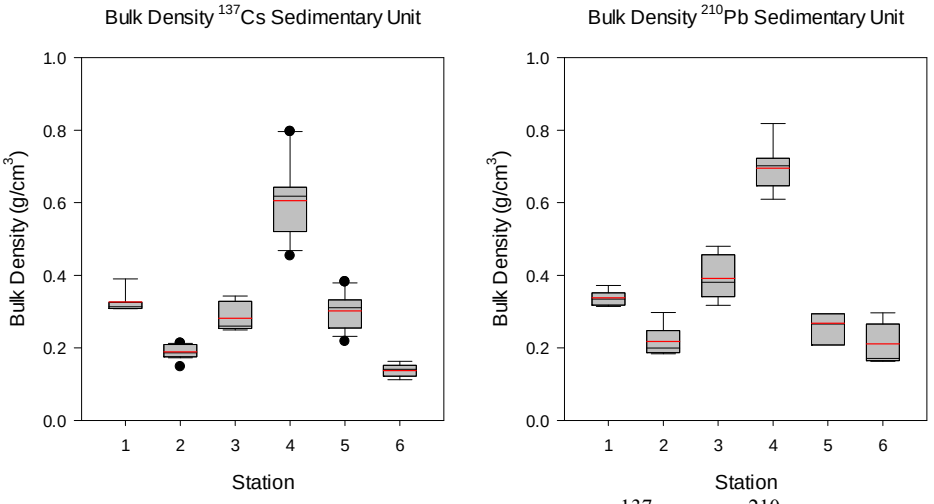

Figure 11. Whisker plots for bulk density in the ^{137}Cs and ^{210}Pb sedimentary units.

The general trend of porosity appears to increase riverward for stations PR01, PR02, and PR03 and then increase toward the marsh interior for stations PR04, PR05, and PR06 (see Figure 12). In both sedimentary units, station PR01 has the lowest median porosity, and station PR06 has the highest median porosity. A significant difference is not apparent in the visual examination of the whisker plots for the porosity property.

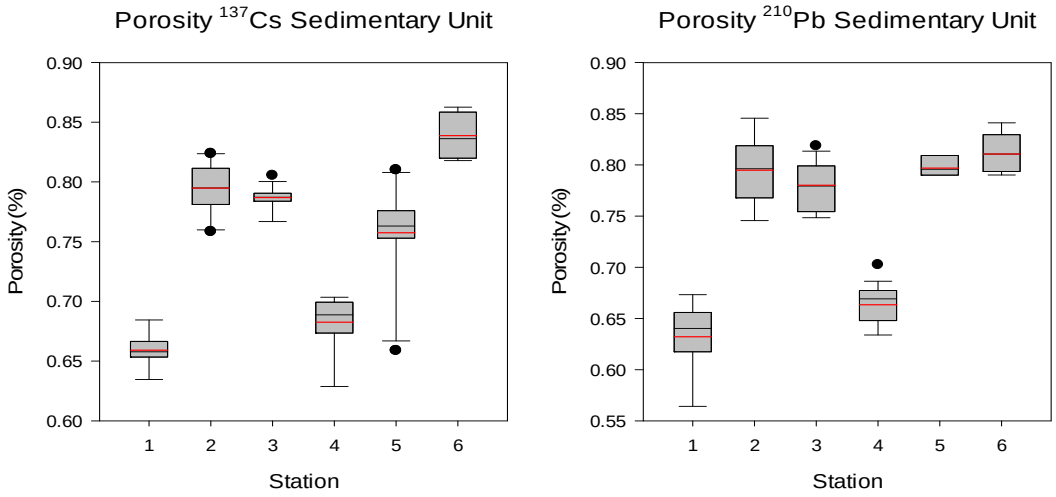

Figure 12. Whisker plots for porosity in the ^{137}Cs and ^{210}Pb sedimentary units.

Median grain size appears to be similar across the transect in both sedimentary units with most stations having a narrow range. There appears to be a general increase in the median d.50 value in the upper sedimentary unit as stations move riverward. However, in the lower sedimentary unit, the median d.50 values for stations PR01, PR02, and PR03 appear to increase away from the river. The greatest median value in the upper sedimentary unit is at station PR04 and in the lower unit at station PR01 (see Figure 13).

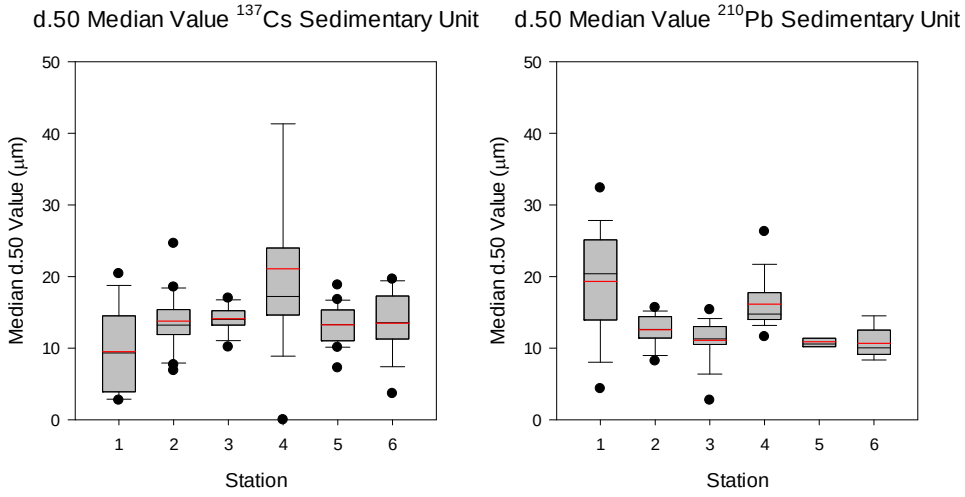

Figure 13. Whisker plots for median d.50 in the ^{137}Cs and ^{210}Pb sedimentary units.

Trends in the water content appear to be similar for both sedimentary units. Both the upper and the lower sedimentary unit show a general increase in water content away from the river edge at stations PR04, PR05, and PR06. Comparing the median water content values of stations PR01, PR02, and PR03, station PR02 appears to have a greater median value than stations PR01 and PR03. It appears that in both sedimentary units there is greater storage of water in the marsh interior at station PR06 than at any other station (see Figure 14).

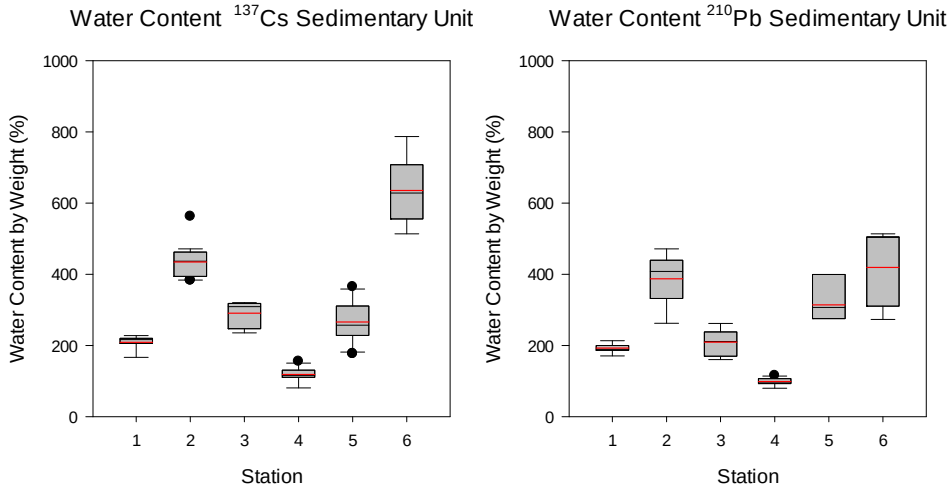

Figure 14. Whisker plots for water content in the ^{137}Cs and ^{210}Pb sedimentary units.

Histogram Distribution

The suite of physical sedimentary data (POC, bulk density, porosity, d.50 and water content) was visually evaluated for normality using a graphical histogram method and the more rigorous Kolmogorov-Smirnov test for normality. The histograms represent all data for each sedimentary property from both sedimentary units. Visual evaluations of the histogram data show the sedimentary variables as definitively non-normal. The histograms appear to show the sedimentary property data is positively skewed except for porosity (see Figure 15).

Rates of Autocompaction, Sedimentation, Accretion, and Elevation

Average rates of autocompaction and average sedimentation were calculated using the Williams (2003) model, and all results have an associated propagated error. This propagated error is the level of uncertainty associated for each of these variables and was calculated using Taylor's (1982) error analysis. Uncertainty is an inherent part of the data collection and analysis that must be fully addressed. Calculated rates of autocompaction and sedimentation show the variation in annual rates of sedimentation and autocompaction for each station. In the upper sedimentary unit, rates of autocompaction and sedimentation are greatest at stations PR02 and PR05. In the lower sedimentary unit, these rates are greatest at station PR02 and PR03 (see Table 3).

Average annual accretion rates were calculated using the Williams (2003) model with all rates having an associated propagated error. The calculated rates of average annual accretion are greatest in the upper sedimentary unit at stations PR02 and PR05 and greatest in the lower sedimentary unit at stations PR02 and PR03 (see Table 4).

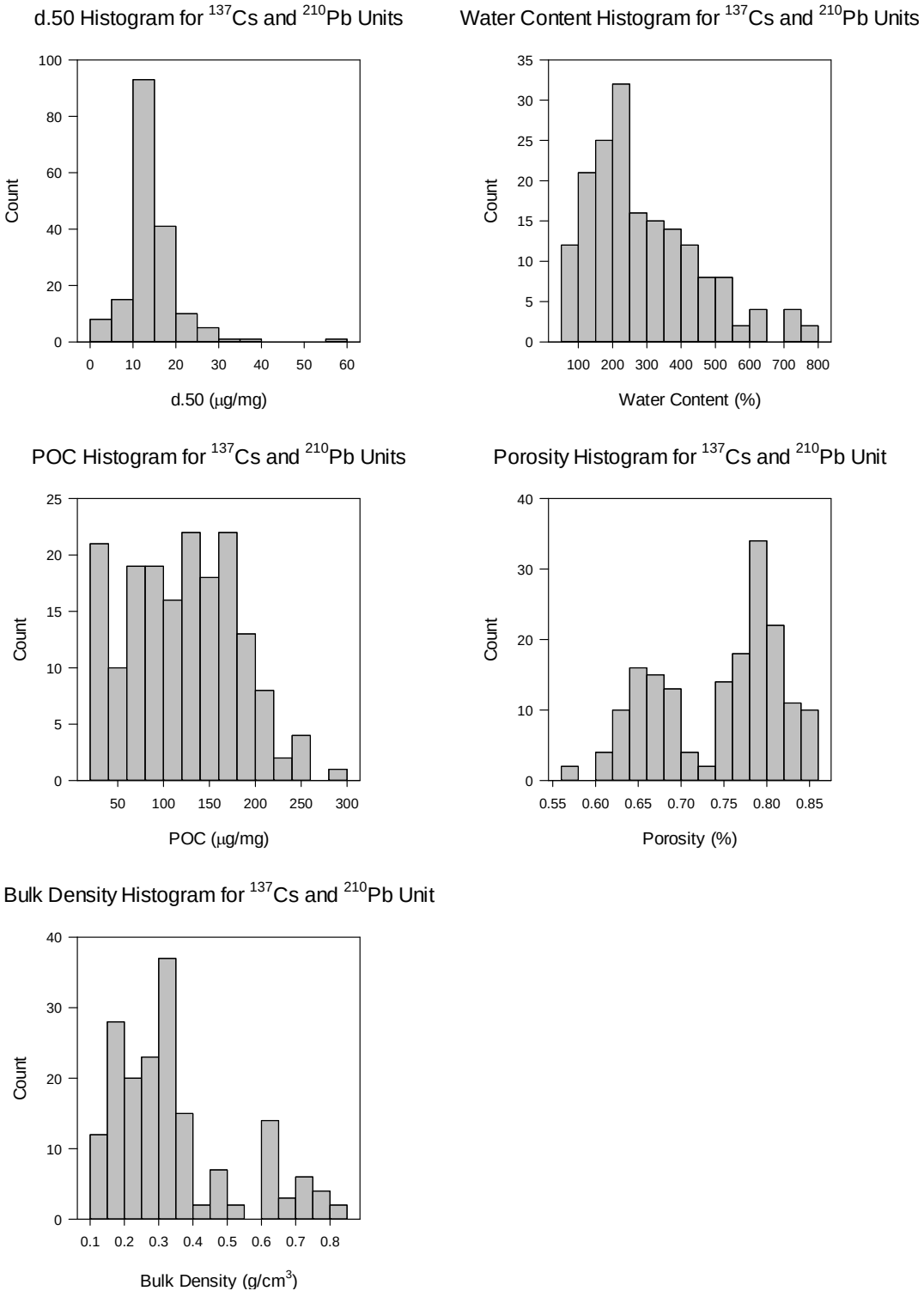

Figure 15. Histograms showing the distribution for each sedimentary property (POC, bulk density, porosity, d.50, and water content).

Table 3

Averaged Rates of Autocompaction and Averaged Rates of Annual Adimentation for ^{137}Cs and $^{210}Pb_{xs}$ Sedimentary Units

Station	^{137}Cs Rate of Autocompaction (cm/y)	^{137}Cs Rate of Sedimentation (cm/y)	$^{210}Pb_{xs}$ Rate of Autocompaction (cm/y)	$^{210}Pb_{xs}$ Rate of Sedimentation (cm/y)
PR_01_08	0.11 ± 0.03	0.29 ± 0.04	0.10 ± 0.02	0.29 ± 0.03
PR_02_08	0.39 ± 0.05	0.46 ± 0.03	0.22 ± 0.08	0.34 ± 0.03
PR_03_08	0.22 ± 0.05	0.39 ± 0.03	0.18 ± 0.06	0.31 ± 0.03
PR_04_08	0.30 ± 0.09	0.43 ± 0.03	0.12 ± 0.03	0.30 ± 0.03
PR_05_08	0.42 ± 0.10	0.48 ± 0.03	0.07 ± 0.02	0.10 ± 0.007
PR_06_08	0.27 ± 0.06	0.41± 0.03	0.12 ± 0.06	0.18 ± 0.06

Table 4

Average Annual Rate of Accretion for the ^{137}Cs and $^{210}Pb_{xs}$ Sediment Unit

Station	^{137}Cs Sediment Unit Average Annual Accretion (cm/y)	$^{210}Pb_{xs}$ Sediment Unit Average Annual Accretion (cm/y)
PR_01_08W	0.31 ± 0.03	0.30 ± 0.02
PR_02_08W	0.58 ± 0.05	0.38 ± 0.08
PR_03_08W	0.40 ± 0.05	0.37 ± 0.06
PR_04_08W	0.58 ± 0.09	0.34 ± 0.03
PR_05_08W	0.67 ± 0.11	0.14 ± 0.02
PR_06_08W	0.44 ± 0.06	0.24 ± 0.06

Rates of average elevation change were calculated from the Williams (2003) model along the associated propagated error. Modeled rates of elevation change in the upper unit are greatest at stations PR04 and PR05, whereas the lower unit stations PR01 and PR04 appear to have the greatest rate of elevation change (see Table 5).

Table 5

Average Annual Rate of Elevation Change for the ^{137}Cs and $^{210}Pb_{xs}$ Sediment Unit

Station	^{137}Cs Sediment Unit Average Annual Elevation Change (cm/y)	$^{210}Pb_{xs}$ Sediment Unit Average Annual Elevation Change (cm/y)
PR_01_08W	0.20 ± 0.01	0.21 ± 0.004
PR_02_08W	0.19 ± 0.01	0.16 ± 0.01
PR_03_08W	0.17 ± 0.01	0.19 ± 0.01
PR_04_08W	0.28 ± 0.03	0.22 ± 0.01
PR_05_08W	0.25 ± 0.03	0.07 ± 0.001
PR_06_08W	0.18 ± 0.01	0.12 ± 0.01

The physical sedimentary data were subjected to the Kolmogorov-Smirnov statistical test of normality. These results showed, with high confidence, the non-normal distribution of all physical properties except for POC. The POC normality result was very close to failing its normality test, so it was treated as non-normal (see Table 6). Treating POC as a non-normal variable allows the test of significance to be uniform across all sedimentary properties.

Table 6

Results of the Test for Normality Using the Kolmogorov-Smirnov Test Measuring the Normality of the Data Distribution

Sedimentary Property	K-S Distribution	P value
POC	0.066	P = 0.054
Bulk Density	0.182	P < 0.001
Porosity	0.152	P < 0.001
d.50	0.169	P < 0.001
Water Content	0.124	P < 0.001

Statistical Analysis of Data

There are significant differences in the sedimentary properties between the two units when the data are evaluated with the Mann-Whitney test. There is at least one significant difference in the sedimentary properties for all cores, except for PR05. The M-W tests for POC content are significant at stations PR_02, PR_03, PR_04, and PR_06. These four stations each have greater POC concentrations in the upper ^{137}Cs sedimentary unit than in the lower unit. Bulk density values are significant at stations PR03, PR04, and PR06, with the larger bulk density values found in the lower ^{210}Pb sedimentary unit. The median grain size (d.50) values at stations PR01 and PR03 are significantly different when the upper and lower sedimentary units are compared. Median d.50 values are higher in the upper sedimentary unit for station PR01 and greater in the lower sedimentary unit for station PR03. Water content is significantly different and greater in the upper sedimentary unit for stations PR03, PR04, and PR06 (see Table 7).

Table 7

Results of the Mann-Whitney Test Comparing the Upper ^{137}Cs Sedimentary Unit to the Lower ^{210}Pb Sedimentary Unit

Sedimentary Property	PR_01_08	PR_02_08	PR_03_08	PR_04_08	PR_05_08	PR_06_08
POC	0.027	0.000	0.000	0.000	0.002	0.001
Bulk Density	0.024	0.049	0.000	0.001	0.135	0.000
Porosity	0.008	1.000	0.770	0.005	0.002	0.004
d.50	0.001	0.369	0.001	0.067	0.018	0.037
Water Content	0.008	0.153	0.000	0.000	0.048	0.000

Note. Level of significance determined with a Bonferroni corrected alpha of 0.00

There are calculated, numerical differences for autocompaction when the rates in the upper unit are compared to the rates in the lower unit. When these different rates are compared using the Mann-Whitney test, results show a significant difference between these two units ($\alpha = 0.05$). Subjecting the average annual sedimentation rate from the upper and lower sedimentary unit to the Mann-Whitney test yields a similar result. There is a significant difference between rates of sedimentation in the two sedimentary units ($\alpha = 0.05$) (see Table 8).

Table 8

Results of the Mann-Whitney Test Comparing Average Annual Autocompaction Rate in the Upper ^{137}Cs Sedimentary Unit to the Lower ^{210}Pb Sedimentary Unit and the Average Annual Sedimentation Rate in the Upper ^{137}Cs Sedimentary Unit to the Lower ^{210}Pb Sedimentary Unit

Mann-Whitney Test	**^{137}Cs Sedimentary Unit vs. ^{210}Pb Sedimentary Unit**
Average Autocompaction Rate	0.041
Average Sedimentation Rate	0.026

Measuring the correlation strength of sedimentary properties with Spearman's test shows how the sedimentary properties correlate to increasing depth. With increasing depth, cores PR01, PR02, PR03, PR04, and PR06 are all strongly correlated to both POC and bulk density in the upper sedimentary unit. These five stations have a negative Spearman correlation for POC and a positive Spearman correlation for bulk density. This relationship is assumed the result of natural sediment compaction of the organic-rich marsh that reduces the volume of the organic matter and increases the mass per unit volume. The POC content at station PR05 also has a negative Spearman correlation with increased depth; however, there is not a significant Spearman correlation between bulk density and depth. Stations PR02, PR04, PR05, and PR06 all have a negative Spearman

correlation when depth and water content are compared. Stations PR02, PR04, and PR06 all have a negative Spearman correlation for increasing depth and decreasing water content, but station PR05 has a significant increase in the water content with increasing depth. Only stations PR05 and PR06 have a significant correlation between increasing depth and a porosity that also increases. Station PR06 has the only significant Spearman correlation between depth and d.50 (see Table 9).

Table 9

Spearman Correlation Between Depth and Sedimentary Properties in the ^{137}Cs Sedimentary Unit

Depth vs.	PR01	PR02	PR03	PR04	PR05	PR06
POC	-0.62	-0.86	-0.75	-0.74	-0.95	-0.82
Bulk Density	0.71	0.56	0.53	0.68	N.S.	0.90
Porosity	N.S.	N.S.	N.S.	N.S.	0.72	0.62
d.50	N.S.	N.S.	N.S.	N.S.	N.S.	-0.52
Water content by weight	N.S.	-0.60	N.S.	-0.70	0.52	-0.90

Note. Negative sign before correlation indicates one variable tends to decrease while the other increases. Values with a *p* value above 0.05 or a Spearman coefficient between 0.49 and -0.49 are not significant (N.S.)

In the lower ^{210}Pb sedimentary unit, there were very few significant Spearman correlations between increasing depth and the sedimentary property values. Stations PR02 and PR06 both have significant POC Spearman correlations, but they are inversely correlated. Station PR02 has a positive Spearman correlation for POC where station PR06 has a negative Spearman correlation. In addition to the negative Spearman correlation, station PR06 has a positive correlation between bulk density and depth. This negative POC and positive bulk density pairing is evident in all cores in the upper sedimentary unit, except for PR05. Stations PR04 and PR06 both have negative

Spearman correlations between water content and increasing depth, and only PR03 has a significant Spearman correlation between increasing depth and d.50 (see Table 10).

Table 10

Spearman Correlation Between Depth and Sedimentary Properties in the ^{210}Pb Sedimentary Unit

Depth vs.	PR01	PR02	PR03	PR04	PR05	PR06
POC	N.S.	0.61	N.S.	N.S.	N.S.	-0.70
Bulk Density	N.S.	N.S.	N.S.	N.S.	N.S.	0.85
Porosity	N.S.	N.S.	0.50	N.S.	N.S.	N.S.
d.50	N.S.	N.S.	N.S.	N.S.	N.S.	N.S.
Water content by weight	N.S.	N.S.	N.S.	-0.77	N.S.	-0.71

Note. Negative sign before correlation indicates one variable tends to decrease while the other increases. Values with a p value above 0.05 or a Spearman coefficient between 0.49 and -0.49 are not significant (N.S.).

Using the Spearman correlation, the median sedimentary property values were compared to the average rates of autocompaction. For both sedimentary units, sedimentation rate is the only property that is significantly correlated with autocompaction (see Table 11).

Table 11

Spearman Correlation Between the Median Sedimentary Property Values,Ssedimentation Rate and the Rates of Average Autocompaction (α=0.05)

Average Autocompaction Rate vs.	**^{137}Cs Sedimentary Unit**	**^{210}Pb Sedimentary Unit**
Median POC	N.S.	N.S.
Median Bulk Density	N.S.	N.S.
Median Porosity	N.S.	N.S.
Median d.50	N.S.	N.S.
Median Water Content	N.S.	N.S.
Average Sedimentation Rate	1.00	0.829

Correlation of the average annual rates of autocompaction and average annual sedimentation using Spearman's test shows a positive and significant relationship ($\alpha = 0.05$) between these two variables. In the lower sedimentary unit, stations PR02 and PR03 have the greatest rates of calculated average annual autocompaction and the highest rates of average annual sedimentation. When correlating the average rates of autocompaction to the rates of sedimentation the Spearman test again shows that these variables are correlated, but the correlation is not significant ($\alpha = 0.05$) (see Table 12).

Table 12

Spearman Correlation Between the Average Annual Autocompaction Rate and the Average Annual Sedimentation Rate for the ^{137}Cs and ^{210}Pb Sedimentary Units

Spearman Correlation	^{137}Cs Sedimentary Unit	^{210}Pb Sedimentary Unit
Average Autocompaction Rate vs. Average Sedimentation Rate	1.00; p = 0.002	0.829; p = 0.058

With the average annual sedimentation and the average annual autocompaction showing a positive Spearman correlation, the data were plotted on a scatter plot with a best-fit trend line. Plotting these two data sets (upper and lower sedimentary units) on scatter plots and then fitting these data points to a trend line shows there is a strong exponential fit between autocompaction and sedimentation in the upper unit. In the upper sedimentary unit, the relationship between autocompaction and sedimentation is strongly and significantly correlated, but in the lower unit the data are less strongly correlated with an alpha of 0.058. A third graph plotting the rates of autocompaction and sedimentation from both sedimentary units does show a significant correlation and exponential fit across the entire core (see Figure 16).

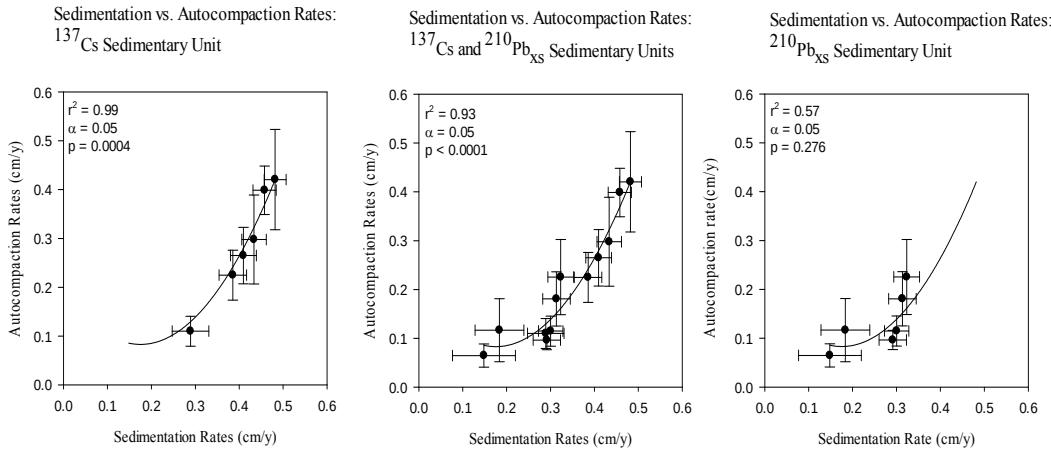

A B C

Figure 16. Scatter plot representing the graphical relationship between average annual autocompaction and the average annual sedimentation rate for the upper 137Cs sedimentary unit (A), the lower sedimentary unit (C), and both the upper and the lower sedimentary units combined (B). Data points are all fitted with an exponential best fit curve line at an $\alpha = 0.05$.

CHAPTER V

SUMMARY

Major Findings

These findings suggest that the rate of average annual autocompaction is strongly tied to the rate of average annual sedimentation. Results of the Spearman statistical test show that greater rates of sedimentation are strongly correlated to greater rates of autocompaction in both sedimentary units. These rates of autocompaction are significantly greater in the upper ^{137}Cs sedimentary unit than in the rates in the lower ^{210}Pb sedimentary unit. Stations with the highest rates of autocompaction in the upper sedimentary unit are found between the natural river levee and the marsh interior (Stations PR02 and PR05). In the lower sedimentary unit, stations with the greatest rate of autocompaction were found on the north bank of the Pearl River closest to the river (PR03) and between the river and the marsh interior (PR02).

The results of this study show rates of autocompaction significantly differ in the first half meter of marsh sediment. Rates of sedimentation at each station influence the amount of overburden pressure exerted on the sediment below. This greater overburden on the sediment leads to higher rates of autocompaction. This relationship of increased overburden stress and higher rates of compaction is also documented in Bayou Lafourche, Louisiana (Törnqvist et al., 2008). Törnqvist et al. (2008) found a well-correlated linear relationship between the rates of compaction and the thickness of the overburden.

In the lower unit, stations on the southern bank of the Pearl River (PR05 and PR06) have annual rates of sedimentation half the rate of the upper unit. This uncoupling

of the sedimentation rate may be the result of a recently discovered growth fault in the PRM (K. Yeager, personal communication October 10, 2011). Stations on the southern bank of the Pearl River are on the down-thrown side of the growth fault, and the northern bank stations are on the up-thrown side. It is possible that increased fault movement over the last 50 years has led to a decrease in the elevation on the south bank of the river. With a decrease in elevation, the sedimentation rates also have increased. In the upper unit, station PR05 has a thick sedimentary unit and one of the highest rates of sedimentation and autocompaction. However, in the lower unit, PR05 has a very thin unit of sediment and the lowest calculated rate of sedimentation and autocompaction.

When the rules of soil mechanics are applied to these two modeled units of different thicknesses, the influence that rates of sedimentation have on compaction are better understood. Increasing the normal stress (downward force) on the sediment leads to the expulsion of water and gas (reducing the pore space) that ultimately reduces the sediments volume (compaction). This physical compaction is correlated to the change in the effective stress (load carried by the grains) (σ'), which is defined as the difference between the total stress (σ) and the pore pressure of the water (u) (Terzaghi, 1943; Terzaghi, Peck, & Mesri, 1996).

$$(\sigma') = (\sigma) - u \tag{10}$$

Equation 10 states that an increase in the total stress is balanced by a decrease in the pore pressure that then maintains a constant effective stress. However, if there is an increase in the total stress and no change in the pore pressure, the effective stress will increase and induce natural compaction (Lambe & Whitman, 1969). Sediments in a thicker unit have more individual grains of sediment to support the downward normal

force associated with higher rates of sedimentation. These thicker units will, therefore, require more time to compact than a thinner unit of sediment. With a thin unit of sediment there are fewer grains to support the overburden, resulting in the sediment grains realigning into a more tightly configured packing (Yuill, Lavoie, & Reed, 2009).

Other Studies

There are three approaches for calculating the autocompaction of surface sediments. The first traditionally focused on thick units (10's of meters) of Holocene sediment overlying a basal peat (Bird et al., 2004; Bloom, 1964; Haslett et al., 1998; Törnqvist et al., 2008). The second method of calculating autocompaction measures thin units of sediments at near the surface (<1m) (Williams, 2003). The third method measures shallow autocompaction of surface sediments from a fixed elevation above the sediment surface using rod surface elevation tables (RSETs) (Cahoon et al., 1995, Cahoon, Marin, Black, & Lynch, 2000; Ford & Grace, 1998; McKee & Cherry, 2009; Rodgers & Saintilan, 2006). Published results of these different methods show similar rates in sediments along the northern Gulf of Mexico.

Modeling compaction in thick units of sediment uses coarse measurements of sedimentary properties which invariably overlook finer-scale features that may drive compaction on a decimeter scale, most notably sedimentation rates. These finer-scale processes vary by location (distance from sediment source, elevation, and floral assemblages) even within the distance of this coring transect (400 m) considered herein. It is believed by Kuecher (1994), Törnqvist et al. (2008), and Williams (2003) that the majority of compaction occurs within the surface two meters or less of marsh sediments; therefore, integrating autocompaction over several vertical meters can overlook areas

reaching the compaction limit very near the surface. Calculating the average compaction rates over thick sequences, deposited over long periods (+1000 years), gives modeled rates of compaction which are up to 100% higher than younger (100-500 years), thinner sequences from the same core (Törnqvist et al., 2008). The variability and complexity of these environments make the process of assigning regional rates of autocompaction impossible (Meckel, 2007; Williams, 2003).

Törnqvist et al. (2008) used basal peat dating to calculate rates of compaction over a thick, overlying, sedimentary unit and derived rates of autocompaction that appear very similar to the rates in the PRM. One of the main objectives of Törnqvist et al. (2008) study included analyzing the relationship between overburden and annual compaction of basal peat. The Törnqvist et al. (2008) study found a significant relationship between the variables as did this study of the PRM. Over time the higher rates of sedimentation will lead to greater overburden stress on the sediment causing the sediment to further compact.

Measuring the difference between accretion and changing surface elevation as a proxy for sediment compaction show large variations. The highest rate and largest range of autocompaction found in the literature are from the rod surface elevation measurements (RSETs) in the salt marshes of the southeast (Cahoon et al. 1995, Cahoon et al., 2000; Rodgers & Saintilan, 2006). This method calculates autocompaction using a technique that measures elevation changes from a fixed level above the sediment surface. The difference between the vertical accretion and the change in elevation below the fixed height is the rate of shallow autocompaction. Cahoon and Frois (2006) conducted measurements over a two-year period and found significant differences in the rates of

accretion and the change in elevation. The high rates of shallow compaction found at the Bayou Chitigue, Louisiana, test plot were the result of passage of Hurricane Andrew and the resulting plant dieback.

Two more recent studies in the PRM investigated changes in marsh elevation and compaction over a short two-year test period. Both studies were conducted in the PRM, with comparable plant species and sediment types. The first study by McKee and Cherry (2009) examined the impact of Hurricane Katrina on marsh elevation changes, soil profiles, and if a large storms passage influences changes in organic matter production. To measure rates compaction, McKee and Cherry (2009) used the RSET method established by Cahoon et al. (1995). Immediately after Hurricane Katrina, RSET measurements recorded the thickness of newly deposited sediment in relation to the initial marsh elevation. During the next 2 years, marsh surface elevation decreased at much higher rates than rates calculated in the Williams (2003) model in this research study. Ford and Grace (1998) also selected sites in the PRM to determine if herbivore feeding patterns resulted in changes of marsh elevation. Quantifying the affect that herbivores influenced marsh accretion and compaction was tested using plots control and test plots. The control marsh plots were fenced to restrict grazing, and the test plots went unfenced. Using RSET measurements spanning a 2-year time period, the rate of marsh accretion was measured at quarterly intervals. To measure shallow compaction of the surface sediments, Ford and Grace (1998) also used the method established by Cahoon et al. (1995). The results showed higher rates of accretion in the grazed plots with higher rates of shallow compaction; whereas, in the ungrazed plots, rates of accretion and shallow compaction were both lower. In both Ford and Grace (1998) and McKee and

Cherry (2009) rates of shallow compaction were attributed to plant mortality and the subsequent compaction of the root zone. It appears when the root zone is included in the sediment column rates of shallow compaction will be higher than expected.

Calculating autocompaction rates in thin sediment units at the near surface (< 1m) was utilized in the PRM and by Williams (2003). The rates of average annual autocompaction and rates of sedimentation in the PRM are less than the results Williams (2003) published from the Trinity River estuary. The rates of autocompaction were expected to be similar to Williams (2003) because the study areas are both river-dominated, contain mostly organic rich silty sediments, and have similar plant species. However, in the Williams (2003) study, unlike the PRM study, the upper 10 to 15 cm of sediment were included in the calculations for average annual autocompaction, giving these modeled rates a less compacted first layer of sediment (see Table 13). By keeping this upper unit of sediment, Williams (2003) also integrated the shallow compaction associated with the root zone. This study expands the original Williams (2003) study by finding another rate of autocompaction using the ^{210}Pb isotope for chronological control. With this additional data set, autocompaction rates for the deeper unit were calculated and further conclusions about the driving force of autocompaction were explored.

Table 13

Overview of Coastal Marsh Autocompaction Rates and Field Methods

Method	Study Site	Sedimentation Rate	Compaction Rate	Source
Bulk density, fallout radionuclides (^{7}Be, ^{137}Cs, ^{210}Pb)	Pearl River marsh, Louisiana	0.10 – 0.48 cm/y	0.10 – 0.42 cm/y	Prouhet et al. (2011) (unpublished)
Bulk density, fallout radionuclide (^{137}Cs)	Trinity River Estuary	0.14 – 1.02 cm/y	0.22 – 0.96 cm/y	Williams (2003)
Stratigraphic cross-sections and ^{14}C dating of basal peat	SW Britain, Connecticut, Mississippi River delta	0.14 – 0.54 cm/y	0.12 – 0.50 cm/y	Haslett et al. (1998), Bloom (1964), Törnqvist et al. (2008)
Surface elevation measurements	Salt Marshes of Louisiana, Florida, and North Carolina	0.39 – 2.60 cm/y	0.23 – 2.5 cm/y	Cahoon et al. (1995, 2000), Rodgers and Saintilan (2006)
	Pearl River Marsh	0.91 –1.24 cm/y	0.54 – 1.13 cm/y	Ford and Grace (1998)
	Pearl River and Big Branch Marsh	4 – 6cm	1.3 – 1.9 cm/y	McKee and Cherry (2009)

Importance of Work

Autocompaction is a difficult field of study and is quantitatively ignored when rates of subsidence are discussed. There also are few direct observations of autocompaction, and monitoring efforts are expensive and time-consuming (Meckel et al., 2006). The results of this study are important because they statistically show there are significant changes in the sedimentary properties in the first half meter of sediment

and further constrain the rates of autocompaction in the understudied near-surface sediments. Despite the large number of borings into the surface sediments of the northern Gulf of Mexico coast, geological and geotechnical data for modeling autocompaction are still unavailable for large areas of the Mississippi Delta region (Meckel et al., 2006). The high-resolution sedimentary data collected from the six wedge and peat cores in the PRM and the rates of autocompaction calculated should help to overcome some of the limitations of sparse low-resolution data sets.

Limitations

There are limitations associated with this study and should be addressed so future work can improve on the results. The average rates of autocompaction modeled in the PRM are not absolute values because of the limitations of the model, depositional history of the marsh, recently discovered faulting in the PRM, and the inherent error associated with data and sample collection. The Williams (2003) model makes three major assumptions about sedimentation:

1. Sedimentation is uniform in composition, rate of delivery, and bulk density on a decadal time scale.
2. As each layer of sediment is buried under successive layer, compaction will be uniform with an exponential rate.
3. Bulk density and layer thickness are inversely proportional and sediment compacts to a finite thickness with a constant bulk density.

Results from this study show that surface sediments have variations in sedimentary properties when the stations are less than 50 meters apart. The surface sediments in the PRM challenge the assumption of uniform sediment composition over a

small spatial area. Inundation of the PRM occurs during monthly spring tides, coastal storms, and up river flooding. Each of these events can alter the sediment fabric by temporarily increasing sedimentation rates or by eroding the marsh surface during floodwater retreat. The sedimentary properties in PRM record these events and through statistical analysis (Mann-Whitney test), it is evident that the sedimentation rate and the types of sediment delivered and retained in the marsh are variable.

A study recently completed in the PRM shows that this reach of the river has been captured by a newly discovered growth fault (K. Yeager, personal communication, October 10, 2011). This growth fault axis is centered in the river channel with the up-thrown side being north of the river and the down-thrown side of the fault being south of the river. This neo-tectonic motion is almost certainly influencing the rates of sedimentation at the marsh surface. By influencing the rates of sedimentation, the growth fault is possibly altering the rates of autocompaction at the near surface.

The modeled values for autocompaction, sedimentation, accretion, and elevation change all have an associated propagated error. These propagated errors are impossible to identify but need be addressed in the data. These errors are the result of sample collection, data analysis, and numerical analysis of the data.

Ideally, modeling rates of autocompaction in the PRM would include the upper 10 -15 cm of sediment, but this upper section is heavily bioturbated with obvious signs of disturbance from Hurricane Katrina. In the PRM down-core trends in bulk density did not satisfy the Williams (2003) model assumption of increasing bulk density with depth, unless the upper mixed layer of the marsh was removed from the study. By removing

this upper section of sediment, the new top layer was first assumed to the surface in 2005 and the first layer of sediment is compacted to an unknown thickness.

Future Work

Six years ago the PRM was heavily influenced by Hurricane Katrina, and the evidence of this storm is still evident in the sedimentary record. This large storm severely altered the PRM near surface sediments leading to the upper 10-15 cm of sediment being ignored for this study. Removal of this mix layer was not ideal, but necessary, to fulfill the assumptions of the Williams (2003) model. Choosing a location to model rates of autocompaction that is devoid of neo-tectonics and has not experienced a large-scale storm event may provide a different outcome in which sedimentary property influences autocompaction the most.

Conclusions

1. The Pearl River Marsh has recorded the passage of Hurricane Katrina in the sedimentary record. This event is most evident in the naturally occurring isotope ^{210}Pb profile and in the POC sedimentary profile.
2. There is a significant difference in the average annual rate of sedimentation between the two-modeled sedimentary units.
3. The rate of average annual accretion in the PRM is greater than the average annual rate of autocompaction.
4. The average annual rate of autocompaction for the upper ^{137}Cs sedimentary unit is significantly correlated to the average annual rate of sedimentation. In the lower ^{210}Pb sedimentary unit, the rate of autocompaction is less strongly correlated to the rate of sedimentation.

5. In the upper and lower sedimentary units, the average annual rate of autocompaction is significantly and exponentially related to the average annual rate of sedimentation.
6. In the first half meter of sediment there are statistically significant differences in at least one of the sedimentary properties (POC, bulk density, porosity, median grain size, or water content) except at station PR05.

APPENDIX A

RAW SEDIMENTARY DATA

A-1: Physical and Radionuclide data for core PR-01B_08W, collected 5/17/2008 at N30° 13' 25.08", W89° 38' 33.36"

Depth interval (cm)	Cumulative mass depth (g cm^{-2})	^{7}Be (mBq g^{-1})	^{137}Cs (mBq g^{-1})	^{210}Pb$_{xs}$ (mBq g^{-1})	% Sand	% Silt	% Clay
0-1	0.45 ± 0.05	5.70 ± 1.30	4.20 ± 0.50	45.54 ± 1.80	1.88	90.39	7.73
1-2	0.89 ± 0.09	0.92 ± 0.32	3.93 ± 0.41	57.70 ± 3.40	8.19	57.79	34.02
2-3	1.37 ± 0.14	3.38 ± 1.38	5.53 ± 0.53	58.93 ± 3.93	--	--	--
3-4	1.86 ± 0.19	0.00	5.57 ± 0.61	68.29 ± 4.07	10.99	67.63	21.38
4-5	2.37 ± 0.24	0.00	5.32 ± 0.51	67.76 ± 3.91	6.43	87.16	6.41
5-6	2.89 ± 0.29	0.00	4.37 ± 0.51	67.35 ± 3.68	9.45	61.43	29.12
6-7	3.30 ± 0.33	0.00	4.83 ± 0.44	79.43 ± 5.46	13.28	78.18	8.54
7-8	3.70 ± 0.37	0.00	5.04 ± 0.58	103.00 ± 4.65	17.34	74.46	8.20
8-9	4.18 ± 0.42	0.00	3.89 ± 0.49	112.61 ± 6.34	7.46	54.19	38.35
9-10	4.66 ± 0.47	0.00	6.37 ± 0.66	158.65 ± 6.68	2.33	82.92	14.75
10-11	5.10 ± 0.51	0.00	6.29 ± 0.78	150.51 ± 10.38	11.81	73.68	14.51
11-12	5.53 ± 0.55	0.00	6.94 ± 0.59	145.77 ± 10.47	3.90	86.27	9.83
12-13	5.85 ± 0.59	0.00	9.61 ± 1.26	156.47 ± 11.05	7.41	80.60	11.99
13-14	6.17 ± 0.62	0.00	9.28 ± 1.22	144.26 ± 8.70	3.02	54.35	42.63
14-15	6.50 ± 0.65	0.00	13.07 ± 0.94	134.03 ± 6.11	1.66	82.05	16.29
15-16	6.82 ± 0.68	0.00	10.02 ± 0.80	144.70 ± 9.12	4.40	40.43	55.17
16-17	7.11 ± 0.71	0.00	13.93 ± 1.72	123.56 ± 6.12	10.34	40.66	49.00
17-18	7.40 ± 0.74	0.00	22.37 ± 1.16	101.46 ± 5.02	8.39	79.23	12.38
18-19	7.70 ± 0.77	0.00	18.04 ± 1.95	138.89 ± 9.69	0.49	44.28	55.23
19-20	7.99 ± 0.80	0.00	29.59 ± 1.33	105.14 ± 3.88	0.18	85.07	14.75
20-21	8.29 ± 0.83	0.00	30.47 ± 1.26	96.51 ± 5.39	0.54	41.56	57.90
21-22	8.58 ± 0.86	0.00	32.14 ± 3.39	89.88 ± 3.58	3.17	45.79	51.04
22-23	8.87 ± 0.89	0.00	43.06 ± 1.93	86.31 ± 6.00	6.34	79.40	14.26
23-24	9.16 ± 0.92	0.00	42.57 ± 2.05	79.65 ± 3.25	8.47	79.21	12.32
24-25	9.52 ± 0.95	0.00	50.69 ± 1.96	70.79 ± 3.29	0.18	83.75	16.07
25-26	9.89 ± 0.99	0.00	84.42 ± 2.40	55.56 ± 2.54	1.90	51.31	46.79
26-27	10.20 ± 1.02	0.00	96.37 ± 9.18	14.75 ± 0.65	10.52	76.96	12.52
27-28	10.51 ± 1.05	0.00	24.92 ± 2.48	56.01 ± 1.86	7.85	85.55	6.60
28-29	10.81 ± 1.08	0.00	87.53 ± 8.40	65.59 ± 2.71	2.77	48.95	48.28
29-30	11.11 ± 1.11	0.00	50.13 ± 1.90	49.78 ± 1.67	1.19	85.29	13.52
30-31	11.47 ± 1.15	0.00	18.36 ± 2.19	43.60 ± 2.03	24.84	66.40	8.76
31-32	11.82 ± 1.18	0.00	13.20 ± 0.80	36.91 ± 1.38	34.15	57.92	7.93
32-33	12.15 ± 1.22	0.00	11.98 ± 0.95	31.91 ± 1.32	12.67	77.71	9.62
33-34	12.48 ± 1.25	0.00	8.28 ± 0.81	37.60± 2.30	22.88	69.25	7.87
34-35	12.78 ± 1.28	0.00	9.03 ± 0.92	28.60 ± 1.55	0.55	80.23	19.22
35-36	13.08 ± 1.31	0.00	12.01 ± 1.34	31.45 ± 1.68	25.38	65.97	8.65
36-37	13.38 ± 1.34	0.00	9.02 ± 1.08	31.65 ± 2.46	19.77	71.32	8.91
37-38	13.68 ± 1.37	0.00	6.83 ± 0.85	24.88 ± 1.80	16.17	74.95	8.88
38-39	13.99 ± 1.40	0.00	6.56 ± 0.73	33.35 ± 1.92	14.32	75.40	10.28
39-40	14.31 ± 1.43	0.00	5.65 ± 0.74	37.54 ± 1.99	8.31	80.20	11.49
40-41	14.64 ± 1.46	--	--	23.31 ± 1.08	13.55	73.30	13.15

Depth interval (cm)	Cumulative mass depth (g cm^{-2})	^{7}Be (mBq g^{-1})	^{137}Cs (mBq g^{-1})	^{210}Pb$_{xs}$ (mBq g^{-1})	% Sand	% Silt	% Clay
41-42	14.96 ± 1.50	--	--	21.89 ± 1.17	11.12	76.80	12.08
42-43	15.29 ± 1.53	--	--	20.62 ± 0.79	27.86	62.02	10.12
43-44	15.63 ± 1.56	--	--	19.06 ± 1.16	9.25	78.10	12.65
44-45	15.97 ± 1.60	--	--	19.44 ± 1.12	8.37	79.98	11.65
45-46	16.32 ± 1.63	--	--	18.85 ± 1.18	11.44	75.23	13.33
46-47	16.66 ± 1.67	--	--	16.48 ± 1.01	16.71	70.05	13.24
47-48	16.99 ± 1.70	--	--	17.42 ± 1.22	13.18	74.87	11.95
48-49	17.34 ± 1.73	--	--	17.84 ± 0.70	15.02	73.34	11.64
49-50	17.67 ± 1.77	--	--	14.54 ± 0.82	11.32	73.25	15.43
50-51	17.99 ± 1.80	--	--	7.60 ± 0.53	22.98	64.98	12.04
51-52	18.32 ± 1.83	--	--	11.60 ± 0.65	15.49	70.62	13.89
52-53	18.62 ± 1.86	--	--	1.20 ± 0.34	14.96	73.08	11.96
53-54	18.91 ± 1.89	--	--	0	25.17	66.11	8.72
54-55	19.22 ± 1.92	--	--	7.33 ± 0.39	19.06	67.91	13.03
55-56	19.52 ± 1.95	--	--	3.89 ± 0.03	30.21	60.10	9.69
56-57	19.82 ± 1.98	--	--	3.23 ± 1.56	24.73	64.40	10.87
57-58	20.12 ± 2.01	--	--	0.66 ± 0.17	17.07	72.59	10.34
58-59	20.42 ± 2.04	--	--	2.68 ± 0.31	10.49	76.62	12.89
59-60	20.72 ± 2.07	--	--	1.57 ± 0.33	20.72	69.39	9.89
60-61	21.03 ± 2.10	--	--	--	22.62	60.02	17.36
61-62	21.33 ± 2.13	--	--	1.04 ± 0.33	11.99	72.80	15.21
62-63	21.62 ± 2.16	--	--	--	14.88	68.49	16.63
63-64	21.92 ± 2.19	--	--	1.65 ± 0.33	4.55	39.27	56.18
64-65	22.23 ± 2.22	--	--	--	19.65	66.01	14.34
65-66	22.53 ± 2.25	--	--	--	19.14	71.17	9.69
66-67	22.83 ± 2.28	--	--	--	11.61	77.17	11.22
67-68	23.13 ± 2.31	--	--	--	8.40	70.00	21.60
68-69	23.42 ± 2.34	--	--	--	13.68	76.17	10.15
69-70	23.71 ± 2.37	--	--	--	21.47	69.29	9.24
70-72	24.34 ± 2.40	--	--	--	38.17	55.86	5.97
72-74	24.99 ± 2.44	--	--	--	9.53	79.19	11.28
74-76	25.65 ± 2.47	--	--	--	15.16	74.79	10.05
76-78	26.29 ± 2.50	--	--	--	13.36	74.73	11.91
78-80	26.91 ± 2.53	--	--	--	14.57	74.50	10.93
80-82	27.53 ± 2.56	--	--	--	7.63	84.82	7.55
82-84	28.19 ± 2.60	--	--	--	10.10	76.94	12.96
84-86	28.86 ± 2.63	--	--	--	7.12	81.93	10.95
86-88	29.49 ± 2.66	--	--	--	10.72	75.76	13.52
88-90	30.11± 2.69	--	--	--	3.89	85.42	10.69
90-95	31.68 ± 2.72	--	--	--	19.76	72.70	7.54
95-100	33.36 ± 2.76	--	--	--	5.16	86.09	8.75

A-2: Physical data for core PR_01_08W, collected 5/17/2008 at N30° 13' 25.08", W89° 38' 33.36"

Depth (cm)	POC (µg/mg)	Bulk Density (g/cm^3)	Porosity φ	d.50 (µm)	Water Content by Weight (%)
0.5	61.23	0.470	0.633	14.85	137.87
1.5	60.08	0.470	0.633	15.12	137.87
2.5	68.80	0.515	0.663		131.78
3.5	73.21	0.515	0.663	18.78	131.78
4.5	97.07	0.539	0.582	22.22	110.69
5.5	75.28	0.539	0.582	18.65	110.69
6.5	115.36	0.430	0.634	27.81	151.04
7.5	140.27	0.430	0.634	31.80	151.04
8.5	148.67	0.508	0.637	8.82	128.68
9.5	218.10	0.508	0.637	14.36	128.68
10.5	198.00	0.455	0.596	15.91	134.27
11.5	240.15	0.455	0.596	17.69	134.27
12.5	221.60	0.337	0.625	17.01	190.01
13.5	258.94	0.337	0.625	5.85	190.01
14.5	207.22	0.348	0.659	11.55	194.22
15.5	239.74	0.348	0.659	3.12	194.22
16.5	212.17	0.308	0.660	4.21	219.71
17.5	211.51	0.308	0.660	14.17	219.71
18.5	196.51	0.315	0.655	3.21	213.08
19.5	235.12	0.315	0.655	9.75	213.08
20.5	198.06	0.311	0.667	2.73	219.60
21.5	207.68	0.311	0.667	3.80	219.60
22.5	200.85	0.308	0.685	12.47	227.54
23.5	252.33	0.308	0.685	14.97	227.54
24.5	160.65	0.390	0.635	8.91	166.66
25.5	142.74	0.390	0.635	4.78	166.66
26.5	172.68	0.326	0.653	14.62	205.49
27.5	181.79	0.326	0.653	20.39	205.49
28.5	191.90	0.320	0.624	4.35	199.80
29.5	170.62	0.320	0.624	10.80	199.80
30.5	151.85	0.372	0.619	26.70	170.51
31.5	153.40	0.372	0.619	32.35	170.51
32.5	155.42	0.349	0.640	20.48	187.87
33.5	170.64	0.349	0.640	25.67	187.87
34.5	166.78	0.316	0.659	8.96	213.61
35.5	193.46	0.316	0.659	24.59	213.61
36.5	176.57	0.314	0.564	24.22	184.16
37.5	189.13	0.314	0.564	23.58	184.16

Depth (cm)	POC (µg/mg)	Bulk Density (g/cm^3)	Porosity φ	d.50 (µm)	Water Content by Weight (%)
38.5	201.99	0.334	0.616	19.12	188.74
39.5	198.15	0.334	0.616	13.39	188.74
40.5	177.59	0.348	0.673	15.80	198.41
41.5	187.95	0.348	0.673	17.02	198.41
42.5	168.41	0.354	0.652	26.30	189.01
43.5	178.95	0.354	0.652	14.51	189.01
44.5	184.29	0.362	0.628	15.51	177.66
45.5	192.93	0.362	0.628	15.07	177.66
46.5	183.42	0.363	0.679	17.44	191.56
47.5	202.70	0.363	0.679	16.41	191.56
48.5	203.39	0.359	0.646	19.05	184.55
49.5	239.00	0.359	0.646	13.35	184.55
50.5	239.23	0.347	0.678	20.86	200.39
51.5	246.25	0.347	0.678	17.57	200.39
52.5	249.91	0.313	0.641	18.43	210.24
53.5	254.67	0.313	0.641	25.85	210.24
54.5	238.70	0.327	0.671	17.63	210.27
55.5	258.96	0.327	0.671	28.32	210.27
56.5	248.35	0.317	0.675	25.37	218.19
57.5	250.16	0.317	0.675	23.05	218.19
58.5	255.20	0.321	0.655	18.54	208.78
59.5	277.64	0.321	0.655	26.06	208.78
60.5	310.70	0.322	0.652	13.14	207.81
61.5	282.67	0.322	0.652	14.34	207.81
62.5	277.55	0.316	0.659	13.95	213.86
63.5	268.44	0.316	0.659	2.88	213.86
64.5	297.22	0.326	0.670	20.37	211.04
65.5	279.55	0.326	0.670	23.42	211.04
66.5	266.58	0.318	0.658	16.26	211.73
67.5	196.68	0.318	0.658	9.27	211.73
68.5	333.06	0.310	0.685	19.31	226.53
69.5	264.10	0.310	0.685	28.38	226.53
71	249.64	0.337	0.668		203.20
73	304.46	0.350	0.659	18.44	193.34
75	258.34	0.346	0.668	22.84	197.62
77	250.28	0.346	0.654	19.36	193.87
79	242.77	0.324	0.658	21.16	208.05
81	236.03	0.333	0.652	22.18	200.69

Depth (cm)	POC (µg/mg)	Bulk Density (g/cm^3)	Porosity φ	d.50 (µm)	Water Content by Weight (%)
83		0.349	0.650	16.12	191.07
85	221.18	0.358	0.683	18.13	195.71
87	220.94	0.340	0.661	16.42	199.43
89	249.00	0.328	0.665	15.92	207.49

A-3: Physical and Radionuclide data for core PR-02B_08W, collected 5/29/2008 at N30° 13' 22.80", W89° 38' 34.40"

Depth interval (cm)	Cumulative mass depth (g cm^{-2})	^{7}Be (mBq g^{-1})	^{137}Cs (mBq g^{-1})	$^{210}Pb_{xs}$ (mBq g^{-1})	POC (µg mg^{-1})	% Sand	% Silt	% Clay
0-1	0.20 ± 0.02	30.88 ± 2.16	1.76 ± 0.18	102.88 ± 3.37	170.19	2.13	88.30	9.57
1-2	0.40 ± 0.04	19.66 ± 1.52	4.05 ± 0.25	79.44 ± 3.55	131.43	13.59	79.47	6.94
2-3	0.60 ± 0.06	0.00	3.18 ± 0.40	73.64 ± 3.41	128.30	13.53	79.65	6.82
3-4	0.80 ± 0.08	0.00	3.69 ± 0.45	70.89 ± 3.41	105.72	16.81	76.89	6.30
4-5	1.01 ± 0.10	0.00	3.05 ± 0.30	91.38 ± 4.84	104.38	8.41	81.61	9.98
5-6	1.22 ± 0.12	0.00	3.17 ± 0.34	75.59 ± 3.11	116.36	8.91	81.71	9.38
6-7	1.39 ± 0.14	0.00	3.15 ± 0.21	101.78 ± 4.60	140.32	11.73	79.70	8.57
7-8	1.57 ± 0.16	0.00	3.52 ± 0.42	116.70 ± 5.13	154.30	15.21	76.23	8.56
8-9	1.71 ± 0.17	0.00	5.42 ± 0.69	129.42 ± 4.91	162.70	6.33	82.34	11.33
9-10	1.86 ± 0.19	0.00	4.99 ± 0.60	132.89 ± 4.84	163.62	1.25	84.94	13.81
10-11	2.05 ± 0.21	0.00	12.08 ± 1.20	121.73 ± 5.30	175.55	13.45	79.96	6.59
11-12	2.24 ± 0.22	0.00	12.03 ± 1.35	116.93 ± 6.03	170.05	12.98	76.56	10.46
12-13	2.42 ± 0.24	0.00	11.54 ± 1.56	113.39 ± 4.34	167.20	8.46	80.88	10.66
13-14	2.60 ± 0.26	0.00	14.53 ± 1.32	125.44 ± 5.16	181.51	3.30	83.56	13.14
14-15	2.80 ± 0.28	0.00	11.76 ± 1.37	106.13 ± 3.86	151.21	0.98	71.11	27.91
15-16	2.99 ± 0.30	0.00	11.10 ± 1.48	107.11 ± 3.92	145.20	6.85	83.18	9.97
16-17	3.17 ± 0.32	0.00	15.54 ± 2.10	101.94 ± 5.08	169.00	5.50	80.10	14.40
17-18	3.34 ± 0.33	0.00	17.55 ± 1.11	108.55 ± 4.77	172.81	2.20	85.65	12.15
18-19	3.52 ± 0.35	0.00	22.69 ± 1.44	98.80 ± 4.02	160.76	9.32	79.61	11.07
19-20	3.69 ± 0.37	0.00	28.74 ± 3.07	75.68 ± 2.54	146.06	0.29	76.82	22.89
20-21	3.87 ± 0.39	0.00	21.48 ± 2.45	95.71 ± 6.09	160.28	2.96	85.31	11.73
21-22	4.06 ± 0.41	0.00	40.45 ± 1.47	82.26 ± 4.87	150.45	2.10	86.81	11.09
22-23	4.27 ± 0.43	0.00	38.82 ± 1.85	88.38 ± 6.87	147.42	5.69	81.53	12.78
23-24	4.48 ± 0.45	0.00	40.65 ± 4.42	57.76 ± 4.15	139.40	2.23	87.65	10.12
24-25	4.69 ± 0.47	0.00	47.88 ± 4.65	71.66 ± 4.07	132.49	0.89	85.66	13.45
25-26	4.90 ± 0.49	0.00	52.05 ± 2.89	67.61 ± 5.21	138.65	2.26	88.87	8.87
26-27	5.11 ± 0.51	0.00	57.86 ± 2.02	48.81 ± 2.53	119.83	2.50	87.48	10.02
27-28	5.32 ± 0.53	0.00	46.88 ± 4.66	53.27 ± 4.00	127.73	2.98	86.72	10.30
28-29	5.51 ± 0.55	0.00	66.13 ± 1.94	50.92 ± 2.79	111.27	1.42	87.28	11.30
29-30	5.69 ± 0.57	0.00	61.32 ± 5.95	33.78 ± 0.79	116.35	0.58	89.70	9.72
30-31	5.90 ± 0.59	0.00	60.88 ± 5.78	50.58 ± 3.00	111.75	2.27	84.91	12.82
31-32	6.11 ± 0.61	0.00	40.53 ± 3.88	46.60 ± 2.88	105.11	0.65	87.44	11.91
32-33	6.40 ± 0.64	0.00	22.84 ± 1.72	36.37 ± 2.39	98.61	3.23	83.80	12.97
33-34	6.68 ± 0.67	0.00	13.39 ± 1.47	29.40 ± 3.17	73.44	0.49	89.64	9.87
34-35	6.98 ± 0.70	0.00	9.79 ± 0.93	26.16 ± 0.76	72.55	1.96	87.50	10.54
35-36	7.27 ± 0.73	0.00	9.33 ± 0.86	35.49 ± 2.26	111.16	2.60	88.23	9.17
36-37	7.48 ± 0.75	0.00	9.16 ± 0.89	39.30 ± 2.24	110.64	0.97	88.93	10.10
37-38	7.69 ± 0.77	0.00	10.54 ± 1.03	29.13 ± 1.74	80.21	1.76	87.46	10.78
38-39	7.88 ± 0.79	0.00	8.42 ± 1.06	34.75 ± 2.61	129.70	1.17	78.28	20.55
39-40	8.07 ± 0.81	0.00	10.62 ± 0.95	37.69 ± 1.37	132.20	2.54	86.49	10.97
40-41	8.26 ± 0.83	0.00	6.79 ± 0.43	29.92 ± 1.87	149.90	11.26	75.29	13.45
41-42	8.45 ± 0.85	0.00	4.72 ± 0.38	28.82 ± 1.99	137.66	0.79	87.38	11.83
42-43	8.63 ± 0.86	--	--	23.21 ± 1.47	134.90	6.61	77.34	16.05
43-44	8.82 ± 0.88	--	--	23.55 ± 1.35	124.72	0.23	86.29	13.48

Depth interval (cm)	Cumulative mass depth (g cm^{-2})	^{7}Be (mBq g^{-1})	^{137}Cs (mBq g^{-1})	^{210}Pb$_{xs}$ (mBq g^{-1})	POC (µg mg^{-1})	% Sand	% Silt	% Clay
44-45	9.02 ± 0.90	--	--	20.46 ± 0.12	132.30	0.05	85.47	14.48
45-46	9.21 ± 0.92	--	--	18.19 ± 1.15	130.24	0.21	86.72	13.07
46-47	9.39 ± 0.94	--	--	17.21 ± 0.81	146.51	0.03	86.63	13.34
47-48	9.57 ± 0.96	--	--	13.34 ± 0.83	147.90	1.38	85.40	13.22
48-49	9.76 ± 0.98	--	--	17.83 ± 1.03	168.76	0.59	88.55	10.86
49-50	9.94 ± 0.99	--	--	17.89 ± 1.56	164.67	6.54	72.87	20.59
50-51	10.09 ± 1.01	--	--	17.48 ± 1.15	167.38	0.05	84.52	15.43
51-52	10.25 ± 1.03	--	--	5.52 ± 0.54	184.46	0.00	84.04	15.96
52-53	10.42 ± 1.04	--	--	7.02 ± 0.50	178.61	0.02	87.07	12.91
53-54	10.59 ± 1.06	--	--	9.00 ± 1.18	182.61	0.72	89.56	9.72
54-55	10.77 ± 1.08	--	--	11.22 ± 0.95	177.89	7.08	77.48	15.44
55-56	10.94 ± 1.09	--	--	14.71 ± 1.07	184.52	1.13	87.48	11.39
56-57	11.11 ± 1.11	--	--	13.46 ± 1.07	162.72	4.61	79.90	15.49
57-58	11.27 ± 1.13	--	--	6.13 ± 0.42	162.00	0.21	84.82	14.97
58-59	11.44 ± 1.14	--	--	7.82 ± 0.41	154.07	5.97	86.85	7.18
59-60	11.62 ± 1.16	--	--	3.07 ± 0.24	192.22	3.91	86.31	9.78
60-61	11.80 ± 1.18	--	--	5.19 ± 0.42	158.04	4.90	85.25	9.85
61-62	11.98 ± 1.20	--	--	4.66 ± 0.24	175.43	1.28	89.54	9.18
62-63	12.15 ± 1.22	--	--	4.17 ± 0.51	186.49	0.31	88.68	11.01
63-64	12.31 ± 1.23	--	--	3.17 ± 0.17	177.74	0.16	89.53	10.31
64-65	12.46 ± 1.25	--	--	--	181.00	1.39	89.52	9.09
65-66	12.60 ± 1.26	--	--	3.50 ± 0.35	178.86	1.35	84.44	14.21
66-67	12.77 ± 1.28	--	--	--	191.09	1.41	88.46	10.13
67-68	12.94 ± 1.29	--	--	--	181.17	1.15	87.46	11.39
68-69	13.10 ± 1.31	--	--	--	173.05	0.55	89.01	10.44
69-70	13.27 ± 1.33	--	--	--	184.86	1.11	86.45	12.44
70-72	13.66 ± 1.35	--	--	--	174.86	0.75	91.39	7.86
72-74	14.03 ± 1.37	--	--	--	160.85	0.10	87.24	12.66
74-76	14.40 ± 1.38	--	--	--	176.09	0.51	90.18	9.31
76-78	14.80 ± 1.40	--	--	--	166.75	0.54	87.75	11.71
78-80	15.19 ± 1.42	--	--	--	149.86	1.22	87.26	11.52
80-82	15.75 ± 1.45	--	--	--	140.36	0.37	88.97	10.66
82-84	16.39 ± 1.48	--	--	--	109.89	0.55	90.79	8.66
84-86	16.93 ± 1.51	--	--	--	124.46	0.54	88.75	10.71
86-88	17.58 ± 1.54	--	--	--	114.71	1.54	87.74	10.72
88-90	18.19 ± 1.57	--	--	--	106.54	1.67	84.05	14.28
90-92	18.89 ± 1.61	--	--	--	97.55	1.19	88.24	10.57
92-94	19.60 ± 1.64	--	--	--	89.39	0.73	86.22	13.05
94-96	20.24 ± 1.68	--	--	--	92.44	0.43	87.80	11.77
96-98	20.83 ± 1.71	--	--	--	103.98	0.23	86.35	13.42
98-100	21.40 ± 1.73	--	--	--	109.19	2.39	86.33	11.28

A-4: Physical data for core PR_02_08W, collected 5/29/2008 at N30° 13' 22.80", W89° 38' 34.40"

Depth (cm)	POC (µg/mg)	Bulk Density (g/cm^3)	Porosity φ	d.50 (µm)	Water Content by Weight (%)
0.5	170.19	0.197	0.780	11.84	404.84
1.5	131.43	0.197	0.780	24.20	404.84
2.5	128.3	0.204	0.800	24.83	401.27
3.5	105.72	0.204	0.800	28.34	401.27
4.5	104.38	0.209	0.785	20.73	384.87
5.5	116.36	0.209	0.785	20.16	384.87
6.5	140.32	0.173	0.804	21.90	475.78
7.5	154.30	0.173	0.804	25.50	475.78
8.5	162.70	0.148	0.812	15.57	562.64
9.5	163.62	0.148	0.812	10.15	562.64
10.5	175.55	0.187	0.782	24.60	429.29
11.5	170.05	0.187	0.782	18.52	429.29
12.5	167.20	0.179	0.824	16.94	471.32
13.5	181.51	0.179	0.824	11.98	471.32
14.5	151.21	0.197	0.772	6.88	401.93
15.5	145.20	0.197	0.772	15.00	401.93
16.5	169.00	0.173	0.758	11.97	449.98
17.5	172.81	0.173	0.758	11.87	449.98
18.5	160.76	0.174	0.786	17.41	463.79
19.5	146.06	0.174	0.786	7.68	463.79
20.5	160.28	0.184	0.822	13.87	459.03
21.5	150.45	0.184	0.822	12.49	459.03
22.5	147.42	0.211	0.811	13.29	393.90
23.5	139.40	0.211	0.811	13.13	393.90
24.5	132.49	0.209	0.781	11.19	383.13
25.5	138.65	0.209	0.781	15.25	383.13
26.5	119.83	0.212	0.804	15.44	387.72
27.5	127.73	0.212	0.804	14.59	387.72
28.5	111.27	0.186	0.806	13.12	443.96
29.5	116.35	0.186	0.806	15.66	443.96
30.5	111.75	0.212	0.795	12.03	383.82
31.5	105.11	0.212	0.795	11.56	383.82
32.5	98.61	0.283	0.774	13.37	280.37
33.5	73.44	0.283	0.774	12.61	280.37
34.5	72.55	0.298	0.762	12.47	262.33
35.5	111.16	0.298	0.762	15.06	262.33
36.5	110.64	0.208	0.796	14.38	391.73

Depth (cm)	POC (µg/mg)	Bulk Density (g/cm^3)	Porosity φ	d.50 (µm)	Water Content by Weight (%)
37.5	80.21	0.208	0.796	12.53	391.73
38.5	129.70	0.187	0.746	8.18	407.67
39.5	132.20	0.187	0.746	13.21	407.67
40.5	149.90	0.193	0.819	14.59	435.31
41.5	137.66	0.193	0.819	14.40	435.31
42.5	134.90	0.184	0.846	11.25	471.37
43.5	124.72	0.184	0.846	10.11	471.37
44.5	132.30	0.199	0.831	9.18	426.98
45.5	130.24	0.199	0.831	11.64	426.98
46.5	146.51	0.179	0.849	10.59	484.79
47.5	147.90	0.179	0.849	10.79	484.79
48.5	168.76	0.184	0.837	12.21	467.24
49.5	164.67	0.184	0.837	9.18	467.24
50.5	167.38	0.154	0.864	8.73	573.90
51.5	184.46	0.154	0.864	9.36	573.90
52.5	178.61	0.173	0.841	10.85	498.93
53.5	182.61	0.173	0.841	15.74	498.93
54.5	177.89	0.176	0.828		481.86
55.5	184.52	0.176	0.828	15.13	481.86
56.5	162.72	0.162	0.847	10.56	536.13
57.5	162	0.162	0.847	8.90	536.13
58.5	154.07	0.176	0.822	24.06	479.67
59.5	192.22	0.176	0.822	20.92	479.67
60.5	158.04	0.181	0.845	18.88	479.12
61.5	175.43	0.181	0.845	16.52	479.12
62.5	186.49	0.167	0.843	13.23	518.47
63.5	177.74	0.167	0.843	12.29	518.47
64.5	181	0.146	0.844	14.74	592.61
65.5	178.86	0.146	0.844	10.74	592.61
66.5	191.09	0.167	0.847	13.04	519.37
67.5	181.17	0.167	0.847	12.71	519.37
68.5		0.167	0.786	13.02	483.18
69.5	184.86	0.167	0.786	10.91	483.18
71	174.86	0.194	0.773	15.81	408.22
73	160.85	0.188	0.859	11.36	468.70
75	176.09	0.182	0.856	17.05	480.82
77	166.75	0.201	0.847	12.63	432.83
79	149.86	0.194	0.860	11.91	454.23
81	140.36	0.283	0.826	12.25	298.80

Depth (cm)	POC (µg/mg)	Bulk Density (g/cm^3)	Porosity φ	d.50 (µm)	Water Content by Weight (%)
83	109.89	0.316	0.812	14.74	263.55
85	124.46	0.272	0.835	10.92	314.32
87	114.71	0.326	0.815	11.42	255.81
89	106.54	0.306	0.817	9.79	274.08
91	97.55	0.346	0.808	11.62	239.47
93	89.39	0.356	0.801	10.48	230.75
95	92.44	0.322	0.817	13.18	263.55

A-5: Physical and Radionuclide data for core PR-03B_08W, collected 6/6/2008 at N30° 13' 22.00", W89° 38' 34.80"

Depth interval (cm)	Cumulative mass depth (g cm^{-2})	^{7}Be (mBq g^{-1})	^{137}Cs (mBq g^{-1})	^{210}Pb$_{xs}$ (mBq g^{-1})	POC (µg mg^{-1})	% Sand	% Silt	% Clay
0-1	0.34 ± 0.03	54.76 ± 5.92	3.61 ± 0.22	71.62 ± 3.79	116.42	8.03	85.17	6.80
1-2	0.68 ± 0.07	15.38 ± 1.06	3.42 ± 0.27	61.02 ± 3.96	85.57	9.45	81.30	9.25
2-3	1.09 ± 0.11	10.19 ± 0.82	4.06 ± 0.44	59.47 ± 4.62	75.51	11.35	82.58	6.07
3-4	1.49 ± 0.15	0.00	5.45 ± 0.57	50.44 ± 3.27	65.30	9.03	84.36	6.61
4-5	1.85 ± 0.19	0.00	5.30 ± 0.45	58.28 ± 2.92	70.55	10.64	79.61	9.75
5-6	2.21 ± 0.22	0.00	3.66 ± 0.48	69.23 ± 4.99	75.99	7.04	81.63	11.33
6-7	2.52 ± 0.25	0.00	5.54 ± 0.62	70.62 ± 4.88	91.61	9.42	82.53	8.05
7-8	2.82 ± 0.28	0.00	6.44 ± 0.68	75.45 ± 4.58	98.60	10.52	80.16	9.32
8-9	3.20 ± 0.32	0.00	5.94 ± 0.40	71.64 ± 3.14	107.70	5.28	83.31	11.41
9-10	3.57 ± 0.36	0.00	6.21 ± 0.58	55.83 ± 4.21	113.20	12.29	73.54	14.17
10-11	3.84 ± 0.38	0.00	7.75 ± 0.46	70.01 ± 3.72	123.68	5.47	84.22	10.31
11-12	4.10 ± 0.41	0.00	6.03 ± 0.72	63.75 ± 2.68	128.24	3.90	84.96	11.14
12-13	4.37 ± 0.44	0.00	7.43 ± 0.66	68.32 ± 3.57	33.34	--	--	--
13-14	4.63 ± 0.46	0.00	9.71 ± 0.73	77.18 ± 4.45	129.35	8.39	82.56	9.05
14-15	4.88 ± 0.49	0.00	8.19 ± 0.59	67.63 ± 3.73	129.85	3.78	85.80	10.42
15-16	5.12 ± 0.51	0.00	9.00 ± 1.06	72.02 ± 3.39	133.45	--	--	--
16-17	5.38 ± 0.54	0.00	12.25 ± 1.36	61.93 ± 3.25	165.62	7.48	82.38	10.14
17-18	5.63 ± 0.56	0.00	17.90 ± 1.45	65.29 ± 2.20	116.78	5.23	85.23	9.54
18-19	5.91 ± 0.59	0.00	20.22 ± 1.57	61.07 ± 2.55	88.31	8.35	84.08	7.57
19-20	6.19 ± 0.62	0.00	21.01 ± 1.62	58.59 ± 3.22	102.56	4.59	83.35	12.06
20-21	6.44 ± 0.64	0.00	27.67 ± 2.74	57.68 ± 2.91	130.82	--	--	--
21-22	6.69 ± 0.67	0.00	23.04 ± 2.33	61.00 ± 2.41	94.93	2.15	86.68	11.17
22-23	7.03 ± 0.70	0.00	28.24 ± 2.09	55.59 ± 2.25	114.68	6.23	82.89	10.88
23-24	7.37 ± 0.74	0.00	35.78 ± 3.43	54.12 ± 1.76	86.49	1.89	89.02	9.09
24-25	7.70 ± 0.77	0.00	36.81 ± 2.62	40.95 ± 1.06	81.06	1.58	79.24	19.18
25-26	8.03 ± 0.80	0.00	36.95 ± 3.55	48.17 ± 2.67	81.56	1.95	87.39	10.66
26-27	8.43 ± 0.84	0.00	30.29 ± 2.20	44.68 ± 2.04	83.81	2.45	84.61	12.94
27-28	8.84 ± 0.88	0.00	25.26 ± 1.89	50.00 ± 2.43	80.82	3.96	85.92	10.12
28-29	9.22 ± 0.92	0.00	31.96 ± 3.09	39.44 ± 1.27	75.75	5.42	81.69	12.89
29-30	9.60 ± 0.96	0.00	25.52 ± 2.54	37.31 ± 2.50	64.36	0.67	76.27	23.06
30-31	10.07 ± 1.01	0.00	20.76 ± 1.59	37.24 ± 1.70	78.03	1.64	86.39	11.97
31-32	10.54 ± 1.05	0.00	17.57 ± 1.80	31.65 ± 1.09	68.10	1.20	84.45	14.35
32-33	11.02 ± 1.10	0.00	17.04 ± 1.77	31.75 ± 1.38	63.93	1.15	85.52	13.33
33-34	11.50 ± 1.15	0.00	15.40 ± 1.05	37.91 ± 2.21	65.47	1.38	86.66	11.96
34-35	11.87 ± 1.19	0.00	12.86 ± 1.11	41.46 ± 3.14	79.58	1.50	85.26	13.24
35-36	12.25 ± 1.23	0.00	9.96 ± 0.92	22.70 ± 1.96	64.11	5.66	77.40	16.94
36-37	12.59 ± 1.26	0.00	6.54 ± 0.72	34.42 ± 2.16	76.94	2.64	84.70	12.66
37-38	12.94 ± 1.29	0.00	3.89 ± 0.47	24.10 ± 1.80	70.47	0.52	89.42	10.06
38-39	13.26 ± 1.33	0.00	3.45 ± 0.41	24.73 ± 0.64	60.57	0.79	85.88	13.33
39-40	13.58 ± 1.36	0.00	4.83 ± 0.58	19.00 ± 0.41	69.88	0.30	42.39	57.31
40-41	13.94 ± 1.39	0.00	2.81 ± 0.27	22.08 ± 0.74	82.64	0.26	84.66	15.08
41-42	14.30 ± 1.43	--	--	13.58 ± 1.11	67.94	0.69	86.40	12.91
42-43	14.67 ± 1.47	--	--	8.95 ± 1.02	70.07	0.71	83.64	15.65
43-44	15.05 ± 1.51	--	--	8.82 ± 0.62	79.06	1.18	82.88	15.94

Depth interval (cm)	Cumulative mass depth (g cm^{-2})	^{7}Be (mBq g^{-1})	^{137}Cs (mBq g^{-1})	^{210}Pb$_{xs}$ (mBq g^{-1})	POC (µg mg^{-1})	% Sand	% Silt	% Clay
44-45	15.42 ± 1.54	--	--	12.17 ± 0.83	70.30	2.04	88.23	9.73
45-46	15.80 ± 1.58	--	--	10.75 ± 0.67	84.44	1.42	81.52	17.06
46-47	16.08 ± 1.61	--	--	5.84 ± 0.24	75.81	2.49	81.75	15.76
47-48	16.36 ± 1.64	--	--	6.08 ± 0.01	55.18	3.12	80.48	16.40
48-49	16.71 ± 1.67	--	--	0.90 ± 0.05	73.43	0.47	82.43	17.10
49-50	17.05 ± 1.71	--	--	9.58 ± 0.56	79.87	0.50	83.73	15.77
50-51	17.39 ± 1.74	--	--	4.56 ± 0.36	75.95	0.55	87.46	11.99
51-52	17.72 ± 1.77	--	--	5.17 ± 0.11	86.82	2.19	83.20	14.61
52-53	18.11 ± 1.81	--	--	8.32 ± 0.80	77.04	0.71	85.69	13.60
53-54	18.50 ± 1.85	--	--	--	88.25	1.73	82.25	16.02
54-55	18.85 ± 1.89	--	--	--	78.74	1.66	83.64	14.70
55-56	19.20 ± 1.92	--	--	--	84.09	0.81	86.88	12.31
56-57	19.60 ± 1.96	--	--	--	77.70	3.09	84.33	12.58
57-58	19.99 ± 2.00	--	--	--	76.54	0.95	88.28	10.77
58-59	20.34 ± 2.03	--	--	--	73.73	1.02	82.75	16.23
59-60	20.69 ± 2.07	--	--	--	82.03	4.30	81.38	14.32
60-61	21.08 ± 2.11	--	--	--	82.81	3.28	81.27	15.45
61-62	21.47 ± 2.15	--	--	--	66.95	2.39	83.21	14.40
62-63	21.80 ± 2.18	--	--	--	71.62	2.25	85.57	12.18
63-64	22.14 ± 2.21	--	--	--	70.46	0.63	83.50	15.87
64-65	22.62 ± 2.26	--	--	--	57.96	2.57	80.35	17.08
65-66	23.10 ± 2.31	--	--	--	92.60	2.15	79.98	17.87
66-67	23.67 ± 2.37	--	--	--	60.30	2.98	81.92	15.10
67-68	24.24 ± 2.42	--	--	--	59.18	2.94	82.10	14.96
68-69	24.72 ± 2.47	--	--	--	59.45	2.63	80.79	16.58
69-70	25.21 ± 2.52	--	--	--	60.73	1.43	86.65	11.92
70-72	26.19 ± 2.57	--	--	--	60.86	2.02	80.73	17.25
72-74	27.31 ± 2.63	--	--	--	65.57	1.15	87.77	11.08
74-76	28.39 ± 2.68	--	--	--	52.82	1.67	87.00	11.33
76-78	29.33 ± 2.73	--	--	--	44.57	4.93	84.38	10.69
78-80	30.46 ± 2.78	--	--	--	44.35	2.22	85.99	11.79
80-82	31.51 ± 2.84	--	--	--	54.02	1.31	85.53	13.16
82-84	32.67 ± 2.89	--	--	--	49.66	3.94	83.06	13.00
84-86	33.71 ± 2.95	--	--	--	49.58	4.08	84.62	11.30
86-88	34.66 ± 2.99	--	--	--	54.83	3.31	86.68	10.01
88-90	35.66 ± 3.04	--	--	--	56.50	1.80	83.84	14.36
90-92	36.82 ± 3.10	--	--	--	50.52	3.36	85.17	11.47
92-94	37.84 ± 3.15	--	--	--	55.66	1.93	82.65	15.42
94-96	38.86 ± 3.20	--	--	--	54.21	3.00	81.79	15.21
96-98	39.81 ± 3.25	--	--	--	59.20	1.98	86.49	11.53
98-100	40.82 ± 3.30	--	--	--	63.93	0.97	88.56	10.47

A-6: Physical data for core PR_03_08W, collected 6/6/2008 at N30° 13' 22.00", W89° 38' 34.80"

Depth (cm)	POC (µg/mg)	Bulk Density (g/cm^3)	Porosity φ	d.50 (µm)	Water Content by Weight (%)
0.5	116.42	0.342	0.701	25.66	209.93
1.5	85.57	0.342	0.701	17.16	209.93
2.5	75.51	0.401	0.731	23.21	186.70
3.5	65.30	0.401	0.731	18.82	186.70
4.5	70.55	0.356	0.713	24.81	205.33
5.5	75.99	0.356	0.713	12.59	205.33
6.5	91.61	0.309	0.748	16.53	248.10
7.5	98.60	0.309	0.748	15.92	248.10
8.5	107.7	0.375	0.758	13.16	207.19
9.5	113.20	0.375	0.758	14.08	207.19
10.5	123.68	0.274	0.806	13.88	300.84
11.5	128.24	0.274	0.806	13.06	300.84
12.5	139.35	0.260	0.784	13.41	309.00
13.5	129.35	0.260	0.784	15.59	309.00
14.5	129.85	0.249	0.767	16.58	315.29
15.5	133.45	0.249	0.767	14.03	315.29
16.5	165.62	0.255	0.797	15.11	320.18
17.5	116.78	0.255	0.797	14.33	320.18
18.5	88.31	0.285	0.788	16.97	283.11
19.5	102.56	0.285	0.788	15.00	283.11
20.5	130.82	0.253	0.787	11.67	318.29
21.5	94.93	0.253	0.787	13.21	318.29
22.5	114.68	0.343	0.787	13.60	235.33
23.5	86.49	0.343	0.787	15.23	235.33
24.5	81.06	0.328	0.791	10.16	246.78
25.5	81.56	0.328	0.791	13.60	246.78
26.5	83.81	0.413	0.766	11.85	190.37
27.5	80.82	0.413	0.766	15.36	190.37
28.5	75.75	0.384	0.799	12.75	213.45
29.5	64.36	0.384	0.799	7.97	213.45
30.5	78.03	0.471	0.748	11.66	162.90
31.5	68.10	0.471	0.748	10.71	162.90
32.5	63.93	0.480	0.750	10.53	160.23
33.5	65.47	0.480	0.750	10.93	160.23
34.5	79.58	0.378	0.768	13.11	208.42
35.5	64.11	0.378	0.768	10.56	208.42
36.5	76.94	0.341	0.792	12.24	237.99

Depth (cm)	POC (µg/mg)	Bulk Density (g/cm^3)	Porosity φ	d.50 (µm)	Water Content by Weight (%)
37.5	70.47	0.341	0.792	13.41	237.99
38.5	60.57	0.317	0.811	10.55	261.97
39.5	69.88	0.317	0.811	2.73	261.97
40.5	82.64	0.362	0.819	9.51	231.65
41.5	67.94	0.362	0.819	12.31	231.65
42.5	70.07	0.382	0.766	9.96	205.75
43.5	79.06	0.382	0.766	10.44	205.75
44.5	70.3	0.384	0.796	16.32	212.67
45.5	84.44	0.384	0.796	9.78	212.67
46.5	75.81	0.283	0.820	11.36	296.40
47.5	55.18	0.283	0.820	10.59	296.40
48.5	73.43	0.339	0.783	9.55	236.67
49.5	79.87	0.339	0.783	9.50	236.67
50.5	75.95	0.339	0.808	11.49	243.90
51.5	86.82	0.339	0.808	12.12	243.90
52.5	77.04	0.384	0.764	10.90	203.99
53.5	88.25	0.384	0.764	9.98	203.99
54.5	78.74	0.352	0.798	11.11	232.24
55.5		0.352	0.798	11.07	232.24
56.5	77.7	0.391	0.774	12.02	202.71
57.5	76.54	0.391	0.774	12.84	202.71
58.5	73.73	0.344	0.742	10.33	220.94
59.5	82.03	0.344	0.742	12.18	220.94
60.5	82.81	0.392	0.790	10.89	206.68
61.5	66.95	0.392	0.790	11.81	206.68
62.5	71.62	0.332	0.810	12.71	249.70
63.5	70.46	0.332	0.810	10.68	249.70
64.5	57.96	0.489	0.746	10.84	156.56
65.5	92.60	0.489	0.746	9.87	156.56
66.5	60.3	0.561	0.735	11.40	134.18
67.5	59.18	0.561	0.735	11.30	134.18
68.5	59.45	0.490	0.747	10.13	156.28
69.5	60.73	0.490	0.747	12.07	156.28
71	60.86	0.491	0.751	9.87	156.68
73	65.57	0.563	0.726	12.56	132.01
75	52.82	0.538	0.738	12.39	140.50
77	44.57	0.472	0.750	15.15	162.96
79	44.35	0.564	0.730	13.09	132.65
81	54.02	0.526	0.720	12.29	140.47

Depth (cm)	POC (µg/mg)	Bulk Density (g/cm^3)	Porosity φ	d.50 (µm)	Water Content by Weight (%)
83	49.66	0.578	0.721	13.65	127.79
85	49.58	0.519	0.731	13.76	144.50
87	54.83	0.475	0.744	13.93	160.46
89	56.5	0.498	0.728	10.98	149.70
91	50.52	0.584	0.783	12.47	137.52
93	55.66	0.507	0.725	11.02	146.65
95	54.21	0.512	0.743	11.35	148.78
97	59.2	0.477	0.743	12.77	159.77
99	63.93	0.505	0.745	13.69	151.27

A-7: Physical and Radionuclide data for core PR-04B_08W, collected 7/12/2008 at N30° 13' 18.50", W89° 38' 36.60"

Depth interval (cm)	Cumulative mass depth (g cm^{-2})	^{7}Be (mBq g^{-1})	^{137}Cs (mBq g^{-1})	^{210}Pb$_{xs}$ (mBq g^{-1})	POC (µg mg^{-1})	% Sand	% Silt	% Clay
0-1	0.39 ± 0.04	47.18 ± 4.29	5.24 ± 0.58	89.53 ± 3.06	102.70	10.78	78.14	11.08
1-2	0.78 ± 0.08	7.55 ± 0.57	4.06 ± 0.47	49.18 ± 2.18	81.89	15.74	72.99	11.27
2-3	1.21 ± 0.12	0.00	4.16 ± 0.38	49.42 ± 2.35	75.37	19.89	67.18	12.93
3-4	1.65 ± 0.16	0.00	4.75 ± 0.55	58.09 ± 3.25	78.24	15.58	73.27	11.15
4-5	2.08 ± 0.21	0.00	4.28 ± 0.47	108.80 ± 3.64	78.44	19.37	70.76	9.87
5-6	2.51 ± 0.25	0.00	4.24 ± 0.45	54.54 ± 3.56	74.45	15.37	73.75	10.88
6-7	2.95 ± 0.30	0.00	3.86 ± 0.44	43.73 ± 2.00	72.65	27.40	60.68	11.92
7-8	3.40 ± 0.34	0.00	3.95 ± 0.38	49.30 ± 2.26	71.46	28.93	60.73	10.34
8-9	3.83 ± 0.38	0.00	2.89 ± 0.28	59.45 ± 3.75	114.03	19.55	68.92	11.53
9-10	4.27 ± 0.43	0.00	4.35 ± 0.47	55.31 ± 2.50	108.44	11.97	76.04	11.99
10-11	4.72 ± 0.47	0.00	5.08 ± 0.69	60.01 ± 2.63	93.48	16.04	69.45	14.51
11-12	5.17 ± 0.52	0.00	4.14 ± 0.38	59.96 ± 1.94	87.17	14.22	72.06	13.72
12-13	5.65 ± 0.57	0.00	4.04 ± 0.39	48.46 ± 2.08	67.14	--	--	--
13-14	6.13 ± 0.61	0.00	4.45 ± 0.50	50.14 ± 3.42	67.23	18.18	69.57	12.25
14-15	6.65 ± 0.67	0.00	4.02 ± 0.35	33.03 ± 2.67	58.99	21.93	67.16	10.91
15-16	7.18 ± 0.72	0.00	4.65 ± 0.49	36.50 ± 1.81	59.47	16.04	71.76	12.20
16-17	7.79 ± 0.78	0.00	4.66 ± 0.41	34.53 ± 1.00	57.85	21.59	67.44	10.97
17-18	8.40 ± 0.84	0.00	5.25 ± 0.51	31.41 ± 1.04	50.25	26.80	63.03	10.17
18-19	9.06 ± 0.91	0.00	7.67 ± 1.00	28.09 ± 1.36	51.26	28.40	62.00	9.60
19-20	9.71 ± 0.97	0.00	5.12 ± 0.54	13.14 ± 0.67	38.34	20.00	70.65	9.35
20-21	10.34 ± 1.03	0.00	5.76 ± 0.64	12.66 ± 0.74	40.97	39.15	52.56	8.29
21-22	10.98 ± 1.10	0.00	4.21 ± 0.49	11.18 ± 0.77	30.46	48.27	44.97	6.76
22-23	11.77 ± 1.18	0.00	5.50 ± 0.63	6.15 ± 0.10	27.47	19.14	68.76	12.10
23-24	12.56 ± 1.26	0.00	4.51 ± 0.39	4.82 ± 0.11	29.68	18.16	70.17	11.67
24-25	13.17 ± 1.32	0.00	7.50 ± 0.75	30.56 ± 1.13	51.53	26.69	64.54	8.77
25-26	13.78 ± 1.38	0.00	16.81 ± 1.60	27.83 ± 2.01	48.37	15.73	71.70	12.57
26-27	14.41 ± 1.44	0.00	18.97 ± 1.31	28.26 ± 1.35	47.93	11.51	70.92	17.57
27-28	15.04 ± 1.50	0.00	25.04 ± 2.37	17.83 ± 0.99	45.48	20.83	64.35	14.82
28-29	15.73 ± 1.57	0.00	18.67 ± 1.47	15.09 ± 0.68	37.56	16.59	72.30	11.11
29-30	16.43 ± 1.64	0.00	20.25 ± 1.52	18.55 ± 0.82	35.77	21.55	68.03	10.42
30-31	17.26 ± 1.73	0.00	22.05 ± 1.65	9.30 ± 0.36	31.69	13.25	72.49	14.26
31-32	18.08 ± 1.81	0.00	29.01 ± 2.85	8.61 ± 0.32	28.37	13.41	73.68	12.91
32-33	18.83 ± 1.88	0.00	27.53 ± 2.39	10.24 ± 0.88	32.18	9.01	75.66	15.33
33-34	19.59 ± 1.96	0.00	30.56 ± 2.99	9.68 ± 0.47	27.71	14.70	73.47	11.83
34-35	20.19 ± 2.02	0.00	27.36 ± 2.74	17.39 ± 0.59	29.54	7.73	77.27	15.00
35-36	20.80 ± 2.08	0.00	23.10 ± 1.71	9.68 ± 0.21	29.54	17.28	71.01	11.71
36-37	21.50 ± 2.15	0.00	20.03 ± 1.55	7.59 ± 0.20	33.41	12.62	75.12	12.26
37-38	22.21 ± 2.22	0.00	16.90 ± 2.12	6.50 ± 0.60	28.68	9.30	75.42	15.28
38-39	22.88 ± 2.29	0.00	8.23 ± 0.84	6.56 ± 0.20	26.25	8.45	80.95	10.60
39-40	23.55 ± 2.35	0.00	9.82 ± 0.81	17.39 ± 0.87	28.80	13.44	71.39	15.17
40-41	24.25 ± 2.43	0.00	8.78 ± 0.86	0.00	26.80	6.89	76.43	16.68
41-42	24.96 ± 2.50	0.00	2.89 ± 0.29	0.00	28.21	8.59	78.79	12.62
42-43	25.62 ± 2.56	0.00	3.66 ± 0.46	0.00	29.43	9.14	75.81	15.05
43-44	26.27 ± 2.63	--	--	0.00	31.37	9.03	77.78	13.19

Depth interval (cm)	Cumulative mass depth (g cm^{-2})	^{7}Be (mBq g^{-1})	^{137}Cs (mBq g^{-1})	^{210}Pb$_{xs}$ (mBq g^{-1})	POC (µg mg^{-1})	% Sand	% Silt	% Clay
44-45	26.94 ± 2.69	--	--	16.23 ± 0.33	32.16	6.95	80.63	12.42
45-46	27.61 ± 2.76	--	--	0.00	37.31	6.96	82.37	10.67
46-47	28.20 ± 2.82	--	--	0.00	36.93	4.48	84.80	10.72
47-48	28.79 ± 2.88	--	--	0.00	34.87	5.67	82.55	11.78
48-49	29.49 ± 2.95	--	--	0.00	39.35	6.69	83.13	10.18
49-50	30.18 ± 3.02	--	--	7.82 ± 0.15	31.01	5.93	81.69	12.38
50-51	30.83 ± 3.08	--	--	7.92 ± 0.41	34.22	8.24	79.42	12.34
51-52	31.47 ± 3.15	--	--	4.17 ± 0.11	35.24	3.95	83.99	12.06
52-53	32.23 ± 3.22	--	--	3.20 ± 0.25	31.34	5.26	84.62	10.12
53-54	33.00 ± 3.30	--	--	4.82 ± 0.20	29.38	6.11	83.56	10.33
54-55	33.71 ± 3.37	--	--	8.48 ± 0.48	25.95	3.52	83.72	12.76
55-56	34.42 ± 3.44	--	--	3.68 ± 0.16	24.87	6.54	82.57	10.89
56-57	35.20 ± 3.52	--	--	1.95 ± 0.10	24.60	5.35	82.80	11.85
57-58	35.97 ± 3.60	--	--	6.31 ± 0.16	23.90	4.97	83.42	11.61
58-59	36.84 ± 3.68	--	--	4.60 ± 0.01	26.72	6.47	81.63	11.90
59-60	37.71 ± 3.77	--	--	1.84 ± 0.25	24.09	5.61	82.36	12.03
60-61	38.42 ± 3.84	--	--	6.03 ± 0.14	28.58	8.04	81.56	10.40
61-62	39.13 ± 3.91	--	--	0.91 ± 0.54	22.53	7.87	81.48	10.65
62-63	39.85 ± 3.99	--	--	2.83 ± 0.18	24.97	9.22	80.87	9.91
63-64	40.58 ± 4.06	--	--	3.68 ± 0.13	24.69	6.17	81.19	12.64
64-65	41.45 ± 4.15	--	--	1.64 ± 0.35	23.42	9.04	77.23	13.73
65-66	42.32 ± 4.23	--	--	--	23.13	9.39	78.01	12.60
66-67	43.05 ± 4.31	--	--	--	23.01	9.45	79.07	11.48
67-68	43.77 ± 4.38	--	--	--	21.00	11.36	78.66	9.98
68-69	44.53 ± 4.45	--	--	--	20.92	8.14	82.53	9.33
69-70	45.29 ± 4.53	--	--	--	21.31	6.39	79.92	13.69
70-71	46.03 ± 4.60	--	--	--	21.98	8.87	81.24	9.89
71-72	46.76 ± 4.68	--	--	--	22.18	7.94	80.75	11.31
72-73	47.50 ± 4.75	--	--	--	22.28	10.39	77.77	11.84
73-74	48.23 ± 4.82	--	--	--	19.12	11.29	77.01	11.70
74-75	49.10 ± 4.91	--	--	--	18.84	9.70	78.51	11.79
75-76	49.97 ± 5.00	--	--	--	19.53	14.08	73.87	12.05
76-77	50.80 ± 5.08	--	--	--	20.49	9.74	79.80	10.46
77-78	51.63 ± 5.16	--	--	--	19.81	8.21	83.07	8.72
78-79	52.57 ± 5.26	--	--	--	19.44	9.88	78.02	12.10
79-80	53.50 ± 5.35	--	--	--	19.48	11.69	75.64	12.67
80-81	54.19 ± 5.42	--	--	--	17.00	5.36	79.02	15.62
81-82	54.88 ± 5.49	--	--	--	17.25	12.70	78.06	9.24
82-83	55.73 ± 5.57	--	--	--	15.72	8.04	80.78	11.18
83-84	56.57 ± 5.66	--	--	--	16.13	12.72	75.39	11.89
84-85	57.22 ± 5.72	--	--	--	15.43	9.54	80.44	10.02
85-86	57.87 ± 5.79	--	--	--	18.21	10.31	76.39	13.30
86-87	58.67 ± 5.87	--	--	--	18.79	7.72	79.27	13.01
87-88	59.46 ± 5.95	--	--	--	17.94	11.10	78.68	10.22
88-89	60.25 ± 6.03	--	--	--	18.46	19.01	71.80	9.19
89-90	61.04 ± 6.10	--	--	--	23.59	8.27	76.44	15.29
90-91	61.75 ± 6.18	--	--	--	25.44	6.13	79.73	14.14

Depth interval (cm)	Cumulative mass depth (g cm^{-2})	^{7}Be (mBq g^{-1})	^{137}Cs (mBq g^{-1})	^{210}Pb$_{xs}$ (mBq g^{-1})	POC (µg mg^{-1})	% Sand	% Silt	% Clay
91-92	62.46 $\pm$ 6.25	--	--	--	24.85	4.12	80.23	15.65
92-93	63.17 $\pm$ 6.32	--	--	--	28.66	4.62	81.53	13.85
93-94	63.87 $\pm$ 6.39	--	--	--	25.72	7.99	79.75	12.26
94-95	64.64 $\pm$ 6.46	--	--	--	24.54	4.85	81.77	13.38
95-96	65.41 $\pm$ 6.54	--	--	--	27.02	3.87	80.25	15.88
96-97	66.10 $\pm$ 6.61	--	--	--	29.09	7.20	79.46	13.34
97-98	66.79 $\pm$ 6.68	--	--	--	26.90	5.99	80.78	13.23
98-99	67.42 $\pm$ 6.74	--	--	--	26.78	6.56	81.62	11.82
99-100	68.05 $\pm$ 6.81	--	--	--	26.29	1.25	84.85	13.90

A-8: Physical data for core PR_04_08W, collected 7/12/2008 at N30° 13' 18.50", W89° 38' 36.60"

Depth (cm)	POC (µg/mg)	Bulk Density (g/cm^3)	Porosity φ	d.50 (µm)	Water Content by Weight (%)
0.5	102.7	0.390	0.691	18.87	181.76
1.5	81.89	0.390	0.691	21.10	181.76
2.5	75.37	0.430	0.712	17.48	169.87
3.5	78.24	0.430	0.712	21.84	169.87
4.5	78.44	0.431	0.701	24.01	166.56
5.5	74.45	0.431	0.701	22.25	166.56
6.5	72.65	0.441	0.692	22.15	160.85
7.5	71.46	0.441	0.692	21.46	160.85
8.5	114.03	0.440	0.697	18.85	162.22
9.5	108.44	0.440	0.697	17.27	162.22
10.5	93.48	0.454	0.689	14.83	155.63
11.5	87.17	0.454	0.689	13.39	155.63
12.5	67.14	0.472	0.684		148.72
13.5	67.23	0.472	0.684	16.69	148.72
14.5	58.99	0.521	0.662	22.74	130.39
15.5	59.47	0.521	0.662	15.14	130.39
16.5	57.85	0.607	0.703	19.19	118.88
17.5	50.25	0.607	0.703	23.15	118.88
18.5	51.26	0.646	0.693	24.52	110.10
19.5	38.34	0.646	0.693	23.43	110.10
20.5	40.97	0.640	0.686	37.19	109.91
21.5	30.46	0.640	0.686	57.75	109.91
22.5	27.47	0.796	0.629	17.21	80.94
23.5	29.68	0.796	0.629	17.10	80.94
24.5	51.53	0.618	0.696	29.73	115.45
25.5	48.37	0.618	0.696	15.77	115.45
26.5	47.93	0.624	0.703	11.10	115.37
27.5	45.48	0.624	0.703	14.11	115.37
28.5	37.56	0.703	0.656	19.48	956.50
29.5	35.77	0.703	0.656	26.26	956.50
30.5	31.69	0.818	0.634	15.88	793.84
31.5	28.37	0.818	0.634	17.39	793.84
32.5	32.18	0.761	0.636	13.80	856.96
33.5	27.71	0.761	0.636	18.84	856.96
34.5	29.54	0.609	0.677	13.43	113.92
35.5	29.54	0.609	0.677	21.21	113.92
36.5	33.41	0.710	0.669	15.99	96.68

Depth (cm)	POC (µg/mg)	Bulk Density (g/cm^3)	Porosity φ	d.50 (µm)	Water Content by Weight (%)
37.5	28.68	0.710	0.669	13.35	96.68
38.5	26.25	0.659	0.685	16.92	106.56
39.5	28.80	0.659	0.685	14.44	106.56
40.5	26.80	0.702	0.652	11.59	95.19
41.5	28.21	0.702	0.652	14.33	95.19
42.5	29.43	0.647	0.674	14.80	106.86
43.5	31.37	0.647	0.674	14.08	106.86
44.5	32.16	0.671	0.670	14.72	102.42
45.5	37.31	0.671	0.670	16.35	102.42
46.5	36.93	0.586	0.711	15.40	124.45
47.5	34.87	0.586	0.711	14.55	124.45
48.5	39.35	0.686	0.685	15.44	102.33
49.5	31.01	0.686	0.685	14.36	102.33
50.5	34.22	0.636	0.714	15.48	115.03
51.5	35.24	0.636	0.714	14.13	115.03
52.5	31.34	0.756	0.662	16.15	89.84
53.5	29.38	0.756	0.662	16.80	89.84
54.5	25.95	0.707	0.672	13.67	97.43
55.5	24.87	0.707	0.672	16.80	97.43
56.5	24.60	0.768	0.635	15.16	84.66
57.5	23.90	0.768	0.635	14.32	84.66
58.5	26.72	0.858	0.634	14.71	75.69
59.5	24.09	0.858	0.634	13.81	75.69
60.5	28.58	0.701	0.685	16.72	100.16
61.5	22.53	0.701	0.685	16.42	100.16
62.5	24.97	0.731	0.656	15.68	92.02
63.5	24.69	0.731	0.656	14.05	92.02
64.5	23.42	0.878	0.608	12.96	70.93
65.5	23.13	0.878	0.608	14.10	70.93
66.5	23.01	0.732	0.666	14.82	93.33
67.5	21.00	0.732	0.666	17.36	93.33
68.5	20.92	0.755	0.652	16.61	88.55
69.5	21.31	0.755	0.652	12.95	88.55
70.5	21.98	0.741	0.650	16.27	89.87
71.5	22.18	0.741	0.650	15.13	89.87
72.5	22.28	0.742	0.666	15.36	92.02
73.5	19.12	0.742	0.666	16.58	92.02
74.5	18.84	0.861	0.614	15.12	73.03
75.5	19.53	0.861	0.614	17.21	73.03
76.5		0.828	0.641	16.54	79.43

Depth (cm)	POC (µg/mg)	Bulk Density (g/cm^3)	Porosity φ	d.50 (µm)	Water Content by Weight (%)
77.5	19.81	0.828	0.641	17.54	79.43
78.5	19.44	0.925	0.663	15.48	73.44
79.5	19.48	0.925	0.663	15.61	73.44
80.5	17.00	0.691	0.689	12.49	102.11
81.5	17.25	0.691	0.689	19.60	102.11
82.5	15.72	0.854	0.618	15.40	74.16
83.5	16.13	0.854	0.618	18.13	74.16
84.5	15.43	0.657	0.677	17.37	105.62
85.5	18.21	0.657	0.677	14.90	105.62
86.5	18.79	0.794	0.630	14.21	81.27
87.5	17.94	0.794	0.630	17.05	81.27
88.5	18.46	0.787	0.650	20.76	84.65
89.5	23.59	0.787	0.650	12.54	84.65
90.5	25.44	0.713	0.678	12.89	97.53
91.5	24.85	0.713	0.678	12.13	97.53
92.5	28.66	0.710	0.669	13.29	96.59
93.5	25.72	0.710	0.669	14.45	96.59
94.5	24.54	0.778	0.666	12.86	87.77
95.5	27.02	0.778	0.666	11.30	87.77
96.5	29.09	0.703	0.685	13.53	99.84
97.5	26.90	0.703	0.685	13.79	99.84
98.5	26.78	0.631	0.678	13.91	110.25
99.5	26.29	0.631	0.678	12.39	110.25

A-9: Physical and Radionuclide data for core PR-05B_08W, collected 7/23/2008 at N30° 13' 17.10", W89° 38' 37.60"

Depth interval (cm)	Cumulative mass depth (g cm^{-2})	^{7}Be (mBq g^{-1})	^{137}Cs (mBq g^{-1})	^{210}Pb$_{xs}$ (mBq g^{-1})	POC (µg mg^{-1})	% Sand	% Silt	% Clay
0-1	0.26 ± 0.03	16.79 ± 1.50	5.03 ± 0.45	61.38 ± 3.97	89.76	2.98	87.12	9.90
1-2	0.53 ± 0.05	13.56 ± 1.32	4.18 ± 0.40	56.33 ± 3.67	93.55	4.21	81.48	14.31
2-3	0.86 ± 0.09	15.60 ± 1.27	4.30 ± 0.39	60.23 ± 3.85	83.94	4.17	79.71	16.12
3-4	1.20 ± 0.12	0.00	3.61 ± 0.39	51.73 ± 2.95	56.05	4.79	80.56	14.65
4-5	1.57 ± 0.16	0.00	5.39 ± 0.58	45.29 ± 2.44	58.12	6.64	82.82	10.54
5-6	1.94 ± 0.19	0.00	3.40 ± 0.33	49.95 ± 2.83	53.87	7.58	82.20	10.22
6-7	2.37 ± 0.24	0.00	3.85 ± 0.42	59.16 ± 3.01	90.35	3.52	83.20	13.28
7-8	2.79 ± 0.28	0.00	5.60 ± 0.65	37.03 ± 2.60	64.35	7.65	80.82	11.53
8-9	3.11 ± 0.31	0.00	4.90 ± 0.55	89.01 ± 5.33	143.80	11.07	80.05	8.88
9-10	3.44 ± 0.34	0.00	6.65 ± 0.88	104.28 ± 5.19	146.07	1.80	56.49	41.71
10-11	3.66 ± 0.37	0.00	6.27 ± 0.69	96.48 ± 5.13	168.75	2.88	85.04	12.08
11-12	3.88 ± 0.39	0.00	6.25 ± 0.80	90.71 ± 4.54	184.07	3.69	81.62	14.69
12-13	4.21 ± 0.42	0.00	5.62 ± 0.69	93.42 ± 4.70	172.56	8.89	77.97	13.14
13-14	4.54 ± 0.45	0.00	6.66 ± 0.57	50.78 ± 3.24	189.07	2.89	84.45	12.66
14-15	4.90 ± 0.49	0.00	4.60 ± 0.49	97.63 ± 4.87	211.01	2.14	82.74	15.12
15-16	5.25 ± 0.53	0.00	9.00 ± 1.01	57.89 ± 2.32	196.53	13.67	74.50	11.83
16-17	5.52 ± 0.55	0.00	7.10 ± 0.81	46.37 ± 2.35	185.54	7.31	81.26	11.43
17-18	5.79 ± 0.58	0.00	6.84 ± 0.82	46.67 ± 1.92	176.74	11.37	76.68	11.95
18-19	6.17 ± 0.62	0.00	10.38 ± 0.79	33.79 ± 1.67	151.15	5.33	82.51	12.16
19-20	6.55 ± 0.66	0.00	10.16 ± 0.81	76.39 ± 5.19	138.91	13.21	76.30	10.49
20-21	6.80 ± 0.68	0.00	9.41 ± 1.09	51.69 ± 4.82	134.38	4.20	79.29	16.51
21-22	7.05 ± 0.71	0.00	10.78 ± 0.69	60.38 ± 4.58	132.07	4.85	78.24	16.91
22-23	7.33 ± 0.73	0.00	10.61 ± 0.97	40.48 ± 2.52	141.50	4.70	78.31	16.99
23-24	7.61 ± 0.76	0.00	11.63 ± 1.40	36.50 ± 2.39	130.23	5.79	79.41	14.80
24-25	7.93 ± 0.79	0.00	12.12 ± 0.67	39.12 ± 2.41	127.26	9.47	78.18	12.35
25-26	8.26 ± 0.83	0.00	12.72 ± 1.26	21.70 ± 1.25	94.11	6.34	79.58	14.08
26-27	8.59 ± 0.86	0.00	17.53 ± 1.34	60.23 ± 4.40	114.34	8.73	78.80	12.47
27-28	8.93 ± 0.89	0.00	33.61 ± 2.29	48.85 ± 3.77	103.93	11.16	76.22	12.62
28-29	9.16 ± 0.92	0.00	40.81 ± 3.88	36.50 ± 2.02	96.30	7.14	78.67	14.19
29-30	9.39 ± 0.94	0.00	22.24 ± 1.68	13.23 ± 0.64	89.55	4.65	57.28	38.07
30-31	9.68 ± 0.97	0.00	46.58 ± 4.42	19.93 ± 1.04	79.66	4.50	78.42	17.08
31-32	9.98 ± 1.00	0.00	60.86 ± 5.69	13.46 ± 0.79	82.52	2.24	84.92	12.84
32-33	10.18 ± 1.02	0.00	105.20 ± 9.74	20.07 ± 1.48	89.99	2.07	80.79	17.14
33-34	10.39 ± 1.04	0.00	77.69 ± 7.22	16.30 ± 0.87	105.77	2.63	80.55	16.82
34-35	10.65 ± 1.07	0.00	87.36 ± 9.82	46.75 ± 1.24	116.47	3.75	80.21	16.04
35-36	10.91 ± 1.09	0.00	41.07 ± 2.86	14.87 ± 0.98	90.01	1.44	80.95	17.61
36-37	11.25 ± 1.13	0.00	25.10 ± 1.84	9.12 ± 0.43	68.30	4.27	78.64	17.09
37-38	11.58 ± 1.16	0.00	15.69 ± 1.34	7.45 ± 0.07	76.52	7.09	78.15	14.76
38-39	11.91 ± 1.19	0.00	11.52 ± 1.02	5.68 ± 0.21	61.87	4.80	79.85	15.35
39-40	12.24 ± 1.22	0.00	9.19 ± 0.96	3.68 ± 0.06	56.66	7.72	75.97	16.31
40-41	12.57 ± 1.26	0.00	7.36 ± 0.63	1.11 ± 0.16	53.89	10.40	74.78	14.82
41-42	12.90 ± 1.29	0.00	11.65 ± 1.00	9.78 ± 0.47	76.45	13.53	73.17	13.30
42-43	13.14 ± 1.31	0.00	10.27 ± 0.98	24.47 ± 0.81	90.50	7.15	76.74	16.11
43-44	13.37 ± 1.34	0.00	13.43 ± 1.76	27.51 ± 1.12	101.53	8.39	78.41	13.20

Depth interval (cm)	Cumulative mass depth (g cm^{-2})	^{7}Be (mBq g^{-1})	^{137}Cs (mBq g^{-1})	^{210}Pb$_{xs}$ (mBq g^{-1})	POC (µg mg^{-1})	% Sand	% Silt	% Clay
44-45	13.59 ± 1.36	0.00	8.90 ± 1.06	19.74 ± 0.38	110.09	4.30	78.00	17.70
45-46	13.81 ± 1.38	0.00	6.31 ± 0.78	22.16 ± 0.50	99.66	3.30	82.16	14.54
46-47	14.02 ± 1.40	--	--	6.65 ± 0.32	108.81	3.65	74.61	21.74
47-48	14.23 ± 1.42	--	--	3.12 ± 0.08	114.62	4.83	78.32	16.85
48-49	14.50 ± 1.45	--	--	5.53 ± 0.34	108.51	5.69	76.87	17.44
49-50	14.77 ± 1.48	--	--	6.13 ± 0.10	92.63	4.58	77.29	18.13
50-51	15.04 ± 1.50	--	--	4.46 ± 0.03	85.62	3.60	80.45	15.95
51-52	15.31 ± 1.53	--	--	7.63 ± 0.35	96.08	2.96	77.46	19.58
52-53	15.54 ± 1.55	--	--	--	100.85	2.46	78.65	18.89
53-54	15.78 ± 1.58	--	--	--	105.98	2.67	77.73	19.60
54-55	16.07 ± 1.61	--	--	--	106.96	4.78	80.63	14.59
55-56	16.36 ± 1.64	--	--	--	103.14	3.74	76.45	19.81
56-57	16.59 ± 1.66	--	--	--	99.91	4.96	79.12	15.92
57-58	16.82 ± 1.68	--	--	--	96.70	3.64	80.57	15.79
58-59	17.06 ± 1.71	--	--	--	104.09	3.32	87.99	8.69
59-60	17.29 ± 1.73	--	--	--	108.49	1.30	88.86	9.84
60-61	17.54 ± 1.75	--	--	--	103.25	0.50	88.34	11.16
61-62	17.78 ± 1.78	--	--	--	112.90	3.51	87.69	8.80
62-63	18.00 ± 1.80	--	--	--	110.52	0.38	89.23	10.39
63-64	18.21 ± 1.82	--	--	--	116.43	2.79	89.76	7.45
64-65	18.43 ± 1.84	--	--	--	142.87	0.01	89.15	10.84
65-66	18.65 ± 1.87	--	--	--	128.56	1.91	89.68	8.41
66-67	18.89 ± 1.89	--	--	--	117.94	1.44	89.60	8.96
67-68	19.12 ± 1.91	--	--	--	116.58	0.92	89.76	9.32
68-69	19.43 ± 1.94	--	--	--	104.63	1.16	90.36	8.48
69-70	19.74 ± 1.97	--	--	--	91.30	2.27	88.42	9.31
70-72	20.35 ± 2.00	--	--	--	81.30	6.09	85.15	8.76
72-74	21.18 ± 2.05	--	--	--	73.69	2.33	90.51	7.16
74-76	22.28 ± 2.10	--	--	--	62.64	1.79	90.95	7.26
76-78	23.15 ± 2.14	--	--	--	60.09	1.40	90.81	7.79
78-80	23.89 ± 2.18	--	--	--	50.33	1.18	89.69	9.13
80-82	24.71 ± 2.22	--	--	--	111.17	0.70	88.46	10.84
82-84	25.53 ± 2.26	--	--	--	71.43	2.76	89.10	8.14
84-86	26.37 ± 2.31	--	--	--	77.26	0.93	90.51	8.56
86-88	27.28 ± 2.35	--	--	--	74.78	--	--	--
88-90	28.02 ± 2.39	--	--	--	70.60	1.72	91.25	7.03
90-92	28.75 ± 2.42	--	--	--	80.20	0.91	87.63	11.46
92-94	29.46 ± 2.46	--	--	--	87.44	1.29	89.71	9.00
94-96	30.27 ± 2.50	--	--	--	94.96	0.82	91.43	7.75
96-98	31.04 ± 2.54	--	--	--	80.49	0.96	90.76	8.28
98-100	31.92 ± 2.58	--	--	--	86.20	2.53	89.36	8.11

A-10: Physical data for core PR_05_08W, collected 7/23/2008 at N30° 13' 17.10", W89° 38' 37.60"

Depth (cm)	POC (µg/mg)	Bulk Density (g/cm^3)	Porosity φ	d.50 (µm)	Water Content by Weight (%)
0.5	89.76	0.262	0.733	16.82	286.61
1.5	93.55	0.262	0.733	14.23	286.61
2.5	83.94	0.335	0.730	12.74	223.48
3.5	56.05	0.335	0.730	14.66	223.48
4.5	58.12	0.370	0.712	20.57	197.02
5.5	53.87	0.370	0.712	21.55	197.02
6.5	90.35	0.433	0.696	12.49	164.73
7.5	64.35	0.433	0.696	16.17	164.73
8.5	143.80	0.322	0.720	25.40	229.36
9.5	146.07	0.322	0.720	5.83	229.36
10.5	168.75	0.218	0.774	11.91	364.86
11.5	184.07	0.218	0.774	11.60	364.86
12.5	172.56	0.332	0.740	14.57	228.03
13.5	189.07	0.332	0.740	13.04	228.03
14.5	211.01	0.353	0.759	10.09	220.53
15.5	196.53	0.353	0.759	15.86	220.53
16.5	185.54	0.269	0.753	14.96	287.37
17.5	176.74	0.269	0.753	15.89	287.37
18.5	151.15	0.382	0.659	14.33	176.90
19.5	138.91	0.382	0.659	18.81	176.90
20.5	134.38	0.250	0.777	10.55	318.57
21.5	132.07	0.250	0.777	10.89	318.57
22.5	141.50	0.287	0.767	10.55	273.52
23.5	130.23	0.287	0.767	11.61	273.52
24.5	127.26	0.328	0.755	16.78	235.95
25.5	94.11	0.328	0.755	13.38	235.95
26.5	114.34	0.330	0.773	15.05	240.20
27.5	103.93	0.330	0.773	15.43	240.20
28.5	96.30	0.232	0.810	13.19	358.41
29.5	89.55	0.232	0.810	7.25	358.41
30.5	79.66	0.294	0.790	11.39	275.40
31.5	82.52	0.294	0.790	13.05	275.40
32.5	89.99	0.208	0.809	10.47	399.14
33.5	105.77	0.208	0.809	10.19	399.14
34.5	116.47	0.266	0.796	10.81	306.78
35.5	90.01	0.266	0.796	9.74	306.78
36.5	68.30	0.340	0.788	10.59	237.61

Depth (cm)	POC (µg/mg)	Bulk Density (g/cm^3)	Porosity φ	d.50 (µm)	Water Content by Weight (%)
37.5	76.52	0.340	0.788	12.97	237.61
38.5	61.87	0.330	0.748	11.23	232.50
39.5	56.66	0.330	0.748	13.45	232.50
40.5	53.89	0.334	0.828	14.15	253.81
41.5	76.45	0.334	0.828	17.47	253.81
42.5	90.50	0.234	0.841	12.07	367.95
43.5	101.53	0.234	0.841	14.63	367.95
44.5	110.09	0.215	0.803	10.26	383.66
45.5	99.66	0.215	0.803	12.47	383.66
46.5	108.81	0.212	0.831	8.57	401.48
47.5	114.62	0.212	0.831	11.33	401.48
48.5	108.51	0.261	0.804	11.11	315.86
49.5	92.63	0.261	0.804	11.22	315.86
50.5	85.62	0.277	0.826	9.74	305.56
51.5	96.08	0.277	0.826	10.28	305.56
52.5	100.85	0.233	0.833	9.19	366.75
53.5	105.98	0.233	0.833	12.35	366.75
54.5	106.96	0.282	0.803	9.68	291.77
55.5	103.14	0.282	0.803	11.04	291.77
56.5	99.91	0.238	0.827	10.94	355.70
57.5	96.70	0.238	0.827		355.70
58.5	104.09	0.237	0.808	19.95	348.93
59.5	108.49	0.237	0.808	15.35	348.93
60.5	103.25	0.243	0.840	12.39	353.94
61.5	112.90	0.243	0.840	18.88	353.94
62.5	110.52	0.213	0.823	14.16	395.51
63.5	116.43	0.213	0.823	19.68	395.51
64.5	142.87	0.217	0.801	13.05	378.82
65.5	128.56	0.217	0.801	16.61	378.82
66.5	117.94	0.230	0.824	15.67	366.83
67.5	116.58	0.230	0.824	15.78	366.83
68.5	104.63	0.308	0.760	15.92	252.61
69.5	91.30	0.308	0.760	12.67	252.61
71	81.30	0.305	0.763	16.61	256.31
73	73.69	0.418	0.748	16.87	183.58
75	62.64	0.548	0.715	16.73	133.80
77	60.09	0.437	0.756	15.11	177.27
79	50.33	0.369	0.768	15.36	213.55
81	111.17	0.412	0.755	12.54	187.76
83	71.43	0.406	0.746	16.56	188.36

Depth (cm)	POC (µg/mg)	Bulk Density (g/cm^3)	Porosity φ	d.50 (µm)	Water Content by Weight (%)
85	77.26	0.423	0.756	13.94	183.12
89	74.78	0.454	0.746		168.58
91	70.60	0.368	0.772	17.10	215.34
93	80.20	0.366	0.784	11.31	219.57
95	87.44	0.359	0.778	14.61	222.35
97	94.96	0.405	0.771		195.37
99	80.49	0.385	0.777	15.54	207.08

A-11: Physical and Radionuclide data for core PR-06B_08W, collected 9/17/2008 at N30° 13' 14.60", W89° 38' 39.90"

Depth interval (cm)	Cumulative mass depth (g cm^{-2})	^{7}Be (mBq g^{-1})	^{137}Cs (mBq g^{-1})	^{210}Pb$_{xs}$ (mBq g^{-1})	POC (µg mg^{-1})	% Sand	% Silt	% Clay
0-1	0.25 ± 0.03	2.14 ± 0.20	3.12 ± 0.38	54.35 ± 3.47	71.15	5.26	83.52	11.22
1-2	0.51 ± 0.05	12.52 ± 1.26	3.59 ± 0.36	49.12 ± 2.59	59.88	8.37	80.32	11.31
2-3	0.80 ± 0.08	0.00	4.88 ± 0.57	33.04 ± 1.78	50.37	8.39	82.38	9.23
3-4	1.09 ± 0.11	0.00	4.32 ± 0.37	54.01 ± 2.59	48.47	5.52	85.66	8.82
4-5	1.46 ± 0.15	0.00	4.23 ± 0.50	65.58 ± 4.35	58.94	5.59	84.83	9.58
5-6	1.83 ± 0.18	0.00	5.09 ± 0.48	56.19 ± 4.26	64.04	8.17	80.08	11.75
6-7	2.17 ± 0.22	0.00	5.41 ± 0.71	70.35 ± 3.93	76.61	7.94	80.82	11.24
7-8	2.52 ± 0.25	0.00	6.09 ± 0.69	62.97 ± 3.23	105.05	5.65	83.00	11.35
8-9	2.78 ± 0.28	0.00	3.63 ± 0.44	89.87 ± 3.45	175.74	5.64	86.63	7.73
9-10	3.04 ± 0.30	0.00	2.45 ± 0.30	113.78 ± 7.28	232.34	15.22	69.79	14.99
10-11	3.21 ± 0.32	0.00	2.11 ± 0.27	155.43 ± 7.01	227.06	8.44	81.50	10.06
11-12	3.39 ± 0.34	0.00	3.47 ± 0.41	181.52 ± 8.47	256.50	7.17	82.77	10.06
12-13	3.51 ± 0.35	0.00	3.89 ± 0.54	177.33 ± 7.49	256.38	3.93	88.44	7.63
13-14	3.64 ± 0.36	0.00	4.20 ± 0.46	175.08 ± 6.78	281.46	8.84	85.40	5.76
14-15	3.76 ± 0.38	0.00	4.52 ± 0.32	224.11 ± 13.50	255.98	3.22	82.44	14.34
15-16	3.88 ± 0.39	0.00	5.68 ± 0.47	174.36 ± 8.89	283.04	9.25	84.59	6.16
16-17	3.99 ± 0.40	0.00	5.09 ± 0.63	156.82 ± 9.90	253.17	14.70	77.79	7.51
17-18	4.11 ± 0.41	0.00	5.86 ± 0.77	147.31 ± 5.99	253.69	12.28	79.98	7.74
18-19	4.23 ± 0.42	0.00	7.76 ± 0.65	126.90 ± 5.79	218.14	11.91	77.21	10.88
19-20	4.36 ± 0.44	0.00	3.63 ± 0.43	148.10 ± 6.86	227.42	0.78	47.38	51.84
20-21	4.50 ± 0.45	0.00	9.48 ± 1.23	103.70 ± 4.83	205.60	11.46	78.47	10.07
21-22	4.65 ± 0.47	0.00	9.54 ± 1.29	85.02 ± 3.40	178.43	9.64	79.49	10.87
22-23	4.81 ± 0.48	0.00	10.09 ± 1.16	66.68 ± 2.97	140.95	8.42	75.51	16.07
23-24	4.97 ± 0.50	0.00	13.99 ± 1.05	55.04 ± 4.34	119.65	12.60	77.10	10.30
24-25	5.11 ± 0.51	0.00	25.23 ± 1.41	81.67 ± 3.86	171.24	1.23	81.64	17.13
25-26	5.25 ± 0.53	0.00	32.27 ± 1.39	55.05 ± 2.25	177.73	8.47	75.01	16.52
26-27	5.39 ± 0.54	0.00	28.54 ± 3.04	44.14 ± 1.88	195.12	8.15	79.31	12.54
27-28	5.53 ± 0.55	0.00	47.52 ± 1.87	50.97 ± 2.70	156.86	5.40	80.71	13.89
28-29	5.70 ± 0.57	0.00	52.19 ± 5.11	49.12 ± 2.12	152.34	6.48	79.74	13.78
29-30	5.86 ± 0.59	0.00	59.93 ± 5.86	64.65 ± 3.64	151.85	2.38	75.92	21.70
30-31	6.02 ± 0.60	0.00	82.29 ± 6.82	43.49 ± 1.86	154.32	3.20	78.03	18.77
31-32	6.19 ± 0.62	0.00	127.13 ± 14.23	48.46 ± 2.22	176.58	3.49	80.77	15.74
32-33	6.36 ± 0.64	0.00	106.91 ± 11.98	35.38 ± 1.88	154.64	4.00	87.20	8.80
33-34	6.53 ± 0.65	0.00	67.30 ± 7.55	33.28 ± 2.17	133.59	7.86	81.32	10.82
34-35	6.83 ± 0.68	0.00	46.98 ± 5.41	41.45 ± 1.63	86.50	3.35	78.81	17.84
35-36	7.12 ± 0.71	0.00	28.91 ± 3.45	20.60 ± 1.64	72.32	2.82	79.49	17.69
36-37	7.36 ± 0.74	--	--	24.00 ± 1.43	95.82	3.55	76.82	19.63
37-38	7.59 ± 0.76	--	--	20.77 ± 0.94	111.25	5.66	79.60	14.74
38-39	7.74 ± 0.77	--	--	32.83 ± 1.89	125.35	6.68	80.05	13.27
39-40	7.89 ± 0.79	--	--	38.51 ± 1.77	148.38	5.02	82.87	12.11
40-41	8.06 ± 0.81	--	--	26.85 ± 1.74	147.30	5.65	81.01	13.34
41-42	8.23 ± 0.82	--	--	23.90 ± 1.68	126.77	5.42	80.95	13.63
42-43	8.39 ± 0.84	--	--	22.51 ± 1.99	168.16	2.53	78.36	19.11

Depth interval (cm)	Cumulative mass depth (g cm^{-2})	^{7}Be (mBq g^{-1})	^{137}Cs (mBq g^{-1})	^{210}Pb$_{xs}$ (mBq g^{-1})	POC (µg mg^{-1})	% Sand	% Silt	% Clay
43-44	8.54 ± 0.85	--	--	12.81 ± 0.82	170.85	2.07	76.44	21.49
44-45	8.73 ± 0.87	--	--	20.62 ± 1.09	121.59	3.98	77.66	18.36
45-46	8.91 ± 0.89	--	--	16.09 ± 0.97	139.80	4.75	79.33	15.92
46-47	9.08 ± 0.91	--	--	12.03 ± 0.96	128.22	5.86	79.27	14.87
47-48	9.25 ± 0.93	--	--	7.11 ± 0.57	144.24	3.22	86.26	10.52
48-49	9.43 ± 0.94	--	--	4.89 ± 0.42	130.33	0.49	90.26	9.25
49-50	9.61 ± 0.96	--	--	19.32 ± 0.86	139.86	2.00	89.67	8.33
50-51	9.77 ± 0.98	--	--	10.69 ± 0.84	106.02	1.50	85.54	12.96
51-52	9.92 ± 0.99	--	--	7.68 ± 0.56	111.19	2.91	88.84	8.25
52-53	10.07 ± 1.01	--	--	4.42 ± 0.30	106.81	1.98	88.74	9.28
53-54	10.21 ± 1.02	--	--	9.74 ± 0.80	125.74	1.13	88.90	9.97
54-55	10.36 ± 1.04	--	--	3.36 ± 0.17	121.36	0.45	90.32	9.23
55-56	10.52 ± 1.05	--	--	4.20 ± 0.16	143.17	0.33	90.93	8.74
56-57	10.71 ± 1.07	--	--	2.44 ± 0.41	130.29	1.21	89.07	9.72
57-58	10.90 ± 1.09	--	--	6.58 ± 0.23	132.17	1.02	90.41	8.57
58-59	11.11 ± 1.11	--	--	--	107.03	0.37	90.35	9.28
59-60	11.32 ± 1.13	--	--	--	126.20	0.86	91.50	7.64
60-61	11.51 ± 1.15	--	--	--	122.23	0.23	91.46	8.31
61-62	11.70 ± 1.17	--	--	--	95.34	0.40	89.91	9.69
62-63	11.87 ± 1.19	--	--	--	99.16	1.56	91.01	7.43
63-64	12.04 ± 1.20	--	--	--	114.95	0.73	91.00	8.27
64-65	12.23 ± 1.22	--	--	--	99.30	0.28	91.58	8.14
65-66	12.42 ± 1.24	--	--	--	72.80	0.59	92.45	6.96
66-67	12.60 ± 1.26	--	--	--	101.06	0.15	92.52	7.33
67-68	12.78 ± 1.28	--	--	--	99.68	0.37	91.31	8.32
68-69	12.96 ± 1.30	--	--	--	134.21	0.55	89.37	10.08
69-70	13.14 ± 1.31	--	--	--	119.14	1.21	90.17	8.62
70-71	13.34 ± 1.33	--	--	--	98.24	2.31	90.12	7.57
71-72	13.53 ± 1.35	--	--	--	127.79	5.49	85.36	9.15
72-73	13.72 ± 1.37	--	--	--	136.72	5.55	87.04	7.41
73-74	13.90 ± 1.39	--	--	--	214.80	3.55	88.60	7.85
74-75	14.06 ± 1.41	--	--	--	140.32	1.43	88.83	9.74
75-76	14.21 ± 1.42	--	--	--	132.74	1.32	86.62	12.06
76-77	14.39 ± 1.44	--	--	--	159.69	0.36	90.87	8.77
77-78	14.56 ± 1.46	--	--	--	147.66	1.55	87.60	10.85
78-79	14.70 ± 1.47	--	--	--	234.51	4.55	88.12	7.33
79-80	14.84 ± 1.48	--	--	--	184.90	3.65	88.84	7.51
80-81	14.99 ± 1.50	--	--	--	138.87	5.64	86.73	7.63
81-82	15.14 ± 1.51	--	--	--	178.85	1.84	90.76	7.40
82-83	15.29 ± 1.53	--	--	--	238.05	2.54	89.89	7.57
83-84	15.43 ± 1.54	--	--	--	134.62	3.21	90.87	5.92
84-85	15.61 ± 1.56	--	--	--	182.88	0.60	87.88	11.52
85-86	15.79 ± 1.58	--	--	--	170.99	2.56	89.83	7.61
86-87	15.97 ± 1.60	--	--	--	201.09	2.25	89.91	7.84
87-88	16.15 ± 1.62	--	--	--	188.61	3.32	88.68	8.00
88-89	16.29 ± 1.63	--	--	--	99.22	0.90	89.37	9.73
89-90	16.42 ± 1.64	--	--	--	176.14	10.23	80.85	8.92

Depth interval (cm)	Cumulative mass depth (g cm^{-2})	^{7}Be (mBq g^{-1})	^{137}Cs (mBq g^{-1})	$^{210}Pb_{xs}$ (mBq g^{-1})	POC (µg mg^{-1})	% Sand	% Silt	% Clay
90-92	16.83 ± 1.66	--	--	--	117.45	5.46	88.52	6.02
92-94	17.23 ± 1.68	--	--	--	170.79	0.04	89.67	10.29
94-96	17.64 ± 1.70	--	--	--	177.81	6.38	86.74	6.88
96-98	17.98 ± 1.72	--	--	--	152.22	1.43	90.13	8.44
98-100	18.31 ± 1.74	--	--	--	182.37	2.48	89.52	8.00

A-12: Physical data for core PR_06_08W, collected 9/17/2008 at N30° 13' 14.60", W89° 38' 39.90"

Depth (cm)	POC (µg/mg)	Bulk Density (g/cm^3)	Porosity φ	d.50 (µm)	Water Content by Weight (%)
0.5	71.15	0.251	0.813	20.67	331.82
1.5	59.88	0.251	0.813	18.23	331.82
2.5	50.37	0.293	0.798	20.58	279.58
3.5	48.47	0.293	0.798	20.55	279.58
4.5	58.94	0.370	0.761	17.06	210.86
5.5	64.04	0.370	0.761	17.98	210.86
6.5	76.61	0.349	0.745	18.89	218.88
7.5	105.05	0.349	0.745	14.78	218.88
8.5	175.74	0.262	0.722	17.50	282.36
9.5	232.34	0.262	0.722	14.11	282.36
10.5	227.06	0.170	0.833	14.27	500.64
11.5	256.50	0.170	0.833	13.10	500.64
12.5	256.38	0.128	0.856	12.61	683.60
13.5	281.46	0.128	0.856	19.35	683.60
14.5	255.98	0.122	0.850	11.65	715.60
15.5	283.04	0.122	0.850	19.63	715.60
16.5	253.17	0.112	0.861	17.75	786.87
17.5	253.69	0.112	0.861	18.69	786.87
18.5	218.14	0.122	0.834	15.00	700.09
19.5	227.42	0.122	0.834	3.67	700.09
20.5	205.60	0.141	0.863	14.57	628.16
21.5	178.43	0.141	0.863	13.55	628.16
22.5	140.95	0.161	0.818	11.73	519.68
23.5	119.65	0.161	0.818	16.82	519.68
24.5	171.24	0.142	0.836	10.93	604.19
25.5	177.73	0.142	0.836	10.35	604.19
26.5	195.12	0.142	0.822	13.68	591.62
27.5	156.86	0.142	0.822	11.62	591.62
28.5	152.34	0.163	0.818	11.77	513.59
29.5	151.85	0.163	0.818	8.35	513.59
30.5	154.32	0.165	0.811	8.61	503.76
31.5	176.58	0.165	0.811	10.05	503.76
32.5	154.64	0.171	0.841	13.85	504.87
33.5	133.59	0.171	0.841	14.52	504.87
34.5	86.50	0.296	0.790	9.72	273.29
35.5	72.32	0.296	0.790	9.65	273.29
36.5	95.82	0.235	0.797	10.11	346.90
37.5	111.25	0.235	0.797	11.19	346.90

Depth (cm)	POC (µg/mg)	Bulk Density (g/cm^3)	Porosity φ	d.50 (µm)	Water Content by Weight (%)
38.5	125.35	0.155	0.848	12.35	558.82
39.5	148.38	0.155	0.848	13.25	558.82
40.5	147.30	0.171	0.860	12.10	515.77
41.5	126.77	0.171	0.860	11.94	515.77
42.5	168.16	0.157	0.847	8.91	554.39
43.5	170.85	0.157	0.847	8.28	554.39
44.5	121.59	0.178	0.834	9.16	480.00
45.5	139.80	0.178	0.834	10.74	480.00
46.5	128.22	0.168	0.812		496.81
47.5	144.24	0.168	0.812	14.25	496.81
48.5	130.33	0.182	0.811	15.89	457.60
49.5	139.86	0.182	0.811	15.30	457.60
50.5	106.02	0.155	0.802	11.45	528.75
51.5	111.19	0.155	0.802	18.87	528.75
52.5	106.81	0.147	0.856	13.54	597.87
53.5	125.74	0.147	0.856	11.85	597.87
54.5	121.36	0.152	0.873	14.45	586.97
55.5	143.17	0.152	0.873	14.19	586.97
56.5	130.29	0.187	0.831	13.36	454.53
57.5	132.17	0.187	0.831	13.60	454.53
58.5	107.03	0.211	0.790	12.89	384.43
59.5	126.20	0.211	0.790	15.35	384.43
60.5	122.23	0.189	0.793	13.11	429.11
61.5	95.34	0.189	0.793	11.36	429.11
62.5	99.16	0.169	0.802	15.94	486.54
63.5	114.95	0.169	0.802	14.38	486.54
64.5	99.30	0.180	0.845	15.33	480.99
65.5	72.80	0.180	0.845	18.20	480.99
66.5	101.06	0.186	0.786	15.00	433.76
67.5	99.68	0.186	0.786	12.49	433.76
68.5	134.21	0.180	0.841	13.42	478.82
69.5	119.14	0.180	0.841	14.04	478.82
70.5	98.24	0.191	0.844	15.69	453.11
71.5	127.79	0.191	0.844	18.07	453.11
72.5	136.72	0.180	0.844		481.65
73.5	214.80	0.180	0.844	16.93	481.65
74.5	140.32	0.161	0.816	12.38	520.61
75.5	132.74	0.161	0.816	16.60	520.61
76.5	159.69	0.168	0.833	13.73	507.52
77.5	147.66	0.168	0.833	12.66	507.52

Depth (cm)	POC (µg/mg)	Bulk Density (g/cm^3)	Porosity φ	d.50 (µm)	Water Content by Weight (%)
78.5	234.51	0.148	0.845		587.24
79.5	184.90	0.148	0.845	18.25	587.24
80.5	138.87	0.150	0.839	21.72	572.13
81.5	178.85	0.150	0.839	17.73	572.13
82.5	238.05	0.144	0.852	20.19	607.25
83.5	134.62	0.144	0.852	17.58	607.25
84.5	182.88	0.173	0.885	12.45	523.18
85.5	170.99	0.173	0.885		523.18
86.5	201.09	0.192	0.958	19.64	511.92
87.5	188.61	0.192	0.958		511.92
88.5	99.22	0.131	0.832	14.26	650.25
89.5	176.14	0.131	0.832		650.25

A-13: Kinematic GPS survey data across coring transect, all elevations relative to the North American Vertical Datum, 1983 (NAVD83)

North Latitude	West Longitude	Elevation (m)
30.223884	-89.642431	0.383
30.223884	-89.642431	0.409
30.223849	-89.642453	0.327
30.223826	-89.642469	0.266
30.223803	-89.642485	0.338
30.223775	-89.642508	0.331
30.223739	-89.642528	0.38
30.223695	-89.642549	0.375
30.223695	-89.642549	0.387
30.223662	-89.642564	0.41
30.223617	89.642588	0.385
30.223581	89.642608	0.365
30.223553	-89.642624	0.388
30.223527	-89.642641	0.352
30.223478	-89.642656	0.425
30.223444	-89.64267	0.338
30.223414	-89.642689	0.397
30.223385	-89.642703	0.343
30.22336	-89.642716	0.356
30.223324	-89.642735	0.333
30.22328	-89.64275	0.345
30.223234	-89.642767	0.326
30.223183	-89.642791	0.363
30.223128	-89.64282	0.365
30.223088	-89.642838	0.272
30.223036	-89.642863	0.287
30.222995	-89.642882	0.311
30.222948	-89.64291	0.237
30.222895	-89.64294	0.26
30.222848	-89.642957	0.318
30.222805	-89.642973	0.25
30.222764	-89.643004	0.185
30.22274	-89.643015	-0.264
30.221816	-89.643488	-0.193
30.221799	-89.643498	0.012

North Latitude	West Longitude	Elevation (m)
30.221782	-89.643508	0.355
30.221751	-89.643525	0.482
30.221701	-89.643558	0.527
30.22165	-89.64358	0.384
30.221611	-89.643603	0.345
30.221573	-89.643624	0.314
30.221534	-89.643645	0.37
30.221495	-89.643667	0.509
30.221449	-89.643701	0.513
30.221411	-89.643725	0.453
30.221376	-89.643748	0.324
30.221337	-89.643773	0.371
30.221294	-89.643796	0.373
30.221238	-89.643833	0.376
30.221197	-89.643869	0.486
30.221166	-89.643886	0.405
30.221124	-89.64391	0.464
30.221069	-89.643938	0.434
30.221022	-89.643968	0.427
30.220969	-89.643998	0.461
30.220923	-89.644031	0.422
30.220869	-89.644077	0.422
30.220827	-89.64413	0.357
30.220781	-89.644184	0.417
30.220743	-89.64423	0.398
30.220718	-89.64427	0.373
30.220671	-89.644324	0.379
30.220641	-89.644364	0.467
30.220589	-89.644432	0.408
30.220589	-89.644432	0.392
30.220589	-89.644432	0.417
30.220589	-89.644432	0.425

APPENDIX B

SPEARMAN CORRELATIONS

N.S. – Not Significant (Spearman Correlation value between -0.49 and 0.49, or $p > 0.05$)
* -- $p <= 0.05$
** -- $p <= 0.01$
*** $p <= 0.001$
$\alpha = 0.05$

B-1: Spearman Correlation Coefficient Matrix showing the interaction between POC and all other parameters within the ^{137}Cs sedimentary unit.

POC	1	2	3	4	5	6
Bulk Density	-0.81***	-0.71***	-0.68**	-0.92***	N.S.	-0.92***
Porosity	0.74**	N.S.	N.S.	N.S.	-0.63**	0.73***
d.50	N.S.	N.S.	N.S.	N.S.	N.S.	N.S.
Water content by weight	0.81***	0.68**	0.67**	0.95***	N.S.	0.92***
Depth	-0.62*	-0.86***	-0.75***	-0.74***	-0.95***	-0.82***

B-2: Spearman Correlation Coefficient Matrix showing the interaction between POC and all other parameters $^{210}Pb_{xs}$ sedimentary unit.

POC	1	2	3	4	5	6
Bulk Density	N.S.	-0.68**	N.S.	N.S.	-0.75*	-0.84**
Porosity	N.S.	0.50*	N.S.	N.S.	0.75*	0.75*
d.50	N.S.	N.S.	0.53*	N.S.	N.S.	N.S.
Water content by weight	N.S.	0.73***	N.S.	N.S.	0.75	0.74*
Depth	N.S.	0.61**	N.S.	N.S.	N.S.	-0.70*

B-3: Spearman Correlation Coefficient Matrix showing the interaction between Bulk Density and all other parameters within the ^{137}Cs sedimentary unit.

Bulk Density	1	2	3	4	5	6
POC	-0.81***	-0.71***	-0.68**	-0.92*	N.S.	-0.92***
Porosity	-0.83***	N.S.	N.S.	N.S.	-0.68***	-0.79***
d.50	N.S.	N.S.	N.S.	N.S.	N.S.	N.S.
Water content by weight	-0.94***	-0.83***	-0.88***	-0.98***	-0.98***	-1.00***
Depth	0.71**	0.56*	0.53*	0.68**	N.S.	0.90***

B-4: Spearman Correlation Coefficient Matrix showing the interaction between Bulk Density and all other parameters $^{210}Pb_{xs}$ sedimentary unit.

Bulk Density	1	2	3	4	5	6
POC	N.S.	-0.68**	N.S.	N.S.	-0.75*	-0.84**
Porosity	N.S.	-0.57*	-0.80***	-0.87***	-1.00***	-0.74*
d.50	N.S.	N.S.	N.S.	N.S.	N.S.	N.S.
Water content by weight	N.S.	-0.96***	-0.98***	N.S.	-1.00***	-0.86***
Depth	N.S.	N.S.	N.S.	N.S.	N.S.	0.85***

B-5: Spearman Correlation Coefficient Matrix showing the interaction between Porosity and all other parameters within the ^{137}Cs sedimentary unit.

Porosity	1	2	3	4	5	6
POC	0.74**	N.S.	N.S.	N.S.	-0.63**	0.73***
Bulk Density	-0.83***	N.S.	N.S.	N.S.	-0.68***	-0.79***
d.50	N.S.	N.S.	N.S.	N.S.	-0.55*	N.S.
Water content by weight	0.94***	N.S.	N.S.	N.S.	0.74***	0.79***
Depth	N.S.	N.S.	N.S.	N.S.	0.72***	0.62*

B-6: Spearman Correlation Coefficient Matrix showing the interaction between Porosity and all other parameters $^{210}Pb_{xs}$ sedimentary unit.

Porosity	1	2	3	4	5	6
POC	N.S.	0.50*	N.S.	N.S.	0.75*	0.75*
Bulk Density	N.S.	-0.57*	-0.80***	-0.87***	-1.00***	-0.74*
d.50	N.S.	N.S.	N.S.	N.S.	N.S.	N.S.
Water content by weight	0.70**	0.76***	0.86***	N.S.	1.00***	0.95***
Depth	N.S.	N.S.	0.50*	N.S.	N.S.	N.S.

B-7: Spearman Correlation Coefficient Matrix showing the interaction between d.50 and all other parameters within the ^{137}Cs sedimentary unit.

d.50	1	2	3	4	5	6
POC	N.S.	N.S.	0.53*	N.S.	N.S.	N.S.
Bulk Density	N.S.	N.S.	N.S.	N.S.	N.S.	N.S.
Porosity	N.S.	N.S.	N.S.	N.S.	N.S.	N.S.
Water content by weight	-0.61**	N.S.	N.S.	0.53*	N.S.	N.S.
Depth	N.S.	N.S.	N.S.	N.S.	N.S.	-0.52*

B-8: Spearman Correlation Coefficient Matrix showing the interaction between d.50 and all other parameters $^{210}Pb_{xs}$ sedimentary unit.

d.50	1	2	3	4	5	6
POC	N.S.	N.S.	0.53*	N.S.	N.S.	N.S.
Bulk Density	N.S.	N.S.	N.S.	N.S.	N.S.	N.S.
Porosity	N.S.	N.S.	N.S.	N.S.	N.S.	N.S.
Water content by weight	-0.61**	N.S.	N.S.	0.53*	N.S.	N.S.
Depth	N.S.	N.S.	N.S.	N.S.	N.S.	N.S.

B-9: Spearman Correlation Coefficient Matrix showing the interaction between water content by weight and all other parameters within the ^{137}Cs sedimentary unit

Water content by weight	1	2	3	4	5	6
POC	0.81***	0.68**	0.67**	0.95***	N.S.	0.92***
Bulk Density	-0.94***	-0.83***	-0.88***	-0.98***	-0.98***	-1.00***
Porosity	0.94***	N.S.	N.S.	N.S.	0.74***	0.79***
d.50	N.S.	N.S.	N.S.	N.S.	N.S.	N.S.
Depth	N.S.	-0.60**	N.S.	-0.70**	0.52*	-0.90***

B-10: Spearman Correlation Coefficient Matrix showing the interaction between water content by weight and all other parameters $^{210}Pb_{xs}$ sedimentary unit

Water content by weight	1	2	3	4	5	6
POC	N.S.	0.73***	N.S.	N.S.	0.75*	0.74*
Bulk Density	N.S.	-0.96***	-0.98***	N.S.	-1.00***	-0.86***
Porosity	0.70**	0.76***	0.86***	N.S.	1.00***	0.95***
d.50	-0.61**	N.S.	N.S.	0.53*	N.S.	N.S.
Depth	N.S.	N.S.	N.S.	-0.77***	N.S.	-0.71*

B-11: Spearman Correlation Coefficient Matrix showing the interaction between depth and all other parameters within the ^{137}Cs sedimentary unit

Depth	1	2	3	4	5	6
POC	-0.62*	-0.86***	-0.75**	-0.74***	-0.95***	-0.82***
Bulk Density	0.71**	0.56*	0.53*	0.68**	N.S.	0.90***
Porosity	N.S.	N.S.	N.S.	N.S.	0.72***	0.62*
d.50	N.S.	N.S.	N.S.	N.S.	N.S.	-0.52*
Water content by weight	N.S.	-0.60**	N.S.	-0.70**	0.52*	-0.90***

B-12: Spearman Correlation Coefficient Matrix showing the interaction between depth and all other parameters $^{210}Pb_{xs}$ sedimentary unit

Depth	1	2	3	4	5	6
POC	N.S.	0.61**	N.S.	N.S.	N.S.	-0.70*
Bulk Density	N.S.	N.S.	N.S.	N.S.	N.S.	0.85***
Porosity	N.S.	N.S.	0.50*	N.S.	N.S.	N.S.
d.50	N.S.	N.S.	N.S.	N.S.	N.S.	N.S.
Water content by weight	N.S.	N.S.	N.S.	-0.77***	N.S.	-0.71*

APPENDIX C

AVERAGED SEDIMENTARY PROPERTY VALUES

C-1: Average bulk density values for the ^{137}Cs and $^{210}Pb_{xs}$ sediment unit

Station	^{137}Cs Sediment Unit Average Bulk Density (g/cm^3)	$^{210}Pb_{xs}$ Sediment Unit Average Bulk Density (g/cm^3)
PR_01_08W	0.327 ± 0.030	0.338 ± 0.020
PR_02_08W	0.189 ± 0.018	0.218 ± 0.043
PR_03_08W	0.282± 0.036	0.391 ± 0.058
PR_04_08W	0.606 ± 0.098	0.695 ± 0.063
PR_05_08W	0.302 ± 0.050	0.268 ± 0.048
PR_06_08W	0.138 ± 0.018	0.211 ± 0.056

C-2: Average water content by weight values for the ^{137}Cs and $^{210}Pb_{xs}$ sediment unit

Station	^{137}Cs Sediment Unit Average Water Content by Weight (%)	$^{210}Pb_{xs}$ Sediment Unit Average Water Content by Weight (%)
PR_01_08W	208.67 ± 20.85	192.33 ± 12.34
PR_02_08W	443.34 ± 44.57	387.07 ± 71.47
PR_03_08W	290.45 ± 33.11	209.32 ± 35.57
PR_04_08W	118.54 ± 20.37	359.49 ± 372.97
PR_05_08W	260.96 ± 55.97	314.32 ± 62.47
PR_06_08W	635.48 ± 90.76	419.03 ± 106.61

C-3: Average POC values for the ^{137}Cs and $^{210}Pb_{xs}$ sediment unit

Station	^{137}Cs Sediment Unit Average POC (µg/mg)	$^{210}Pb_{xs}$ Sediment Unit Average POC (µg/mg)
PR_01_08W	197.67 ± 30.40	177.33 ± 15.35
PR_02_08W	151.53 ± 19.31	113.67 ± 22.60
PR_03_08W	114.87 ± 24.93	72.88 ± 7.84
PR_04_08W	50.57 ± 15.31	31.27 ± 4.64
PR_05_08W	142.45 ± 39.47	90.39 ± 16.24
PR_06_08W	201.33 ± 51.03	126.32 ± 36.19

C-4: Average porosity values for the ^{137}Cs and $^{210}Pb_{xs}$ sediment unit

Station	^{137}Cs Sediment Unit Average Porosity (%)	$^{210}Pb_{xs}$ Sediment Unit Average Porosity (%)
PR_01_08W	65.91 ± 1.57	63.22 ± 3.20
PR_02_08W	79.50 ± 2.15	79.50 ± 2.15
PR_03_08W	78.70 ± 1.00	78.01 ± 2.45
PR_04_08W	68.25 ± 2.37	66.34 ± 1.99
PR_05_08W	75.75 ± 3.87	79.69 ± 0.89
PR_06_08W	83.88 ± 1.78	81.06 ± 1.98

C-5: Average d.50 values for the ^{137}Cs and $^{210}Pb_{xs}$ sediment unit

Station	^{137}Cs Sediment Unit Average d. 50 Value (µm)	$^{210}Pb_{xs}$ Sediment Unit Average d. 50 Value (µm)
PR_01_08W	9.50 ± 5.83	19.31 ± 7.36
PR_02_08W	13.77 ± 3.89	12.57 ± 2.06
PR_03_08W	14.10 ± 1.77	11.09 ± 2.85
PR_04_08W	22.39 ± 11.55	16.14 ± 3.50
PR_05_08W	13.26 ± 2.77	10.89 ± 1.08
PR_06_08W	13.48 ± 4.21	10.67 ± 2.16

C-6: Average annual rate of autocompaction for the ^{137}Cs and $^{210}Pb_{xs}$ sediment unit

Station	^{137}Cs Sediment Unit Average Rate of Autocompaction (cm/y)	$^{210}Pb_{xs}$ Sediment Unit Average Rate of Autocompaction (cm/y)
PR_01_08W	0.11 ± 0.03	0.10 ± 0.02
PR_02_08W	0.39 ± 0.05	0.22 ± 0.08
PR_03_08W	0.22 ± 0.05	0.18 ± 0.06
PR_04_08W	0.30 ± 0.09	0.12 ± 0.03
PR_05_08W	0.42 ± 0.10	0.07 ± 0.02
PR_06_08W	0.27 ± 0.06	0.12 ± 0.06

C-7: Average annual rate of accretion for the ^{137}Cs and $^{210}Pb_{xs}$ sediment unit

Station	^{137}Cs Sediment Unit Average Annual Accretion (cm/y)	$^{210}Pb_{xs}$ Sediment Unit Average Annual Accretion (cm/y)
PR_01_08W	0.31 ± 0.03	0.30 ± 0.02
PR_02_08W	0.58 ± 0.05	0.38 ± 0.08
PR_03_08W	0.40 ± 0.05	0.37 ± 0.06
PR_04_08W	0.58 ± 0.09	0.34 ± 0.03
PR_05_08W	0.67 ± 0.11	0.14 ± 0.02
PR_06_08W	0.44 ± 0.06	0.24 ± 0.06

C-8: Average annual rate of sedimentation for the ^{137}Cs and $^{210}Pb_{xs}$ sediment unit

Station	^{137}Cs Sediment Unit Average Annual Sedimentation (cm/y)	$^{210}Pb_{xs}$ Sediment Unit Average Annual Sedimentation (cm/y)
PR_01_08W	0.29 ± 0.04	0.29 ± 0.03
PR_02_08W	0.46 ± 0.03	0.32 ± 0.03
PR_03_08W	0.39 ± 0.03	0.31 ± 0.03
PR_04_08W	0.43 ± 0.03	0.30 ± 0.03
PR_05_08W	0.48 ± 0.03	0.15 ± 0.007
PR_06_08W	0.41± 0.03	0.18 ± 0.06

C-9: Average annual rate of elevation change for the ^{137}Cs and $^{210}Pb_{xs}$ sediment unit

Station	^{137}Cs Sediment Unit Average Annual Elevation Change (cm/y)	$^{210}Pb_{xs}$ Sediment Unit Average Annual Elevation Change (cm/y)
PR_01_08W	0.20 ± 0.01	0.21 ± 0.004
PR_02_08W	0.19 ± 0.01	0.16 ± 0.01
PR_03_08W	0.17 ± 0.01	0.19 ± 0.01
PR_04_08W	0.28 ± 0.03	0.22 ± 0.01
PR_05_08W	0.25 ± 0.03	0.07 ± 0.001
PR_06_08W	0.18 ± 0.01	0.12 ± 0.01

APPENDIX D

CALCULATIONS

Abbreviations for ^{137}Cs Sedimentary Unit:

p – Number of annual layers

D_p – Depth to the 1963/1964 ^{137}Cs peak (cm)

D_n – Depth to the compaction limit (cm)

B_1 – Bulk density of layer 1 (g/cm3)

B_p – Density of the layer at the 1963/1964 ^{137}Cs peak horizon (g/cm3)

B_n – Compaction limit of sediment (g/cm3)

$B_{av1\text{-}p}$ – Average bulk density of the ^{137}Cs sedimentary unit (g/cm3)

T_1 – Thickness of layer 1 (cm)

T_n – Thickness of layer n (cm)

T_p – Thickness of layer p (cm)

C – Average annual rate of autocompaction (cm/y)

$T_1/(D_p/p)$ – Average annual accretion vs. Average annual sedimentation

T_1 / T_n – Average annual accretion vs. Average annual elevation change

$(D_p/p) / T_n$ – Average annual sedimentation vs. Average annual elevation change

Example of calculations for PR_01_08

$$\mathbf{T_1 = ((D_p/p) / (B_1/B_{av1\text{-}p})}$$

$T_1 = ((12/41.5) / (0.308/0.327)) = 0.31$ cm

$$\mathbf{T_p = (B_1/B_p) * T_1}$$

$T_p = (0.308/0.327) * 0.31 = 0.28$ cm

$$\mathbf{T_n = (B_1/B_n) * T_1}$$

T_n= (0.308/0.479) * 0.31 = 0.21

$C = T_1 - T_n$

C = 0.31 – 0.20 = 0.11

E-1: Physical properties and calculated values

Core #	P	D_p	D_n	B_1	B_p	B_n	$B_{av1\text{-}p}$	T_1	T_p	T_n	C
1	41.5	12	323	0.308	0.327	0.479	0.327	0.31	0.29	0.20	0.11
2	41.5	19	351	0.148	0.186	0.453	0.189	0.58	0.47	0.19	0.39
3	41.5	16	107	0.274	0.328	0.635	0.281	0.40	0.33	0.17	0.22
4	41.5	18	337	0.454	0.624	0.95	0.606	0.58	0.42	0.28	0.30
5	41.5	20	303	0.218	0.294	0.589	0.302	0.67	0.50	0.25	0.42
6	41.5	17	381	0.128	0.163	0.320	0.138	0.44	0.35	0.18	0.26

E-2: Averaged bulk density values with standard of deviations

Bulk Density	PR_01_08	PR_02_08	PR_03_08	PR_04_08	PR_05_08	PR_06_08
Average	0.327	0.189	0.282	0.606	0.302	0.138
STDEV	0.030	0.018	0.036	0.098	0.050	0.018

Propagation of error for PR_01_08 ^{137}Cs Sedimentary Unit:

$T_1 = T_1 * ((B_{av1\text{-}p}\ STDEV/B_{av1\text{-}p}) + (D_p\ error/D_p))^{1/2}$

$T1 = 0.31 * ((0.030/0.327) + (0.5/0.29))^{1/2} = 0.03$

$T_p = (T_{1\ propogated\ error})*T_p$

$T_p = (0.03) * 0.29 = 0.01$

$T_n = (T_{1\ propogated\ error})*T_n$

$Tn = 0.03 * 0.20 = 0.01$

$C = ((T_{1\ propogated\ error})^{\wedge 2} - (T_{n\ propogated\ error}{}^{\wedge 2}))^{1/2}$

$C = (0.03)^2 - (0.01)^2)^{1/2} = 0.03$

E-3: Comparing changing elevation, annual sedimentation, and annual accretion in the ^{137}Cs sedimentary unit

Core #	p	D_p	T_1	T_n	D_p/p	$T_1/(D_p/p)$	T_1/T_n	$(D_p/p)/T_n$
1	41.5	12	0.31	0.20	0.29	1.06	1.56	1.46
2	41.5	19	0.58	0.19	0.46	1.28	3.06	2.40
3	41.5	16	0.40	0.17	0.39	1.03	2.32	2.26
4	41.5	18	0.58	0.28	0.43	1.33	2.09	1.57
5	41.5	20	0.67	0.25	0.48	1.39	2.70	1.95
6	41.5	17	0.44	0.18	0.41	1.08	2.50	2.32

$T_1/(D_p/p) = 0.31 / 0.29 = 1.06$

$T_1 / T_n = 0.31 / 0.20 = 1.56$

$(D_p/p) / T_n = 0.29 / 0.20 = 1.46$

E-4: Propagation of error for the changing elevation, annual sedimentation, and annual accretion in the ^{137}Cs sedimentary unit

Core #	$T_1/(D_p/p)$	T_1 Error	T_1/T_n	D_p/p Error	T_n Error	$(D_p/p)/T_n$
1	0.1	0.03	0.2	0.04	0.01	0.1
2	0.1	0.05	0.3	0.03	0.01	0.1
3	0.1	0.05	0.3	0.03	0.01	0.1
4	0.2	0.09	0.4	0.03	0.03	0.2
5	0.2	0.11	0.5	0.03	0.03	0.2
6	0.1	0.06	0.4	0.03	0.01	0.2

Propagation of error for PR_01_08 ^{137}Cs Sedimentary Unit:

$$\mathbf{T_1/(D_p/p) = T_1/(D_p/p) * ((T_{1\ propogated\ error} / T_1)^2 + (0.5 / D_p)^2)^{1/2}}$$

$T_1/(D_p/p) = 1.06 * ((0.03 / 0.31)^2 + (0.5 / 12)^2)^{1/2} = 0.1$

$$\mathbf{T_1/T_n = T_1/T_n * ((T_{n\ propogated\ error} / T_n)^2 + (T_{1\ propogated\ error} / T_1)^2)^{1/2}}$$

$T_1/T_n = 1.56 * ((0.03 / 0.20)^2 + (0.03 / 0.31)^2)^{1/2} = 0.2$

$$\mathbf{(D_p/p)/ T_n = (D_p/p)/ T_n * ((((T_{n\ propogated\ error} / T_n)^2 + (T_{1\ propogated\ error} / T_1)^2)^{1/2}}$$

$(D_p/p)/ T_n = 1.46 ((0.03 / 0.20)^2 + (0.03 / 0.31)^2)^{1/2} = 0.1$

REFERENCES

Allen, J. (1998). The geoarchaeology of land-claim in the coastal wetlands: A sketch from Britain and the northwest European Atlantic and North Sea coasts. *Archaeological Journal, 154*, 1-54.

Allen, J. (2000). Holocene coastal lowlands in NW Europe: Autocompaction and the uncertain ground. In K. Pye & J. R. Allen (Eds.), *Coastal and estuarine environments: Sedimentology, geomorphology, and geoarchaeology* (pp. 239-252). Special Publication, Geological Society of London.

Allen, J., Rae, J., Longworth, G., Haster, S., & Ivanovich, M. (1993). A comparison of ^{210}Pb dating technique with three independent dating methods in an estuarine salt-marsh sequence. *Estuaries, 16*, 670–677.

Appleby, P., & Oldfield, F. (1978). The calculation of lead-210 dates assuming a constant rate of supply of unsupported ^{210}Pb to the sediment. *Catena, 5*, 5-18.

Appleby, P., Richardson, N., & Nolan, P. (1991). ^{241}Am dating of lake sediments. *Hydrobiologia. 214*, 317-331.

Bianchi, T. (2007). *Biogeochemistry of estuaries*. New York: Oxford University Press.

Bird, M., Fifield, L., Chua, S., & Goh, B. (2004). Calculating sediment compaction for radiocarbon dating of intertidal sediments. *Radiocarbon, 46*, 421–435.

Bloom, A. (1964). Peat accumulation and compaction in a Connecticut coastal marsh. *Journal of Sedimentary Petrology, 34*, 599–603.

Cahoon, D. (2006). A review of major storm impacts on coastal wetland elevations. *Estuaries and Coasts,* 29, 889–898.

Cahoon, D., Marin, P., Black, B., & Lynch, J. (2000). A method for measuring vertical accretion, elevation, and compaction of soft, shallow water sediments. *Journal of Sedimentary Research,* 70, 1250 – 1253.

Cahoon, D. R., Reed, D., & Day, J. (1995). Estimating shallow subsidence in microtidal salt marshes of the southeastern United States: Kaye and Barghoorn revisited. *Marine Geology, 128*, 1-9.

Calhoun, M., & Frois, J. (2006). Louisiana Almanac: 2006-2007 (17th ed.). Gretana, La. : Pelican.

Callaway, J., & Day, J. (1996). A relative elevation model (REM) for a subsiding coastal forested wetland receiving wastewater effluent. *Ecological Modeling, 112*, 23-44.

Catuneanu, O. (2003). *Sequence stratigraphy of clastic systems*. Canada: Geology Association.

Charman, D. (2002). *Peat land systems and environmental change*. Chichester, UK: John Wiley and Sons.

Dalrymple, R. W., Zaitlin, B. A., & Boyd, R. (1992). Estuarine facies models: Conceptual basis and stratigraphic implications. *Journal of Sedimentary Petrology, 62*(6), 1130-1146.

DeLaune, R., Nyman, J., & Patric, W. (1994). Peat collapse and wetland loss in a rapidly subsiding coastal marsh. *Journal of Coastal Research, 10*, 1021-1030.

DeLaune, R., & Pezeshki, S. (2003). The role of soil organic carbon in maintaining surface elevation in rapidly subsiding U.S. Gulf of Mexico coastal marshes. *Water, Air, and Soil Pollution, 3*, 167-179.

Dokka, R. (2008). Earth science and public policy: Have we failed New Orleans? *EOS, 89*(10), 96-97.

Dokka, R., Sella, G., & Dixon, T. (2006). Tectonic control of subsidence and southward displacement of southeast Louisiana with respect to stable North America. *Geophys. Res. Lett., 33*, 1-5.

El-Daoushy, F., Tolonen, K., & Rosenberg, R. (1982). Lead-210 and moss increment dating of two Finnish Sphagnum peat moss. *Nature, 296*, 429-431.

Fairbanks, R. G. (1989). A 17,000-year glacio-eustatic sea level record: Influence of glacia-melting rates on the Younger Dryas event and deep-ocean circulation. *Nature, 342*, 637-642.

Faulkner, S., Barrow, W., Doyel, T., Baldwin, M., Michot, T., Wells, C., & Jeske, C. (2006). Sediment deposition from Hurricane Rita on Hackberry Beach Chenier in southwestern Louisiana. *Science and the Storms: The USGS Response to the Hurricanes of 2005*, 157-162.

Fisk, H. N., & McFarlan, E., Jr. (1955). Late Quaternary deltaic deposits of the Mississippi River. *Geological Society America Special Publication, 62*, 279-302.

Flint, R. F. (1963). Status of the Pleistocene Wisconsin stage in central North America. *Science. 139*, 402-404.

Foote, A., & Reynolds, K. (1997). Decomposition of saltmeadow cordgrass (*Spartina patens*) in Louisiana coastal marshes. *Estuaries. 3*, 579 -588.

Ford, M., & Grace, J. (1998). Effects of herbivores on soil processes, plant biomass, litter accumulation, and soil elevation changes in coastal marshes. *Journal of Ecology, 86*, 974-982.

Frazier, D. E. (1974). Depositional episodes: Their relationship to the Quaternary stratigraphic framework in the northwestern portion of the Gulf basin. *Texas Bureau Economic Geology Circular, 74*(1), 28.

Gagliano, S. (2005). Effects of earthquakes, fault movements, and subsidence on the south Louisiana landscape. *Louisiana Civil Engineer Journal of the Louisiana Section of the American Society of Civil Engineers, 13*(2), 5-7, 19-22.

Galloway, W. E. (2001). Cenozoic evolution of sediment accumulation in deltaic and shore-zone depositional systems, Northern Gulf of Mexico basin. *Marine and Petroleum Geology, 18*, 1031-1040.

Gambolati, G,. Putti, M., Teatini, P., & Gasparetto-Stori, G. (2006). Subsidence due to peat oxidation and impact on drainage infrastructures in a farmland catchment south of the Venice lagoon. *Environmental Geology, 49*, 814-820.

Goldberg, E. (1963). *Geochronology with ^{210}Pb in radioactive dating, Radioactive Dating* (pp. 121-132. Paper presented at meeting of the International Atomic Energy Agency, Vienna, Austria.

Gonzales, J., & Törnqvist, T. (2006). Coastal Louisiana in crisis: Subsidence or sea level rise? *EOS, 87*, 493-508.

Greene, D. L., Rodriguez, A. B., & Anderson, J. B. (2007). Seaward-branching coastal-plain and piedmont incised-valley systems through multiple sea-level cycles; late

Quaternary examples from Mobile Bay and Mississippi Sound, U.S.A. *Journal of Sedimentary Research, 77*, 139-158.

Hanson, R. A. (2000). *The Holocene paleoenvironment of the Pearl River Marsh determined by foraminiferal assemblages* (Unpublished master's thesis). The University of Southern Mississippi, Hattiesburg, MS.

Harris, D., Horwath, W., & Van Kessel, C. (2001). Acid fumigation of soils to remove carbonates prior to total organic carbon or carbon 13 isotopic analysis. *Soil Science Society of America Journal, 65*, 1853-1856.

Haslett, S., Davies, P., Curr, R., Davies, C., Kennington, K., King, C., & Margetts, A. (1998). Evaluating late-Holocene relative sea-level change in the Somerset Levels, southwest Britain. *Holocene,* 8, 197-207.

Hedges, J., & Stern, J. (1984). Carbon and nitrogen determination of carbonate-containing soils. *Limnology and Oceanography, 29*(3), 657-663.

Heinrich, P. V. (2006). Pleistocene and Holocene fluvial systems of the lower Pearl River, Mississippi and Louisiana, USA. *Gulf Coast Association of Geological Societies Transactions, 56,* 267-278.

Hippensteel, S., Martin, R., Nikitina, D., & Pizzuto, J. (2002). Interannual variation of marsh foraminiferal assemblages (Bombay Hook National Wildlife Refuge, Smyrna, DE): Do foraminiferal assemblages have memories? *Journal of Foraminiferal Research, 32*, 97-109.

Horton, B., Rossi, V., & Hawkes, A. (2008). The sedimentary record of the 2005 hurricane season from the Mississippi and Alabama coastlines. *Quaternary International, 195*(1-2), 15-30.

Inglett, P., Vollier, E., Roychoudhury, A., & van Cappellen, P. (2004). A new idea in marsh coring: The wedge. *Soil Science Society of America, 68*, 705-708.

Kaye, C., & Barghoorn, E. (1964). Late Quaternary sea level change and crustal rise at Boston, Massachusetts, with notes on autocompaction of peat. *Geological Society of America Bulletin, 75,* 63–80.

Kendall, C., & McDonald, J. (1998). Isotope tracers in catchment hydrology. Oxford Press: New York.

Kindinger, J. L. (1998). Holocene geologic framework of Lake Pontchartrain basin and lakes of southeastern Louisiana. *USGS Open-File Report No. 98-805*.

Kindinger, J. L., Balson, P. S., & Flocks, J. G. (1994). Stratigraphy of the Mississippi–Alabama shelf and the Mobile River incised-valley system. In R. W. Dalrymple, R. Boyd, & B. A. Zaitlin (Eds.), *Incised-valley systems: Origin and sedimentary sequences* (Vol. 51, pp. 83-95). New York: University Press.

Kooi, H., & De Vries, J. J. (1998). Land subsidence and hydrodynamic compaction of sedimentary basins. *Hydrology and Earth System Sciences 2*, 159–171.

Kuecher, G. (1994). *Geological framework and consolidation settlement potential of the Lafourche delta, Topstratum Valley fill: Implications for wetland loss in Terrebonne Parishes. Louisiana* (Unpublished doctoral dissertation). Louisiana State University, Baton Rouge, LA.

Kuykendall, J. I. (2010). *Paleoenvironmental history of the Pearl River marsh (Louisiana and Mississippi) using lithology and foraminiferal analysis* (Unpublished master's thesis). The University of Southern Mississippi, Hattiesburg, MS.

Lambe, T., & Whitman, R. (1969). *Soil mechanics*. New York, NY: John Wiley & Sons.

Lehmann, E., & D'Abrera, H. (1998). Nonparametrics: Statistical methods based on ranks (Rev. ed.). Englewood Cliffs, NJ: Prentice-Hall.

Leibowitz, S., & Hill, J. (1987). Spatial analyses of Louisiana coastal land loss. In R. E. Turner & D. R. Cahoon (Eds.), *Causes of wetland loss in the coastal central Gulf of Mexico: Minerals Management Service Outer Continental Shelf (OCS) Study MS87-0120 [Technical narrative]* (Vol. 2, pp. 331-355). New Orleans, LA: Minerals Management Service.

Lefebvre, G., Langlois, P., Lupien, C., & Lavallée, J. G. (1984). Laboratory testing and in situ behaviour of peat as embankment foundation. *Canadian Geotechnical Journal, 21*, 322–337.

Leorri, E., Martin, R., & Horton, B. (2009). Field experiments on bioturbation in salt marshed (Bombay Hook National Wildlife Refuge, Smyrna, De, USA): implications for sea-level studies. *Journal of Quaternary Science, 24*, 139-149.

Li, X. (1994). *A 6200-year environmental history of the Pearl River marsh, Louisiana* (Unpublished master's thesis). Louisiana State University, Baton Rouge, LA.

Long, A., Waller, M., & Stupples, P. (2006). Driving mechanisms of coastal change: Peat compaction and the destruction of late Holocene coastal wetlands. *Marine Geology, 225*, 63-84.

Massey, A., Paul, M., Gehrels, W., & Charman, D. (2006). Autocompaction in Holocene coastal back-barrier sediments from South Devon, southwest England, UK. *Marine Geology, 226*, 225–241.

McBride, B. C., 1998. The evolution of allochthonous salt along a mega-regional profile across the northern Gulf of Mexico basin. *AAPG Bull.* 82: 1,037-1,054.

McCraith, B., Gardner, L., Welthey, D., & Moore, W. (2003). The effect of fiddler crab burrowing on sediment mixing and radionuclide profiles along a topographical gradient in a southeastern salt marsh. *Journal of Marine Research*, 61, 359-390.

McGookey, D. P. (1975). Gulf Coast Cenozoic sediments and structures: An excellent example of extra-continental sedimentation. *Gulf Coast Association of Geological Societies Transactions, 25*, 104-120.

McKee, K., & Cherry, J. (2009). Hurricane Katrina sediment slowed elevation loss in subsiding brackish marshes of the Mississippi River delta. *Wetlands*, *29*(1), 2-15.

McKee, K., & Mendelssohn, I. (1989). Response of a freshwater marsh plant community to increased salinity and increased water level. *Aquatic Botany, 34*, 301-316.

Meckel, T. (2007). An attempt to reconcile subsidence rates determined from various techniques in southern Louisiana. *Quaternary Science Reviews, 27*, 1517-1522.

Meckel, T., Brink, U., & Williams, J. (2006). Current subsidence rates due to compaction of Holocene sediments in southern Louisiana. *Geophyiscal Research Letters, 33*, L11403.

Meckel, T., Brink, U., & Williams, J. (2007). Sediment compaction rates and subsidence in delta plains: Numerical constraints and stratigraphic influences. *Basin Research, 19*, 19-31.

Morton, R., Bernier, J., & Ferina, N. (2005, December 15). Rapid subsidence and historical wetland loss in the Mississippi river delta plain: Likely causes and future implications. *U.S. Geological Survey.* Washington, DC: U.S. Government Printing Office.

Morton, R., & White, W. (1997). Characteristics of and corrections for core shortening in unconsolidated sediments. *Journal of Coastal Research, 13*(3), 761-769.

Morton, R., Tiling, G., & Ferina, N. (2003). Causes of hotspot wetland loss in the Mississippi delta plain. *Environmental Geosciences, 10*, 71-80.

Neubauer, S. (2008). Contributions of mineral and organic components to tidal freshwater marsh accretion. *Estuarine, Coastal, and Shelf Science, 78*, 78-88.

Neubauer, S., Anderson, I., Constantine, J., & Kuehl, D. (2002). Sediment deposition and accretion in the Mid-Atlantic (U.S.A.) tidal freshwater marsh. *Estuarine, Coastal, and Shelf Research, 5*4, 713-727.

Nunn, A. (2003). Land surface subsidence caused by groundwater withdrawal in southeastern Louisiana, Transactions of the 53rd Annual Convention; 50th GCSSEPM Anniversary Transactions. *Gulf Coast Association of Geological Societies, 53*, 630–638.

Oldfield, F., & Appleby, P. (1984). Empirical testing of 210Pb-dating models for lake sediments. Leicester University Press: England.

Oldfield, F., Appleby, P., Cambray, R., Eakins, J., Barber, K. Battarbee, R.,Pearson, G., & Williams, J. (1979). Pb210, Cs137, and Pu239 profiles in ombrotrophic peat. *Oikos, 33*, 40-45.

Olid, J., Ordellana, J., Cortizas, A., Masque, P., Peiteado, E., & Cabeza, J. (2008). Roles of surface vegetation in Pb210 dating of peat cores. *Environmental Science and Technology, 42*, 8858-8864.

Orson, R., Warren, R., & Niering, W. (1998). Interpreting sea level rise and rates of vertical marsh accretion in a Southern New England tidal marsh. *Estuarine, Coastal and Self Science, 47*, 419-429.

Otvos, E. G. (2005). Numerical chronology of Pleistocene coastal plain and valley development: Extensive aggradation during glacial low sea-level stands. *Quaternary International, 135*, 91-113.

Otvos, E. G., & Giardino, M. (2004). Interlinked barrier island chain and delta lobe development northern Gulf of Mexico. *Sedimentary Geology, 169*, 47-73.

Owens, P., & Walling, D. (1996). Spatial variability of caesium-137 inventories at reference sites: An example from two contrasting sites in England and Zimbabwe. *Applied Radiation and Isotopes, 47*, 699-707.

Penland, S., & Ramsey, R. (1990). Relative sea level rise in Louisiana and the Gulf of Mexico: 1908-1988. *Journal of Coastal Research, 6*, 322-342.

Pennington, W., Cambray, R., Eakins, J., & Harkness, D. (1976). Radionuclide dating of the recent sediments of Belkham Tarn. *Freshwater Biology, 6*, 317-331.

Pizzuto, J., & Schwendt, A. (1997). Mathematical modeling of autocompaction of a Holocene transgressive valley-fill deposit, Wolfe Glade, Delaware. Geology, *25*, 57–60.

Reed, D. (1989). Patterns of sediment deposition in subsiding coastal salt marshes, Terrebone Bay, La: The role of winter storms. *Estuaries, 4*, 222-227.

Robbins, J. (1978). Geochemical and geophysical applications of radioactive lead. In J. O. Nriagu (Ed.), *Biogeochemistry of Lead in the Environment* (pp. 285-393). Amsterdam: Elsever Scientific.

Rogers, K., & Saintilan, N. (2007) Vegetation change and surface elevation dynamics in estuarine wetlands of southeast Australia. *Estuarine, Coastal and Shelf Science*, *66*, 559-569.

Rybcyzk , J., Curco, C., Canico, A., Prat, N., & Day, J. (1996). In integrated wetland elevation model for the Ebre delta. Presented at the Impact of Climate Change on Northwestern Mediterranean Deltas final workshop. Vol. 2: *The present and the future, commissions of the European community*, Directorate-General XII, Science Research and Development, Venice, 1.17-1.31.

Rybcyzk , J., Day, J., Rismond, A., Scarton, F., & Are, D. (1996). In integrated wetland elevation model for the Po delta, Italy. Presented at the Impact of Climate Change on Northwestern Mediterranean Deltas Final Workshop Vol. 2: The present and the future, commissions of the European community, Directorate-General XII, Science Research and Development, Venice, 1.17-1.31.

Santschi, P., Allison, M., Asbill, S., Perlet, A., Cappellino, S., Dobbs, C., & McShea, L. (1999). Sediment transport and Hg recovery in Lavaca Bay, as evaluated from radionuclide and Hg distributions. *Environmental Science Technology, 33*, 378-391.

Santschi, P., Li, Y., Bell, J., Trier, R., & Kawtaluk, K. (1980). Plutonium in the coastal marine environment. *Earth and Planetary Science Letters, 51*, 248-265.

Saucier, R. T. (1994). *Geomorphology and quaternary geologic history of the lower Mississippi valley* (Vol. 1364). Vicksburg, MS: U.S. Army Engineer Waterways Experiment Station.

Saucier, R. T., & Snead, J. L. (1989). *Quaternary geology of the lower Mississippi valley: Louisiana geological survey*. Baton Rouge, LA: Scale 1:1,100,000.

Schumm, S. A., Dumont, J. F., & Holbrook, J. M. (2000). *Active tectonics and alluvial rivers*. Melbourne, NY: Cambridge University Press.

Shennan, I., & Horton, B. (2002). Holocene land-and sea-level changes in Great Britain. *Journal of Quaternary Science 17*, 511–526.

Shinkle, K., & Dokka, R. (2004, July). Rates of vertical displacement at benchmarks in the lower Mississippi valley and northern Gulf Coast. In *National Oceanic and Atmospheric Administration Technical Report, National Ocean Service/National Geodetic Survey*, p. 135.

Snowden, J., & Forsthoff, G. (1976). Clay sedimentation in the Pearl River delta, Louisiana-Mississippi. *Transactions GCAGS, 26*, 298-304.

Spencer, K., Cundy, A., & Croudance, I. (2003). Heavy metal distribution and early-diagenesis in salt marsh sediments from the Medway Estuary, Kent, UK. *Estuarine, Coastal, and Shelf Science, 57*(1-2), 43-54.

Sturmpf, P. (1983). The process of sedimentation on the surface of a salt marsh. *Estuarine, Coastal and Shelf Science, 17*, 495-508.

Tailfort, M., Neuhubuer, S., and Bristow, G. (2007). The effects of tidal forcing on biogeochemical processes in salt marsh sediments. *Geochemical Transactions, 8*(6), 1-15.

Taylor, J. (1982). An introduction to error analysis: The study of uncertainties in physical measurements. Sausaltio, CA: University Science Books.

Terzaghi, K. (1943). *Theoretical soil mechanics*. New York: John Wiley & Sons.

Terzaghi, K., Peck, R., & Mesri, G. (1996). Soil mechanics in engineering practice. New York: John Wiley & Sons.

Törnqvist, T., Bick, S., van der Bord, K., & de Jong, A. (2006). How stable is the Mississippi delta? *Geology, 34*, 697-700.

Törnqvist, T., Newsome, L., Borg, K., Jong, A., & Kurnik, C. (2004). Deciphering Holocene sea-level history on the U.S. Gulf Coast: A high resolution record from the Mississippi River delta. *GSA Bulletin, 116*(7/8), 1026-1039.

Törnqvist, T., Wallace, D., Storms, J., Wallinga, J., van Dam, R., Blaauw, M., Derksen, M., Klerks, C., Meijneken, C., & Snijders, E. (2008). Mississippi delta subsidence primarily caused by compaction of Holocene strata. *Nature, 1*, 173-176.

Turner, R. E, Milan, C. S, & Swenson, E. M. (2006). Recent volumetric changes in salt marsh soils. *Estuarine Coastal and Shelf Science, 69*, 352-359.

Valiela, I., Teal, J., & Allen, S. (1985). Decomposition in salt marsh ecosystems: The phase and major factors affecting disappearance of above ground organic matter. *Journal of Experimental Marine Biology, 87*, 493-498.

van Asselen, S., Stouthamer, E., & van Asch, W. J. (2009). Effects of peat compaction on delta evolution: A review on processes, response, measuring, and modeling. *Earth-Science Reviews, 92*, 35-51.

Wallbrink, P., & Murray, A. (1996). Distribution and variability of (super 7) Be in soils under different surface cover conditions and its potential for describing soil redistribution processes. *Water Resources Research, 32*, 467-476.

Wardenaar, E. (1987). A new hand tool for cutting peat profiles. *Canadian Journal of Botany, 65*, 1772–1773.

Wasserman, M., Bartoly, F., Portilho, A., Rochedo, E., Viana, A., Perez, D., & Conti., C. (2008). The effect of organic amernment on potential mobility and bioavailability of ^{137}Cs and ^{60}Co in tropical soils. *Journal of Environmental Radioactivity, 99*(33), 554-562.

White, D.A. (1983). Plant communities of the Pearl River basin, Louisiana. *American Midland Naturalist, 110*, 381-396.

Williams, H. (2003). Modeling shallow autocompaction in coastal marshes using Cesium-137 fallout: Preliminary results from the Trinity River Estuary, Texas. *Journal of Coastal Research, 19*(1), 180-188.

Wilson, G., & Grace, H. (1942). The settlement of London due to underdrainage of the London clay. *Journal of Institute of Civil Engineering (London), 19*, 100–127.

Yeager, K., Santschi, P., Phillips, J., & Herberet, B. (2005). Suspended sediment sources and tributary effects in the lower reaches of a coastal plain stream as indicated by radionuclides, Loco Bayou, Texas. *Environmental Geology, 47*, 382-395.

Yeager, K., Santschi, P., Rifai, H., Suarez, M., Brinkmyer, R., Hung, C. C., Schindler, K., Andres, M., & Weaver, E. (2007). Dioxin chronology and fluxes in sediments of the Houston Ship Channel, Texas: Influences of non-steady state sediment

transport and total organic carbon. *Environmental Science and Technology, 41*, 5291-5298.

Yeager, K, Santschi, P., & Rowe, T. (2004). Sediment accumulation and radionuclide inventories (^{239,240}Pu, ^{210}Pb and ^{234}Th) in the northern Gulf of Mexico, as influenced by organic matter and macrofaunal density. *Marine Chemistry,* 91(1-4), 1-14.

Yeager, K., Santschi, P., Schindler, K., Andres, M., & Weaver, E. (2006). The relative importance of terrestrial versus marine sediment sources to the Nueces-Corpus Christi Estuary, Texas: An isotopic approach. *Estuaries and Coasts, 29*, 443-459.

Yuill, B., Lavoie, D., & Reed, D. (2009). Understanding subsidence processes in coastal Louisiana. *Journal of Coastal Research, 54*, 23-36.

Zar, J. (1984). *Biostatistical analysis* (2nd ed.). Englewood Cliffs, NJ: Prentice Hall.